Chapter 3

RADIATIVE TRANSFER

3.1 The Radiative Transfer Equation

Light scattering by a single macroscopic particle can be studied in the framework of electrodynamics of continuous media. The same applies to clusters of particles or scattering volumes, where multiple light scattering does not play an important role. This is not the case for clouds. Here multiple scattering dominates the registered signal. Therefore, generally speaking, techniques of multiple wave scattering should be used in this case. However, they are quite complex and do not always lead to results, which can be used as a base for the numerical algorithm.

Moreover, electromagnetic fields $\vec{E}$ cannot be measured in the optical range. This is mostly due to their high oscillations ($\approx 10^{15}$ oscillations per second). Clearly, any measuring device makes temporal and spatial averaging of registered radiation. Also optical instruments measure quantities quadratic with respect to the field. This is similar to quantum mechanics, where the amplitude ψ is the main notion of the theory, but it is $|\psi|^2$, which is measured.

Therefore, this is of importance to formulate multiple light scattering theory not in terms of field vectors but in terms of quadratic values, which can be easily measured. The Stokes-vector parameter $\vec{I}$ with components I, Q, U, V is usually used in this case. Of course, this leads to the omission of a number of theoretical details (e.g., related to the phase effects). However, such an approach allows an interpretation of most optical measurements. Also note that light beams having the same values I, Q, U, V (but in principle different values of $\vec{E}$) cannot be distinguished by optical instruments, which measure quadratic values. Therefore, the main point is to force multiple light scattering theory to deal with intensities rather than fields from the very beginning. Then we do not need to make the

averaging procedures at the end of calculations to bring calculated values in correspondence to the measured ones. The main task of this section is to introduce an equation, which governs the transformation of the Stokes vector $\vec{I}$ in cloudy media. The Stokes vector used in this section is defined via Eqs. (2.215)-(2.218) with averaging procedures (in time and space domains) applied as discussed by Rozenberg (1973) and Mishchenko (2002).

For the sake of simplicity, we consider now the transformation of light intensity and ignore other components of the Stokes vector. Clearly, if the process of scattering is ignored we can write in the linear approximation:

$$dI = -\sigma_{ext} I dl. \tag{3.1}$$

This underlines the experimental fact that the reduction of light intensity on the length dl in this case is proportional to this length and the value of I itself. The coefficient of proportionality is called the extinction coefficient. Actually it coincides in this simple case with the absorption coefficient ($\sigma_{sca} = 0$). It follows that

$$I = I_0 \exp(-\sigma_{ext} l) \tag{3.2}$$

for a homogeneous ($\sigma_{ext} = const$) layer, which is the well-known extinction law. Here I_0 is the incident intensity at $l = 0$. This formula should be modified for light scattering media to account for light scattering from all other directions to a given direction $\vec{\Omega}$. Then we have:

$$dI(\vec{\Omega}) = -\sigma_{ext} I(\vec{\Omega}) dl + \int_{4\pi} \sigma_{sca}(\vec{\Omega}, \vec{\Omega}') I(\vec{\Omega}') d\vec{\Omega}' dl, \tag{3.3}$$

where $\sigma_{sca}(\vec{\Omega}, \vec{\Omega}')$ describes the local scattering law. Unfortunately, Eq. (3.3) cannot be solved in such a simple way as for the case of Eq. (3.1) (no scattering). This explains the mathematical complexity of the radiative transfer theory. Equation (3.3) is called the radiative transfer equation. It can be written in the following form:

$$\frac{dI(\vec{\Omega})}{dl} = -\sigma_{ext} I(\vec{\Omega}) + \int_{4\pi} \sigma_{sca}(\vec{\Omega}, \vec{\Omega}') I(\vec{\Omega}') d\vec{\Omega}'. \tag{3.4}$$

The radiative transfer theory is concerned with the solution of this equation for scattering volumes (e.g., clouds), having different shapes, types of illuminations, and microstructure. Actually, the Stokes vector $\vec{I}$ is governed by the same equation (Mishchenko, 2002) but σ_{ext} and σ_{sca} become matrices in this case:

$$\frac{d\vec{I}(\vec{\Omega})}{dl} = -\hat{\sigma}_{ext} \vec{I}(\vec{\Omega}) + \int_{4\pi} \hat{L}_2 \hat{\sigma}_{sca} \left(\vec{\Omega}, \vec{\Omega}'\right) \hat{L}_1 \vec{I}(\vec{\Omega}') d\vec{\Omega}'. \tag{3.5}$$

The matrix $\hat{L}_1$ transforms the Stokes vector defined in the meridional plane holding the normal to the scattering layer and the direction $\vec{\Omega}'$ to the Stokes vector in the scattering plane. The matrix $\hat{L}_2$ is needed for the transformation of the Stokes vector of scattered light from the scattering plane back to the meridional plane. This

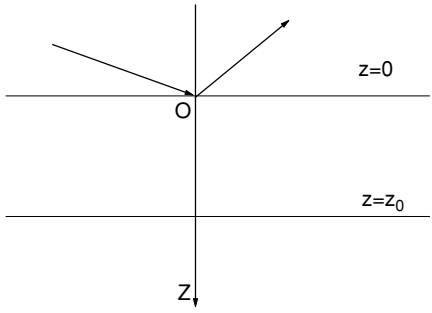

Fig. 3.1. Geometry of the problem.

is due to the fact that the matrix $\hat{\sigma}_{sca}$ in Eq. (3.5) is defined in the scattering plane and the vector $\vec{I}$ is defined with respect to the meridional plane. For spherical water droplets the matrix $\hat{\sigma}_{ext}$ is reduced to a scalar value and

$$\frac{d\vec{I}(\vec{\Omega})}{dl} = -\sigma_{ext}\vec{I}(\vec{\Omega}) + \int_{4\pi} \hat{L}_2\hat{\sigma}_{sca}\left(\vec{\Omega}, \vec{\Omega}'\right)\hat{L}_1\vec{I}(\vec{\Omega}')d\vec{\Omega}'. \tag{3.6}$$

However, for crystalline media, where particles can have a preferential orientation and be anisotropic, this is not the case. This fact adds an additional complexity in radiative transfer studies for the case of ice clouds.

We will be mostly concerned with solutions of Eq. (3.6) for a plane-parallel cloud layer illuminated by the Sun. The interaction of solar radiation with extended cloud fields is well approximated by the solution of this idealized problem. The geometry of the problem is given in Fig. 3.1. The solar light with the zenith angle ϑ_0 uniformly illuminates a plane-parallel scattering layer from above. We will assume that properties of the layer do not change in the horizontal direction. Then properties of light field depend only on the vertical coordinate Z (see Fig. 3.1) and the direction $\vec{\Omega}$, specified by the zenith angle ϑ and the azimuth φ. The main task is to calculate distributions $\vec{I}(\vartheta, \varphi, z)$. Usually only measurements of $\vec{I}(\vartheta, \varphi, 0)$ at the top of the cloud (reflected light) and $\vec{I}(\vartheta, \varphi, z_0)$ at the cloud base (transmitted light) are made (see Fig. 3.1). Therefore, we will be concerned mostly with these two angular distributions.

Equation (3.6) takes the following form for the case shown in Fig. 3.1:

$$\cos\vartheta\frac{d\vec{I}(\vartheta, \varphi)}{dz} = -\sigma_{ext}\vec{I}(\vartheta, \varphi) + \int_0^{2\pi} d\varphi' \int_0^{\pi} d\vartheta' \hat{L}_2\hat{\sigma}_{sca}\left(\vartheta', \varphi' \to \vartheta, \varphi\right) \times \hat{L}_1\vec{I}(\vartheta', \varphi') \tag{3.7}$$

The most simple case to study is that of idealized homogeneous clouds with values of σ_{ext} and $\hat{\sigma}_{sca}$ not dependent on the position inside the cloud. Then we

have from Eq. (3.7):

$$\cos\vartheta \frac{d\vec{I}(\vartheta,\varphi)}{d\tau} = -\vec{I}(\vartheta,\varphi) + \frac{\omega_0}{4\pi}\int_0^{2\pi} d\varphi' \int_0^{\pi} d\vartheta' \hat{L}_2 \hat{P}(\vartheta',\varphi' \to \vartheta,\varphi) \times \hat{L}_1 \vec{I}(\vartheta',\varphi'), \tag{3.8}$$

where we introduced the optical depth

$$\tau = \sigma_{ext} l, \tag{3.9}$$

the phase matrix

$$\hat{P} = \frac{4\pi \hat{\sigma}_{sca}(\vartheta',\varphi' \to \vartheta,\varphi)}{\sigma_{sca}} \tag{3.10}$$

and the single-scattering albedo:

$$\omega_0 = \frac{\sigma_{sca}}{\sigma_{ext}}. \tag{3.11}$$

Studies of Eq. (3.8) open ways to treat more complex cases, including clouds with spatial varying microstructure characteristics and also cases of broken clouds and clouds having various complex shapes. Equation (3.8) is reduced to the following simpler form:

$$\cos\vartheta \frac{dI(\vartheta,\varphi)}{d\tau} = -I(\vartheta,\varphi) + \frac{\omega_0}{4\pi}\int_0^{2\pi} d\varphi' \int_0^{\pi} d\vartheta' p(\vartheta',\varphi' \to \vartheta,\varphi) I(\vartheta',\varphi'), \tag{3.12}$$

if the polarization effects are ignored. Here

$$p(\vartheta',\varphi' \to \vartheta,\varphi) = \frac{4\pi\sigma_{sca}(\vartheta',\varphi' \to \vartheta,\varphi)}{\sigma_{sca}} \text{ is the phase function.}$$

It is useful to distinguish between diffuse $\vec{I}_d$ and direct (or coherent) $\vec{I}_c = \vec{J}_0 \delta(\mu - \mu_0)\delta(\varphi - \varphi_0)$ light in the general solution $\vec{I}(\vartheta,\varphi)$. Here $\vec{J}_0$ describes the Stokes vector of the incident attenuated flux. It is assumed that the layer is illuminated in the direction defined by the incidence zenith angle $\vartheta_0 = \arccos(\mu_0)$ and the azimuthal angle φ_0. The multiply scattered light is observed in the direction specified by the zenith observation angle $\vartheta = \arccos(\mu)$ and the azimuth φ. Namely, we write: $\vec{I}(\vartheta,\varphi) = \vec{I}_d(\vartheta,\varphi) + \vec{I}_c(\vartheta,\varphi)$. The substitution of this formula in Eq. (3.8) gives

$$\cos\vartheta \frac{d\vec{I}_d(\vartheta,\varphi)}{d\tau} = -\vec{I}_d(\vartheta,\varphi) + \frac{\omega_0}{4\pi}\int_0^{2\pi} d\varphi' \int_0^{\pi} d\vartheta' \hat{L}_2 \hat{P}(\vartheta',\varphi' \to \vartheta,\varphi)\hat{L}_1 \times \vec{I}_d(\vartheta',\varphi') + \frac{\omega_0}{4\pi}\hat{P}_*(\vartheta_0,\varphi_0 \to \vartheta,\varphi)\vec{F}\exp\left(-\frac{\tau}{\cos\vartheta_0}\right) \tag{3.13}$$

or

$$\cos\vartheta\frac{dI_d(\vartheta,\varphi)}{d\tau}=-I_d(\vartheta,\varphi)+\frac{\omega_0}{4\pi}\int_0^{2\pi}d\varphi'\int_0^{\pi}d\vartheta' p(\vartheta',\varphi'\to\vartheta,\varphi)I_d(\vartheta',\varphi') + \frac{\omega_0}{4\pi}p(\vartheta_0,\varphi_0\to\vartheta,\varphi)F\exp\left(-\frac{\tau}{\cos\vartheta_0}\right) \tag{3.14}$$

for the scalar case. Here $\hat{P}_*$ is the scattering matrix defined with respect to the meridional plane, $\vec{F}(F, Q_0, U_0, V_0)$ is the Stokes vector of incident light flux at the top of a cloud. It follows for unpolarized solar light: $Q_0 = U_0 = V_0$. The solution of this equation under boundary conditions stating that there is no diffuse light entering the cloud from above and below, allows to find $\vec{I}_d(\vartheta,\varphi)$. Also it follows from Eqs. (3.8) and (3.13) that $\vec{I}_c(\vartheta,\varphi)$ is given simply by:

$$\vec{I}_c(\vartheta,\varphi)=\vec{F}(\vartheta,\varphi)\delta(\cos\vartheta-\cos\vartheta_0)\delta(\varphi-\varphi_0)\exp\left(-\frac{\tau}{\cos\vartheta_0}\right) \tag{3.15}$$

or

$$I_c(\vartheta,\varphi)=F(\vartheta,\varphi)\delta(\cos\vartheta-\cos\vartheta_0)\delta(\varphi-\varphi_0)\exp\left(-\frac{\tau}{\cos\vartheta_0}\right) \tag{3.16}$$

for the scalar case.

The solution of Eq. (3.13) is a more easy task than that of Eq. (3.8) because we avoid the necessity to deal with the divergence in the direction of incident light in the framework of Eq. (3.13).

3.2 Reflection and Transmission Functions

Reflectance and transmittance of light by cloud layers is usually defined in terms of reflection R and transmission T functions. They relate incident light intensity $I_0(\vartheta_0,\varphi_0)$ with reflected $I_R(\mu,\varphi)$ and transmitted $I_T(\mu,\varphi)$ light intensities. Namely, it follows by definition:

$$I_R(\mu,\varphi)=\frac{1}{\pi}\int_0^1 d\varphi'\int_0^{2\pi}R(\tau,\mu,\varphi,\mu',\varphi')I_0(\mu',\varphi')\mu' d\mu', \tag{3.17}$$

$$I_T(\mu,\varphi)=\frac{1}{\pi}\int_0^{2\pi}d\varphi'\int_0^1 T(\tau,\mu,\varphi,\mu',\varphi')I_0(\mu',\varphi')\mu' d\mu'. \tag{3.18}$$

Reflection and transmission functions allow to find the intensity of reflected and transmitted light for arbitrary angular distributions of incident light with the intensity $I_0(\mu',\varphi')$.

If incident light is azimuthally independent, these formulae simplify:

$$I_R(\mu, \varphi) = 2 \int_0^1 \bar{R}(\tau, \mu, \mu') I_0(\mu') \mu' d\mu', \tag{3.19}$$

$$I_T(\mu, \varphi) = 2 \int_0^1 \bar{T}(\tau, \mu, \mu') I_0(\mu') \mu' d\mu', \tag{3.20}$$

where

$$\bar{R}(\tau, \mu, \mu') = \frac{1}{2\pi} \int_0^{2\pi} R(\tau, \mu, \mu' \varphi') d\varphi', \tag{3.21}$$

$$\bar{T}(\tau, \mu, \mu') = \frac{1}{2\pi} \int_0^{2\pi} T(\tau, \mu, \mu' \varphi') d\varphi'. \tag{3.22}$$

Note that relations (3.19) and (3.20) simplify for unidirectional illumination of a cloud by a wide beam (e.g., solar light). Then we can assume that

$$I_0(\mu', \varphi') = \delta(\mu' - \mu_0) \delta(\varphi' - \varphi_0) F, \tag{3.23}$$

where F is the solar flux density at the elementary area positioned at the top of a cloud perpendicular to the incident light beam and $\delta(x)$ is the delta function, having the following property:

$$f(x_0) = \int_0^\infty \delta(x - x_0) f(x) dx. \tag{3.24}$$

Using this relation and equations for reflection and transmission functions given above, we arrive at the following results:

$$I_R(\mu, \varphi) = \frac{F \mu_0 R(\tau, \mu, \varphi, \mu_0, \varphi_0)}{\pi}, \tag{3.25}$$

$$I_T(\mu, \varphi) = \frac{F \mu_0 T(\tau, \mu, \varphi, \mu_0, \varphi_0)}{\pi}, \tag{3.26}$$

and, therefore,

$$R(\tau, \mu, \varphi, \mu_0, \varphi_0) = \frac{\pi I_R(\mu, \varphi)}{F \mu_0}, \tag{3.27}$$

$$T(\tau, \mu, \varphi, \mu_0, \varphi_0) = \frac{\pi I_T(\mu, \varphi)}{F \mu_0}. \tag{3.28}$$

These equations allow us to make the following interpretation of reflection and transmission functions. Indeed, we have for an absolutely white Lambertian surface by definition:

$$\begin{aligned} P_R^L(\mu, \varphi) &= \int_{2\pi} I_R^L(\mu, \mu', \varphi, \varphi') \mu' d\Omega' = \int_0^{2\pi} d\varphi' \int_0^1 I_R^L(\mu, \mu', \varphi, \varphi') \mu' d\mu' \\ &= \int_0^{2\pi} d\varphi' \int_0^1 C \mu_0 \mu' d\mu' = \pi C \mu_0, \end{aligned} \tag{3.29}$$

where $P_R^L(\vartheta, \varphi)$ is the total power scattered by a unit area of a Lambertian surface into the upper hemisphere and we used the fact that intensity of light reflected from a Lambertian surface is proportional to the cosine of the incidence angle $\mu_0 (I_R^L = C\mu_0)$. The constant C can be found from the condition that the scattered and incident powers are equal in the case of an absolutely white Lambertian surface by definition. We have for the incident power:

$$P_0 = \int_{2\pi} I_0(\mu', \mu_0, \varphi', \varphi_0)\mu' d\Omega' = \int_0^{2\pi} d\varphi \int_0^1 \delta(\mu' - \mu_0)\delta(\varphi' - \varphi_0) F\mu' d\mu' = F\mu_0 \tag{3.30}$$

and, therefore: $C = F/\pi$. It means that intensity of light reflected from an absolutely white Lambertian surface is given by:

$$I_R^L = \frac{F}{\pi}\mu_0, \tag{3.31}$$

and, therefore, $R(\tau, \mu, \varphi, \mu_0, \varphi_0)$ [see Eq. (3.25)] is equal to the ratio of light reflected from a given surface I_R to the value of I_R^L:

$$R = I_R / I_R^L. \tag{3.32}$$

Also it means that $R \equiv 1$ by definition for a Lambertian ideally white surface.

Accordingly, it follows:

$$T = I_T \big/ I_R^L. \tag{3.33}$$

The results of calculations and measurements of cloud reflectance and transmittance will be mostly presented in terms of functions R and T in this book. They do not depend on the intensity of incident light and characterize inherent properties of a cloud layer. The intensity of reflected and transmitted light can be calculated using Eqs. (3.17) and (3.18) for an arbitrary angular distribution of incident light. The integration of reflection and transmission functions with respect to angles allows us to find the cloud plane (r_d) and spherical (r) albedo, the cloud diffuse (t_d) and the global (t) transmittance, the cloud absorptance a_d and the global absorptance a (see Table 3.1 for definitions).

3.3 Polarization Characteristics

Clearly, Eqs. (3.15) and (3.16) should be modified if one would like to account for light polarization. Namely, it follows:

$$\vec{I}_R(\mu, \varphi) = \frac{1}{\pi} \int_0^{2\pi} d\varphi \int_0^1 \hat{R}(\tau, \mu, \varphi, \mu', \varphi')\vec{I}_0(\mu', \varphi')\mu' d\mu', \tag{3.34}$$

$$\vec{I}_T(\mu, \varphi) = \frac{1}{\pi} \int_0^{2\pi} d\varphi \int_0^1 \hat{T}(\tau, \mu, \varphi, \mu', \varphi')\vec{I}_0(\mu', \varphi')\mu' d\mu'. \tag{3.35}$$

Table 3.1. Radiative transfer characteristics $\left\{\bar{R} \equiv \frac{1}{2\pi}\int_0^{2\pi} R(\mu_0, \mu, \varphi)d\varphi,\ \ \bar{T} \equiv \frac{1}{2\pi}\int_0^{2\pi} T(\mu_0, \mu, \varphi)\mathrm{d}\varphi\right\}$.

Radiative characteristic	Symbol	Definition
Plane albedo	$r_d(\mu_0)$	$2\int_0^1 \bar{R}(\mu)\mu d\mu$
Spherical albedo	r	$2\int_0^1 r_d(\mu_0)\mu_0 d\mu_0$
Diffuse transmittance	$t_d(\mu_0)$	$2\int_0^1 \bar{T}(\mu_0, \mu)\mu d\mu$
Global transmittance	t	$2\int_0^1 t_d(\mu_0)\mu_0 d\mu_0$
Absorptance	$a_d(\mu_0)$	$1 - r_d(\mu_0) - t_d(\mu_0)$
Global absorptance	a	$1 - r - t$

Here $\vec{I}_R(\mu, \varphi)$ is the Stokes vector of reflected light, $\vec{I}_T(\mu, \varphi)$ is the Stokes vector of transmitted light, $\vec{I}_0(\mu, \varphi)$ is the Stokes vector of incident light, $\hat{R}$ and $\hat{T}$ are 4×4 reflection and transmission matrices, respectively, for illumination from above. Clearly, we have: $R \equiv R_{11}$, $T \equiv T_{11}$. The Stokes vector for unidirectional illumination of a cloud by a wide beam is

$$\vec{I}_0(\mu', \varphi') = \delta(\mu' - \mu_0)\delta(\varphi' - \varphi_0)\vec{F}. \tag{3.36}$$

The first element of $\vec{F}$ equals to the incident net flux F per unit perpendicular area at the top of a cloud. Other elements of this vector (Q_0, U_0, V_0) describe the polarization state of incident light. They equal to zero for incident unpolarized solar light. Obviously, we have in this case [see also Eqs. (3.25) and (3.26)]:

$$\vec{I}_R(\vartheta_0, \vartheta, \varphi) = \frac{\hat{R}\vec{F}}{\pi}\mu_0, \tag{3.37}$$

$$\vec{I}_T(\vartheta_0, \vartheta, \varphi) = \frac{\hat{T}\vec{F}}{\pi}\mu_0. \tag{3.38}$$

Let us assume that incident light is unpolarized. Then we have for the components of the Stokes vector of reflected light:

$$I_R(\vartheta_0, \vartheta, \varphi) = \frac{R_{11}F}{\pi}\mu_0, \quad Q_R(\vartheta_0, \vartheta, \varphi) = \frac{R_{21}F}{\pi}\mu_0, \tag{3.39}$$

$$U_R(\vartheta_0, \vartheta, \varphi) = \frac{R_{31}F}{\pi}\mu_0, \quad V_R(\vartheta_0, \vartheta, \varphi) = \frac{R_{41}F}{\pi}\mu_0, \tag{3.40}$$

and

$$I_T(\vartheta_0, \vartheta, \varphi) = \frac{T_{11}F}{\pi}\mu_0, \quad Q_T(\vartheta_0, \vartheta, \varphi) = \frac{T_{21}F}{\pi}\mu_0, \tag{3.41}$$

$$U_T(\vartheta_0, \vartheta, \varphi) = \frac{T_{31}F}{\pi}\mu_0, \quad V_T(\vartheta_0, \vartheta, \varphi) = \frac{T_{41}F}{\pi}\mu_0 \tag{3.42}$$

for transmitted light. The degree of linear polarization of reflected light is defined as

$$p_l^r \equiv -\frac{\sqrt{Q_R^2 + U_R^2}}{I_R}. \tag{3.43}$$

Therefore, it follows:

$$p_l^r \equiv -\frac{\sqrt{R_{21}^2 + R_{31}^2}}{R_{11}}. \tag{3.44}$$

It follows for the total degree of polarization:

$$p^r \equiv -\frac{\sqrt{R_{21}^2 + R_{31}^2 + R_{41}^2}}{R_{11}}. \tag{3.45}$$

The degree of circular polarization is given by:

$$p_c^r \equiv -\frac{R_{41}}{R_{11}}. \tag{3.46}$$

Note that the following relation holds for the total degree of polarization:

$$p^r \equiv \sqrt{p_l^r + p_c^r}. \tag{3.47}$$

Similar characteristics can be defined for the transmitted light:

$$p_l^t \equiv -\frac{\sqrt{T_{21}^2 + T_{31}^2}}{T_{11}}, \quad p_c^t \equiv \frac{T_{41}}{T_{11}}, \quad p^t \equiv -\frac{\sqrt{T_{21}^2 + T_{31}^2 + T_{41}^2}}{T_{11}}. \tag{3.48}$$

A number of simplifications arise for particular observation and incidence directions. For instance, if incidence and observation directions coincide and perpendicular to the scattering layer, then the principal plane is not defined and the reflection matrix for media with randomly oriented particles has the same structure as the scattering matrix for a local scattering volume. Therefore, light reflected in the nadir direction for the nadir illumination conditions is unpolarized. Also it follows that $p_c^r = p_c^t = 0$ and

$$p_l^r \equiv -\frac{R_{21}}{R_{11}}, \quad p_l^t \equiv -\frac{T_{21}}{T_{11}} \tag{3.49}$$

at $\mu_0 = 1$ and any observation conditions. Similarly, we have $p_c^r = p_c^t = 0$ at $\mu = 1$ for arbitrary illumination conditions. Equations (3.49) hold at $\mu = 1$ and $\varphi = \varphi_0$ as well.

3.4 Optically Thin Clouds

The radiative transfer in thin clouds (e.g., subvisual Cirrus) can be studied using the single-scattering approximation. Indeed multiple light scattering is of no importance in this case and the integral term in Eq. (3.13) can be omitted. Then it follows from Eq. (3.13)

$$\frac{d\vec{I}_d(x)}{dx} = -\vec{I}_d(x) + \frac{\omega_0(x)}{4\pi}\hat{P}(x)\vec{F}\exp(-sx), \tag{3.50}$$

where $x = \tau/\cos\vartheta, s = \cos\vartheta/\cos\vartheta_0$ and we omitted other arguments for simplicity. The matrix $\hat{P}$ in Eq. (3.50) is defined with respect to the meridional plane. This equation can be solved analytically. For this we multiply both sides of Eq. (3.50) by e^x. Then it follows:

$$\exp(x)\frac{d\vec{I}_d(x)}{dx} + \exp(x)\vec{I}_d(x) = \frac{\omega_0(x)}{4\pi}\hat{P}(x)\vec{F}\exp(-(s-1)x) \tag{3.51}$$

or

$$\frac{d\left[\vec{I}_d(x)e^x\right]}{dx} = \frac{\omega_0(x)}{4\pi}\hat{P}(x)\vec{F}\exp(-(s-1)x). \tag{3.52}$$

It means that

$$\vec{I}_d(x) = \frac{1}{4\pi}e^{-x}\int_a^x \omega_0(x')\hat{P}(x')\vec{F}\exp(-(s-1)x'). \tag{3.53}$$

Let us apply boundary conditions now:

$$\vec{I}_{d\uparrow}(x=0) = 0, \cos\vartheta > 0, \tag{3.54}$$

$$\vec{I}_{d\downarrow}(x=x_0) = 0, \cos\vartheta < 0. \tag{3.55}$$

They mean that there is no diffuse light entering the medium from above ($x = 0$) or below ($x = x_0 = (\tau_0/\cos\vartheta)$), τ_0 is the optical thickness of a scattering layer. So we have:

$$\vec{I}_{d\downarrow}(x) = \frac{1}{4\pi}e^{-x}\int_0^x \omega_0(x')\hat{P}(x')\vec{F}\exp(-(s-1)x'), \tag{3.56}$$

$$\vec{I}_{d\uparrow}(x) = \frac{1}{4\pi}e^{-x}\int_{x_0}^x \omega_0(x')\hat{P}(x')\vec{F}\exp(-(s-1)x') \tag{3.57}$$

and boundary conditions are satisfied automatically. A simple integration under the assumption of a homogeneous cloud layer gives:

$$\vec{I}_{d\downarrow}(x) = \frac{\omega_0\hat{P}\vec{F}}{4\pi(s-1)}\{e^{-x} - e^{-sx}\}, \tag{3.58}$$

$$\vec{I}_{d\uparrow}(x) = \frac{\omega_0\hat{P}\vec{F}}{4\pi(s-1)}\{e^{-x-(s-1)x_0} - e^{-sx}\} \tag{3.59}$$

for arbitrary x. It follows at the boundaries of a layer:

$$\vec{I}_{d\downarrow}(x) = \frac{\omega_0 \hat{P}\vec{F}}{4\pi(s-1)}\{e^{-x_0} - e^{-sx_0}\},\ \vec{I}_{d\uparrow}(x) = \frac{\omega_0 \hat{P}\vec{F}}{4\pi(s-1)}\{e^{-(s-1)x_0} - 1\} \tag{3.60}$$

So we have for the reflection and transmission vectors:

$$\vec{I}_r = \frac{\omega_0 \hat{P}\vec{h}}{4(\xi+\eta)}\left\{1 - \exp\left[-\left(\frac{1}{\xi}+\frac{1}{\eta}\right)\tau_0\right]\right\},$$
$$\vec{I}_T = \frac{\omega_0 \hat{P}\vec{h}}{4(\xi-\eta)}\left\{\exp\left[-\frac{\tau_0}{\xi}\right] - \exp\left[-\frac{\tau_0}{\eta}\right]\right\}, \tag{3.61}$$

where $\eta = |\cos\vartheta|$, $\xi = \cos\vartheta_0$, τ_0 is the optical thickness of the scattering layer, and $\vec{h} = \vec{F}/F_1$. We see that matrices $\hat{R}$ and $\hat{T}$ introduced above are proportional to $\hat{P}$ and have the same structure.

Obviously, it follows for unpolarized incident light

$$R = \frac{\omega_0 p(\theta)}{4(\xi+\eta)}\left\{1 - \exp\left[-\left(\frac{1}{\xi}+\frac{1}{\eta}\right)\tau_0\right]\right\}, \tag{3.62}$$

$$T = \frac{\omega_0 p(\theta)}{4(\xi-\eta)}\left\{\exp\left[-\frac{\tau_0}{\xi}\right] - \exp\left[-\frac{\tau_0}{\eta}\right]\right\}. \tag{3.63}$$

Equations given above are very useful in estimations of the influence of thin ($\tau_0 \to 0$) clouds on light fluxes in the terrestrial atmosphere.

3.5 Small-Angle Approximation

Let us consider now the case of a highly anisotropically light scattering layer (the asymmetry parameter $g \to 1$) illuminated along the normal. In this case most scattered photons propagate within the small-angle scattering region and there is a possibility to simplify the radiative transfer equation. Thus, we assume that $\cos\vartheta = 1$ in Eq. (3.12) and obtain:

$$\frac{dI(\tau,\mu)}{d\tau} = -I(\tau,\mu) + \frac{\omega_0}{2}\int_0^1 d\mu' I(\tau,\mu')p(\mu,\mu'), \tag{3.64}$$

where

$$p(\mu,\mu') = \frac{1}{2\pi}\int_{-1}^{2\pi} p(\mu,\mu',\phi)d\phi. \tag{3.65}$$

We used the fact that the intensity of scattered light field for layers with randomly oriented particles does not depend on the azimuth for the illumination of a layer along the normal. Note, that the value of $I(\tau,\mu)$ is the total intensity in

the direction given by arccos(μ), not the diffuse intensity as in Eq. (3.14), and it includes the direct light. The phase function $p(\mu, \mu', \varphi)$ in Eq. (3.65) can be represented in the following form (Minin, 1988)

$$p(\mu, \mu', \phi) = p(\mu, \mu') + 2\sum_{m=1}^{\infty} \cos m(\phi - \phi') \sum_{i=m}^{\infty} x_i \frac{(i-m)!}{(i+m)!} P_i^m(\mu) P_i^m(\mu'), \tag{3.66}$$

where

$$p(\mu, \mu') = \sum_{i=0}^{\infty} x_i P_i(\mu) P_i(\mu') \tag{3.67}$$

and $P_i(\mu)$ and $P_i^m(\mu)$ are Legendre and associated Legendre polynomials, respectively. Note that it follows:

$$x_i = \frac{2i+1}{2} \int p(\theta) P_i(\theta) \sin\theta d\theta. \tag{3.68}$$

We seek the solution of Eq. (3.64) in the following form:

$$I(\tau, \mu) = \sum_{i=0}^{\infty} b_i(\tau) P_i(\mu). \tag{3.69}$$

Substituting Eqs. (3.67) and (3.69) in Eq. (3.64), one obtains:

$$\frac{db_i(\tau)}{d\tau} = -c_i b_i(\tau), \tag{3.70}$$

where

$$c_i = 1 - \omega_0 \frac{x_i}{2i+1} \tag{3.71}$$

and the orthogonality of Legendre polynomials was used. Thus, it follows:

$$b_i(\tau) = A_i \exp(-c_i \tau), \tag{3.72}$$

where $A_i = const$.

We see that it is possible to obtain the intensity of the transmitted light with the following formula:

$$I(\tau, \mu) = \sum_{i=0}^{\infty} A_i e^{-c_i \tau} P_i(\mu). \tag{3.73}$$

Values of A_i are found from initial conditions. We will assume that

$$I(0, \mu) = I_0 \delta(1 - \mu), \tag{3.74}$$

where $\delta(1-\mu)$ is the delta function, I_0 is the density of incident light flux. The delta function can be represented in the following form:

$$\delta(1-\mu) = \frac{1}{4\pi}\sum_{i=0}^{\infty}(2i+1)P_i(\mu). \tag{3.75}$$

Thus, it follows:

$$A_i = \frac{2i+1}{4\pi} \tag{3.76}$$

and, finally,

$$I(\tau,\mu) = B\sum_{i=0}^{\infty}\frac{2i+1}{2}e^{-c_i\tau}P_i(\mu), \tag{3.77}$$

where $B = I_0/2\pi$.

This is a solution of the problem under consideration. Equation (3.77) describes the angular distribution of the transmitted light at small angles for the normal incidence of a light beam. This important formula can be rewritten in the integral form. Indeed, the phase function $p(\theta)$ has a sharp peak in the forward-scattering direction ($\theta = 0$) for cloudy media and the main contribution to the integral Eq. (3.68) comes from the small-angle scattering region. Thus, it follows from Eq. (3.68) that

$$x_i = \frac{2i+1}{2}\int_0^{\infty} p(\theta)J_0\left(\theta\left(i+\frac{1}{2}\right)\right)\theta d\theta, \tag{3.78}$$

where the asymptotic relationship

$$\lim_{\theta\to 0} P_i(\cos\theta) = J_0\left(\theta\left(i+\frac{1}{2}\right)\right) \tag{3.79}$$

was used.

From Eqs. must be (3.77)-(3.79) and the sum formula

$$\sum_{i=0}^{\infty} f\left(i+\tfrac{1}{2}\right) \approx \int_0^{\infty} f(\sigma)d\sigma, \tag{3.80}$$

it follows:

$$I(\tau,\vartheta) = \frac{I_0}{2\pi}\int_0^{\infty} d\sigma J_0(\sigma\vartheta)\exp(-\tau(1-\omega_0 P(\sigma))), \tag{3.81}$$

where

$$P(\sigma) = \frac{1}{2}\int_0^{\infty} p(\theta)J_0(\theta\sigma)\theta d\theta. \tag{3.82}$$

Table 3.2. Phase functions $p(\theta)$ and their Fourier–Bessel transforms $P(\sigma)$ (Υ is the normalization constant, x is the size parameter).

$p(\theta)$	$P(\sigma)$
$\dfrac{2\Upsilon \exp(-\Upsilon\theta)}{\theta}$	$\dfrac{\Upsilon}{\sqrt{\Upsilon^2+\sigma^2}}$
$2\Upsilon^2 \exp(-\Upsilon\theta)$	$\dfrac{\Upsilon^3}{(\Upsilon^2+\sigma^2)^{3/2}}$
$\dfrac{2}{\Upsilon^2}\exp\left(-\dfrac{\theta^2}{2\Upsilon^2}\right)$	$\exp\left(-\dfrac{\Upsilon^2\sigma^2}{2}\right)$
$\dfrac{4J_1^2(\theta x)}{\theta^2}$	$\begin{cases}\dfrac{2}{\pi}\left\{\arccos\left(\dfrac{\sigma}{2x}\right)-\dfrac{\sigma}{2x}\sqrt{1-\left(\dfrac{\sigma}{2x}\right)^2}\right\}, & \sigma \le 2x \\ 0, & \sigma > 2x\end{cases}$

Equation (3.81) in many cases is more easy to handle than Eq. (3.77). For instance, Eq. (3.82) can be analytically integrated for special types of phase functions $p(\theta)$ (see Table 3.2).

It follows from Eq. (3.81) for the diffuse intensity $I_d(\tau, \vartheta)$:

$$I_d(\tau, \vartheta) = \frac{I_0}{2\pi}\int_0^\infty \left[e^{-\tau(1-\omega_0 P(\sigma))} - e^{-\tau}\right] J_0(\sigma\vartheta)\sigma\, d\sigma, \tag{3.83}$$

where we extracted the peak of light intensity exactly in the forward direction using the equality:

$$\frac{I_0}{2\pi}e^{-\tau}\int_0^\infty J_0(\sigma\vartheta)\sigma\, d\sigma = I_0 e^{-\tau}\delta(\vartheta). \tag{3.84}$$

Equation (3.83) is often used for the solution of both direct and inverse problems of cloud optics. It is valid at $\tau \le 5$ and $\vartheta \to 0$. It follows that the phenomenon of multiple light scattering is responsible for broadening of the angular spectrum of the light transmitted by a scattering layer at small angles. The same effect is also observed in the single-scattering regime if the sizes of particles decrease. This remark is of importance for optical particle sizing in cloudy media.

The approximation, which was considered in this section, is called the small-angle approximation (SAA). Moments of different radiative characteristics in this approximation were studied by Lutomirski et al. (1995).

3.6 Optically thick clouds

3.6.1 Fundamental Relationships

Another case, where simple analytical results can be obtained, is that of thick ($\tau_0 \to \infty$) clouds. Note that final equations derived here can be actually applied at

$\tau_0 \geq 10$ or at somewhat smaller values depending on the accuracy requirements. This means that this case covers most cloudy situations occurring in the terrestrial atmosphere. Before we proceed to the derivation of analytical equations for functions R and T at $\tau_0 \gg 1$, we need to establish some auxiliary asymptotic relations.

It is known that light intensity in deep layers of optically thick media is azimuthally independent. The azimuthally integrated radiative transfer equation [see Eq. (3.14)] can be written in the following form:

$$\eta \frac{dI(\tau, \eta)}{d\tau} = -I(\tau, \eta) + B(\tau, \eta) + B_0(\tau, \eta), \tag{3.85}$$

where

$$B(\tau, \eta) = \frac{\omega_0}{2} \int_{-1}^{1} p(\eta, \eta') I(\tau, \eta') d\eta', \tag{3.86}$$

$$B_0(\tau, \eta) = \frac{\omega_0 F}{4\pi} p(\eta, \xi) e^{-\tau/\xi}, \tag{3.87}$$

and

$$p(\eta, \xi) = \frac{1}{2\pi} \int_{0}^{2\pi} p(\eta, \xi, \varphi) d\varphi \tag{3.88}$$

is the azimuthally averaged phase function. We also neglect polarization effects.

Let us assume that $\tau \to \infty$. Then it follows: $B_0(\tau, \eta) \to 0$ and

$$I(\tau, \eta) = i(\eta) e^{-k\tau}. \tag{3.89}$$

The last equation corresponds to the so-called deep-layer regime, when parameters η and τ are decoupled. Then the overall light flux f decreases with the distance from the illuminated boundary preserving the scattered light angular pattern given by the function $i(\eta)$. The value of f decreases in e times on the optical depth $\tau_e = 1/k$. Both the function $i(\eta)$ and the diffusion exponent k, play an important role in the theory considered here. These characteristics of the deep-layer regime also define the intensity of transmitted and reflected light as will be shown below.

So we have from Eq. (3.85):

$$(1 - k\eta) i(\eta) = \frac{\omega_0}{2} \int_{-1}^{1} p(\eta, \eta') i(\eta') d\eta'. \tag{3.90}$$

This integral equation is usually solved numerically. Let us assume that $p = 1$. Then we have:

$$i(\eta) = \frac{\omega_0}{2(1 - k\eta)} \int_{-1}^{1} i(\eta') d\eta' \tag{3.91}$$

or

$$i(\eta) = \frac{D}{1 - k\eta}, \tag{3.92}$$

where

$$D = \frac{\omega_0}{2} \int_{-1}^{1} i(\eta') d\eta' \tag{3.93}$$

does not depend on the angle. Note that $i(\eta)$ satisfies the radiative transfer equation (3.90) for any constant D and, therefore,

$$i(\eta) = \frac{1}{1 - k\eta} \tag{3.94}$$

and

$$I(\tau, \eta) = \frac{\exp(-k\tau)}{1 - k\eta}, \tag{3.95}$$

where we used the normalization condition: $D = 1$. The diffusion constant k can be found as follows. Let us substitute (3.92) in (3.91) taking into account that $D = 1$. Then we have:

$$\frac{\omega_0}{2k} \ln\left(\frac{1 + k}{1 - k}\right) = 1. \tag{3.96}$$

This equation allows to find k at arbitrary ω_0 and $p(\theta) = 1$. Clearly, we have at $\omega_0 = 1 : k = 0$. The dependence $k(\omega_0)$ at $p(\theta) = 1$ is given in Fig. 3.2. For more complex phase functions a numerical solution is needed. The results of correspondent calculations for the Heney–Greenstein phase function

$$p(\theta) = \sum_{n=1}^{\infty} g^n P_n(\cos\theta) \tag{3.97}$$

at the asymmetry parameters $g = 0.75$ (ice clouds) and $g = 0.85$ (water clouds) are also given in Fig. 3.2. We see that $0 \le k \le 1$. This means that the decrease rate of the diffuse light in the deep-layer regime ($\exp(-k\tau)$) for absorbing media is smaller than that of the direct light ($\exp(-\tau)$).

It follows also:

$$(1 + k\eta) i(-\eta) = \frac{\omega_0}{2} \int_{-1}^{1} p(-\eta, \eta') i(\eta') d\eta' \tag{3.98}$$

or

$$(1 + k\eta) i(-\eta) = \frac{\omega_0}{2} \int_{-1}^{1} p(\eta, \eta') i(-\eta') d\eta', \tag{3.99}$$

where we used the property: $p(-\eta, -\eta') = p(\eta, \eta')$.

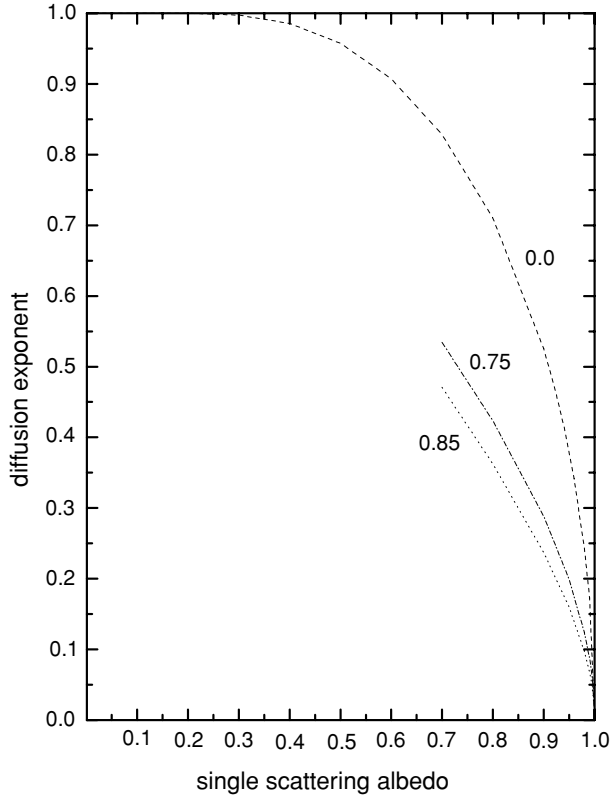

Fig. 3.2. Dependence of the diffusion exponent on the single-scattering albedo for isotropic scattering. Calculations of the diffusion exponent for single-scattering albedos typical for water (0.85) and ice (0.75) clouds are also shown. It follows that the value of k decreases with g for a given ω_0.

Let us establish now the relationship between the intensity $i^{\downarrow}(\eta)$ for light propagated downwards and the intensity $i^{\uparrow}(-\eta)$ for light propagated upwards. Arrows show the direction of light propagation. The value of $\eta = |\cos\vartheta|$ is positive by definition. Note that negative $\cos\vartheta$ corresponds to upwelling light flux. We consider a cut parallel to the upper boundary but at a large optical depth. The corresponding plane at $\tau \gg 1$ is illuminated not only by light coming from above and having the intensity i_a but also by light coming from below and reflected from the layer laying above the plane of cut. We denote this contribution to the total intensity as i_b. Clearly, we have:

$$i^{\downarrow}(\eta) = i_a(\eta) + i_b(\eta). \tag{3.100}$$

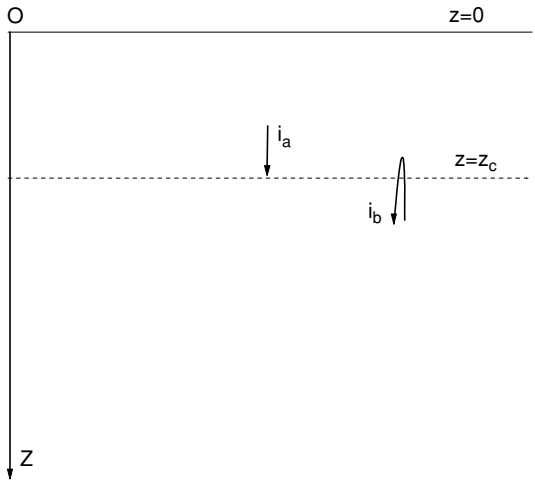

Fig. 3.3. Contributions to downward light flux.

So the function $i^{\downarrow}(\eta)$ can be presented as a sum of two terms (see Fig. 3.3). Clearly, $i_a(\eta)$ is proportional to the angular distribution $u(\eta)$ of light transmitted by the upper layer:

$$i_a(\eta) = Mu(\eta), \tag{3.101}$$

where M is the unknown proportionality constant. We will find this constant at later stages of our derivations. Also it follows from Eq. (3.19) for the intensity $i_b(\eta)$:

$$i_b(\eta) = 2\int_0^1 R(\eta, \eta')i(-\eta')\eta' d\eta', \tag{3.102}$$

where $R(\eta, \eta')$ is the azimuthally averaged reflection function of the upper layer under illumination from below ($\eta > 0, \eta' > 0$). This layer could be chosen to be arbitrary thick. So we will assume that $R(\eta, \eta')$ coincides with the azimuthally averaged reflection function of a semi-infinite layer $R_\infty(\eta, \eta')$.

Summing up, it follows:

$$i^{\downarrow}(\eta) = Mu(\eta) + 2\int_0^1 R_\infty(\eta, \xi)i(-\xi)\xi d\xi. \tag{3.103}$$

Let us find M. For this we multiply the last equation by $\eta i^{\downarrow}(\eta)$ and integrate it from 0 to 1 with respect to η. Then we have:

$$\int_0^1 \eta i^{\downarrow 2}(\eta)d\eta = M\int_0^1 u(\eta)i^{\downarrow}(\eta)\eta d\eta + \Im \tag{3.104}$$

where the two-dimensional integral

$$\Im = 2\int_0^1 i^{\downarrow}(\eta)\eta d\eta \int_0^1 R_\infty(\eta,\xi)i^{\uparrow}(-\xi)\xi d\xi \tag{3.105}$$

can be simplified. For this we note that it follows

$$i^{\uparrow}(-\xi) = 2\int_0^1 i^{\downarrow}(\eta)R_\infty(\eta,\xi)\eta d\eta \tag{3.106}$$

and, therefore,

$$\Im = \int_0^1 i^{\uparrow 2}(-\xi)\xi d\xi \tag{3.107}$$

or

$$\Im = -\int_{-1}^0 i^{\downarrow 2}(\xi)\xi d\xi. \tag{3.108}$$

Therefore, it follows:

$$M = \mathbb{C}\int_{-1}^1 i^2(\eta)\eta d\eta, \tag{3.109}$$

where

$$\mathbb{C} = \left[\int_0^1 u(\eta)i(\eta)d\eta\right]^{-1}. \tag{3.110}$$

We will use the normalization condition: $\mathbb{C} = 2$. Then one derives:

$$M = 2\int_{-1}^1 i^2(\eta)\eta d\eta. \tag{3.111}$$

We present the equation for M together with other important relationships in Table 3.3. The constant N defined in the property 8 (see Table 3.3) will be used in further derivations devoted to studies of relationships between auxiliary functions defined as

$$P(\tau) = \int_{-1}^1 \eta i(\eta)I(\tau,\eta)d\eta \tag{3.112}$$

and

$$Q(\tau) = \int_{-1}^1 \eta i(-\eta)I(\tau,\eta)d\eta. \tag{3.113}$$

The relationships between functions $P(\tau)$ and $Q(\tau)$ can be used for the derivation of asymptotic equations for reflection and transmission functions valid as $\tau_0 \to \infty$. Let us show this.

Table 3.3. Main equations and constants ($u_0 \equiv u(\omega_0 = 1)$, $R_{0\infty} \equiv R_{0\infty}(\omega_0 = 1)$).

N	Property
1	$(1 - k\eta)i(\eta) = \frac{\omega_0}{2}\int_{-1}^{1} p(\eta, \eta')i(\eta')d\eta'$
2	$(1 + k\eta)i(-\eta) = \frac{\omega_0}{2}\int_{-1}^{1} p(\eta, \eta')i(-\eta')d\eta'$
3	$\frac{\omega_0}{2}\int_{-1}^{1} i(\eta)d\eta = 1$
4	$i(-\eta) = 2\int_0^1 i(\xi)R_\infty(\xi, \eta)\xi d\xi$
5	$i(\eta) = 2\int_0^1 i(-\xi)R_\infty(\xi, \eta)\xi d\xi + Mu(\eta)$
6	$2\int_0^1 u(\eta)i(\eta)\eta d\eta = 1$
7	$M = 2\int_{-1}^{1} i^2(\eta)\eta d\eta$
8	$N = 2\int_0^1 i(-\eta)u(\eta)\eta d\eta$
9	$\delta = \int_0^1 u_0(\xi)\xi^2 d\xi$
10	$u_0(\xi) = \frac{3}{4}\left(\xi + 2\int_0^1 R_{0\infty}(\xi, \eta)\eta^2 d\eta\right)$
11	$2\int_0^1 u_0(\eta)\eta d\eta = 1$
12	$2\int_0^1 R_{0\infty}(\xi, \eta)\eta d\eta = 1$

First of all, we note that it follows from Eq. (3.90) after multiplication of this equation by $i(\eta)$ and integration from –1 to 1:

$$\frac{dP(\tau)}{d\tau} = -kP(\tau) + P_0(\tau), \tag{3.114}$$

where

$$P_0(\tau) = \int_{-1}^{1} i(\eta)B_0(\tau, \eta)d\eta \tag{3.115}$$

and we used the equality

$$-kP(\tau) = \int_{-1}^{1} B(\tau, \eta)i(\eta)d\eta - \int_{-1}^{1} i(\eta)I(\tau, \eta)d\eta. \tag{3.116}$$

This equality can be obtained from property 1 in Table 3.3. Namely, we have after multiplying Eq. (1) in Table 3.3 by $I(\tau, \eta)$ and integrating this equation from –1 to 1 with respect to η:

$$\int_{-1}^{1} I(\tau, \eta)i(\eta)d\eta - kP(\tau) = \frac{\omega_0}{2}\int_{-1}^{1} d\eta \int_{-1}^{1} I(\tau, \eta)p(\eta, \eta')i(\eta')d\eta' \tag{3.117}$$

or

$$\int_{-1}^{1} I(\tau, \eta) i(\eta) d\eta - kP(\tau) = \int_{-1}^{1} d\eta' B(\tau, \eta') i(\eta') d\eta', \tag{3.118}$$

where we used the property: $p(\eta, \eta') = p(\eta', \eta)$. The last equation coincides with Eq. (3.116).

The next step is to find $P(\tau)$. For this we use the following substitution in Eq. (3.114):

$$P(\tau) = f(\tau) e^{-k\tau}. \tag{3.119}$$

Then it follows:

$$\frac{df(\tau)}{d\tau} = P_0(\tau) e^{k\tau} \tag{3.120}$$

or

$$f \Big|_{\tau_1}^{\tau} = \int_{\tau_1}^{\tau} P_0(t) e^{kt} dt. \tag{3.121}$$

It means that

$$f(\tau) = f(\tau_1) + \int_{\tau_1}^{\tau} P_0(t) e^{kt} dt. \tag{3.122}$$

So we we have:

$$P(\tau) = f(\tau_1) e^{-k\tau} + e^{-k\tau} \int_{\tau_1}^{\tau} P_0(t) e^{kt} dt. \tag{3.123}$$

The value of τ_1 can be found from boundary conditions. In particular, we are interested in the diffuse light. Diffuse light does not enter the medium from above or below ($I(0, \eta) = 0$ for $\eta > 0$ and $I(\tau_0, \eta) = 0$ for $\eta < 0$). Therefore, we have: $\tau_1 = 0$. Then the boundary condition at the upper boundary is satisfied. Finally, it follows

$$P(\tau) = P(0) e^{-k\tau} + \int_{0}^{\tau} P_0(t) e^{k(t-\tau)} dt. \tag{3.124}$$

A similar relationship can be obtained for $Q(\tau, \eta)$. Then we have:

$$\frac{dQ(\tau)}{d\tau} = kQ(\tau) + Q_0(\tau), \tag{3.125}$$

where

$$Q_0(\tau) = \int_{-1}^{1} i(-\eta) B_0(\tau, \eta) d\eta. \tag{3.126}$$

This equation differs for the correspondent equation for P only by the sign before k. So we have:

$$Q(\tau, \eta) = \psi\left(\tau_1^*\right) e^{k\tau} + e^{k\tau} \int_{\tau_1^*}^{\tau} Q_0(t) e^{-kt} dt, \tag{3.127}$$

where it was assumed that

$$Q(\tau) = \psi(\tau)e^{k\tau}. \tag{3.128}$$

The value of τ_1^* can be found from the boundary condition at the lower boundary of a medium. Namely, we have: $\tau_1^* = \tau_0$. Therefore, it follows:

$$Q(\tau) = Q(\tau_0)e^{k(\tau-\tau_0)} + \int_{\tau_0}^{\tau} Q_0(t)e^{-k(t-\tau)}dt. \tag{3.129}$$

This equation is satisfied automatically at $\tau = \tau_0$ due to the accurate account for the boundary conditions.

Summing up, we have the following important relationships:

$$P(\tau) = P(0)e^{-k\tau} + V(\tau), \tag{3.130}$$

$$Q(\tau) = Q(\tau_0)e^{k(\tau-\tau_0)} + W(\tau), \tag{3.131}$$

where

$$V(\tau) = \int_0^{\tau} P_0(t)e^{k(t-\tau)}dt, \tag{3.132}$$

$$W(\tau) = \int_{\tau_0}^{\tau} Q_0(t)e^{-k(t-\tau)}dt. \tag{3.133}$$

These fundamental relationships are valid for any τ and for any light sources represented by B_0 (Sobolev, 1975). They can be used for the derivation of a number of important results of cloud optics.

We will use a particular case at $\tau = 0$ in the first equation and a case $\tau = \tau_0$ in the second equation. Then it follows:

$$P(\tau_0) = P(0)\exp(-k\tau_0) + V(\tau_0), \tag{3.134}$$

$$Q(0) = Q(\tau_0)\exp(-k\tau_0) + W(0), \tag{3.135}$$

where

$$\begin{aligned} V(\tau_0, \eta) &= e^{-k\tau_0}\int_0^{\tau} P_0 dt \int_{-1}^{1} i(\eta)\frac{\omega_0}{4}p(\eta, \xi)e^{-t((1/\xi)-k)}d\xi \\ &= \frac{1}{2}\left(e^{k\tau_0} - e^{-\tau_0/\xi}\right)\xi i(-\xi), \end{aligned} \tag{3.136}$$

and we used property 2 in Table 3.3. Also we have:

$$\begin{aligned} W(0, \eta) &= \int_{\tau_0}^{0} e^{-kt}dt \int_{-1}^{1} i(-\eta)\frac{\omega_0}{4}p(\eta, \xi)e^{-t/\xi}d\eta \\ &= -\frac{1}{2}\left(1 - e^{-(k+(1/\xi))\tau_0}\right)\xi i(-\xi). \end{aligned} \tag{3.137}$$

Therefore, neglecting small numbers $e^{-\tau_0/\xi}$, it follows as $\tau_0 \to \infty$:

$$P(0, \eta) = -P(\tau_0, \eta)e^{k\tau_0} + \frac{1}{2}\xi i(-\xi), \tag{3.138}$$

$$Q(0, \eta) = Q(\tau_0, \eta)e^{-k\tau_0} - \frac{1}{2}\xi i(-\xi). \tag{3.139}$$

These are auxiliary relations we were bound to establish from the very start. They can be also written in the following form:

$$i(\xi) = 2\int_{-1}^{1} T(\eta, \xi, \tau_0)i(\eta)\eta d\eta + 2e^{-k\tau_0}\int_{-1}^{1} R(\eta, \xi, \tau_0)i(-\eta)d\eta, \tag{3.140}$$

$$i(-\xi) = 2\int_{-1}^{1} R(\eta, \xi, \tau_0)i(\eta)\eta d\eta + 2e^{-k\tau_0}\int_{-1}^{1} T(\eta, \xi, \tau_0)i(-\eta)\eta d\eta, \tag{3.141}$$

where T and R are determined as

$$R = \frac{\pi I_R}{\mu_0 F}, \quad T = \frac{\pi I_T}{\mu_0 F}. \tag{3.142}$$

3.6.2 Asymptotic Equations

The general form of functions $R(\eta, \xi, \tau_0)$ and $T(\eta, \xi, \tau_0)$ can be obtained using physical arguments. In particular T should be proportional to $u(\eta)$ (and, actually due to the reciprocity principal also to $u(\xi)$). Therefore, we have:

$$T(\eta, \xi, \tau_0) = \alpha(\tau_0)u(\eta)u(\xi). \tag{3.143}$$

Let us consider now a semi-infinite layer (see Fig. 3.4) and make a cut at a large optical thickness τ_0. Then we can represent $R_\infty(\eta, \xi)$ as a sum of reflection

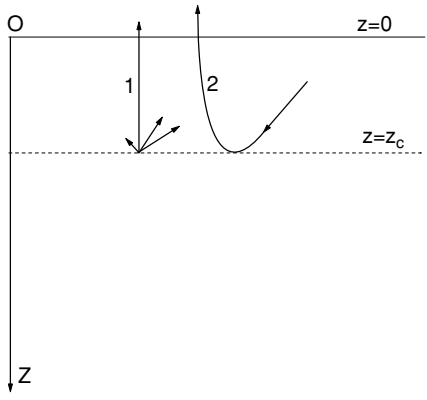

Fig. 3.4. Contributions to upward light flux.

from upper layer $R(\tau_0, \eta, \xi)$ (contribution 1, see Fig. 3.4) and light transmitted by the upper layer and reflected back (contribution 2, see Fig. 3.4). The angular distribution of the transmitted light should be proportional to $u(\eta)$ as it was specified above. So we have:

$$R_\infty(\eta, \xi) = R(\eta, \xi, \tau_0) + \beta(\tau_0)u(\eta)u(\xi). \tag{3.144}$$

Let us find α and β substituting two last equations in asymptotic formulae (3.140), (3.141). Then it follows:

$$i(\xi) = 2e^{k\tau_0}\int_{-1}^{1}\alpha(\tau_0)u(\eta)u(\xi)i(\eta)\eta d\eta + 2\int_{-1}^{1}(R_\infty(\eta, \xi) - \beta(\tau_0)u(\eta)u(\xi))i(-\eta)\eta d\eta, \tag{3.145}$$

$$i(-\xi) = 2\int_{-1}^{1}(R_\infty(\eta, \xi) - \beta(\tau_0)u(\eta)u(\xi))i(\eta)d\eta + 2e^{-k\tau_0}\int_{-1}^{1}\alpha(\tau_0)u(\eta)u(\xi)i(-\eta)\eta d\eta, \tag{3.146}$$

and, therefore,

$$i(\xi) = e^{k\tau_0}\alpha(\tau_0)u(\xi) + i(\xi) - Mu(\xi) - \beta(\tau_0)u(\xi)N, \tag{3.147}$$

$$i(-\xi) = i(-\xi) - \beta(\tau_0)u(\xi) + \alpha Ne^{-k\tau_0}u(\xi), \tag{3.148}$$

where we introduced the integral (see Table 3.3)

$$N = 2\int_{-1}^{1}u(\eta)i(-\eta)\eta d\eta. \tag{3.149}$$

It follows:

$$\alpha(\tau_0) - Me^{-k\tau_0} - \beta Ne^{-k\tau_0} = 0, \tag{3.150}$$

$$\beta(\tau_0) = \alpha(\tau_0)Ne^{-k\tau_0} \tag{3.151}$$

and, therefore,

$$\alpha(\tau_0) = \frac{Me^{-k\tau_0}}{1 - N^2e^{-2k\tau_0}}. \tag{3.151}$$

Finally, we have (Sobolev, 1975, 1984):

$$R(\eta, \xi, \varphi, \tau_0) = R_\infty(\eta, \xi, \varphi) - T(\xi, \eta, \tau_0)Ne^{-k\tau_0}, \tag{3.152}$$

$$T(\xi, \eta) = \frac{Me^{-k\tau_0}}{1 - N^2e^{-2k\tau_0}}u(\eta)u(\xi), \tag{3.153}$$

where we accounted for the fact that the transmitted light does not depend on the azimuth φ.

These formulae are central equations of the cloud optics. The importance of these equations is due to the fact that the dependence on τ_0 is given explicitly. Our next task is to derive approximate equations for constants k, M, N and functions

$u(\eta)$, $R_\infty(\eta, \xi, \varphi)$ in a number of particular cases. Numerical calculations of these functions have been performed by Nakajima and King (1992). The accuracy of Eqs. (3.152), (3.153) was studied by Konovalov (1975), Melnikova and Vasyliev (2005), and Kokhanovsky and Nauss (2006).

3.6.3 Weak Absorption Limit

Equations given above can be simplified considerably for the case of values of ω_0 close to one. This case is of particular importance for cloud optics due to weak absorption of water in the visible and near-infrared. Therefore, we need to find approximate expressions for functions $R_\infty(\eta, \xi)$, $u(\eta)$ and also for parameters k, M, N as $\omega_0 \to 1$. Let us concentrate on this problem now.

3.6.3.1 The constants k, M and the diffuse light field in deep layers

The parameter M depends on the diffuse light intensity $i(\eta)$ in deep layers of a cloud:

$$M = 2\int_{-1}^{1} i^2(\eta)\eta d\eta. \tag{3.154}$$

So we need to study functions $i(\eta)$ as $\omega_0 \to 1$. The radiative transfer equation for the normalized light intensity $i(\eta)$ deep inside of a homogeneous cloudy medium has the following form as it was discussed above:

$$(1 - k\eta)i(\eta) = \frac{\omega_0}{2}\int_{-1}^{1} p(\eta, \eta')i(\eta')d\eta', \tag{3.155}$$

where $p(\eta, \eta')$ is the azimuthally averaged phase function, ω_0 is the single-scattering albedo and k is the diffusion exponent. The normalization condition for $i(\eta)$ has the following form:

$$\frac{\omega_0}{2}\int_{-1}^{1} i(\eta')d\eta' = 1. \tag{3.156}$$

We introduce the following expansions:

$$p(\eta, \eta') = \sum_{n=0}^{\infty} x_n P_n(\eta)P_n(\eta') \tag{3.157}$$

and

$$i(\eta) = \sum_{n=0}^{\infty} \sigma_n P_n(\eta). \tag{3.158}$$

The task is to find σ_n knowing x_n and using Eq. (3.155). So we have from Eq. (3.155):

$$B = \sum_{n=0}^{\infty} \sigma_n P_n(\eta) - k\eta \sum_{n=0}^{\infty} \sigma_n P_n(\eta), \tag{3.159}$$

where

$$B = \frac{\omega_0}{2} \sum_{l=0}^{\infty} \sum_{n=0}^{\infty} \int_{-1}^{1} x_l \sigma_n P_l(\eta) P_l(\eta') P_n(\eta') d\eta' \tag{3.160}$$

or

$$B = \omega_0 \sum_{l=0}^{\infty} \sum_{n=0}^{\infty} \sigma_n x_l \delta_{nl} [2n+1]^{-1} P_n(\eta) \tag{3.161}$$

and after simplifications:

$$B = \omega_0 \sum_{n=0}^{\infty} x_n \sigma_n [2n+1]^{-1} P_n(\eta). \tag{3.162}$$

We used the following orthogonality relationship:

$$\int_{-1}^{1} P_n(\eta) P_l(\eta) d\eta = 2\delta_{nl} [2n+1]^{-1}, \tag{3.163}$$

where δ_{nl} is the Kronecker symbol.

Therefore, it follows:

$$\frac{1}{k} \sum_{n=0}^{\infty} \sigma_n \left\{ 1 - \frac{x_n \omega_0}{2n+1} \right\} P_n(\eta) = \sum_{n=0}^{\infty} \sigma_n \left\{ \frac{n+1}{2n+1} P_{n+1}(\eta) + \frac{n}{2n+1} P_{n-1}(\eta) \right\}, \tag{3.164}$$

where we used the property:

$$P_n(\eta) = \frac{n+1}{2n+1} P_{n+1}(\eta) + \frac{n}{2n+1} P_{n-1}(\eta). \tag{3.165}$$

The expressions for

$$\varsigma(\eta) = \sum_{n=0}^{\infty} \sigma_n \frac{n+1}{2n+1} P_{n+1}(\eta) \tag{3.166}$$

and

$$\upsilon(\eta) = \sum_{n=0}^{\infty} \sigma_n \frac{n}{2n+1} P_{n-1}(\eta) \tag{3.167}$$

can be written as

$$\varsigma(\eta) = \sum_{l=1}^{\infty} \sigma_{l-1} \frac{l}{2l-1} P_l(\eta) \tag{3.168}$$

and

$$\upsilon(\eta) = \sum_{s=0}^{\infty} \sigma_{s+1} \frac{s+1}{2s+3} P_s(\eta), \tag{3.169}$$

where $l = n + 1$, $s = n - 1$.

Therefore, it follows:

$$\sum_{m=0}^{\infty} \left[\frac{1}{k}\sigma_m - \frac{x_m \omega_0}{(2m+1)k}\sigma_m - \frac{m}{2m-1}\sigma_{m-1} - \frac{m+1}{2m+3}\sigma_{m+1} \right] P_m(\eta) = 0 \tag{3.170}$$

for arbitrary η. This means that

$$\frac{1}{k}\sigma_m - \frac{x_m \omega_0}{(2m+1)k}\sigma_m - \frac{m}{2m-1}\sigma_{m-1} - \frac{m+1}{2m+3}\sigma_{m+1} = 0 \tag{3.171}$$

or

$$\sigma_{m+1} = \frac{(2m+3)(2m - \omega_0 x_m + 1)}{(2m+1)(m+1)k}\sigma_m + \frac{(2m+3)m}{(2m-1)(m+1)}\sigma_{m-1}. \tag{3.172}$$

Let us assume that $m = 0$. Then we have:

$$\sigma_1 = \frac{3\sigma_0(1-\omega_0)}{k}. \tag{3.173}$$

It is easy to derive the analytical expression for the value of σ_0. It follows that

$$\sigma_m = \frac{2m+1}{2} \int_{-1}^{1} i(\eta) P_n(\eta) d\eta \tag{3.174}$$

and, therefore,

$$\sigma_0 = \frac{1}{2} \int_{-1}^{1} i(\eta) d\eta. \tag{3.175}$$

So we can derive (see property 3 in Table 3.3): $\sigma_0 = \omega_0^{-1}$ and, therefore,

$$\sigma_1 = \frac{3(1-\omega_0)}{k\omega_0}. \tag{3.176}$$

This allows to obtain the following asymptotic expression from Eq. (3.158):

$$i(\eta) = \omega_0^{-1} \left\{ 1 + 3k^{-1}(1-\omega_0)\eta \right\}, \tag{3.177}$$

where we neglected higher order terms. It follows as $\omega_0 \to 1$:

$$i(\eta) = 1 + 3k^{-1}(1 - \omega_0)\eta. \tag{3.178}$$

Recurrence relations (3.172) allow us to find σ_m and $i(\eta)$ at any k. We will not consider correspondent results here, however, but rather concentrate on the derivation of the approximate equation for k valid as $\omega_0 \to 1$.

For this we introduce:

$$\Upsilon_m = \frac{\sigma_m}{\sigma_{m-1}}. \tag{3.179}$$

Then it follows from Eq. (3.172):

$$\Upsilon_{m+1} = \frac{(2m+3)(2m - \omega_0 x_m + 1)}{(2m+1)(m+1)k} - \frac{(2m+3)m}{(2m-1)(m+1)\Upsilon_m} \tag{3.180}$$

and

$$\Upsilon_m = \frac{(2m+3)m}{(2m-1)(m+1)\left[\frac{(2m+3)(2m+1-\omega_0 x_m)}{(2m+1)(m+1)k} - \Upsilon_{m+1}\right]} \tag{3.181}$$

or

$$\Upsilon_m = \frac{(2m+3)(2m+1)mk}{(2m+3)(2m-1)(2m+1-\omega_0 x_m) - \varepsilon_m}, \tag{3.182}$$

where

$$\varepsilon_m = k(4m^2 - 1)(m+1)\Upsilon_{m+1}. \tag{3.183}$$

Because we are interested in the asymptotic solution valid as $k \to 0$, we can ignore ε_m and derive at $m = 1$:

$$\Upsilon_1 = \frac{3k}{(3 - \omega_0 x_1)}. \tag{3.184}$$

So it follows:

$$\sigma_1 = \frac{3k}{(3 - \omega_0 x_1)}\sigma_0 \tag{3.185}$$

or

$$\sigma_1 = \frac{3k}{(3 - \omega_0 x_1)\omega_0}. \tag{3.186}$$

Therefore, we finally derive (see also Eq. (3.176)):

$$k = \sqrt{3(1 - \omega_0)(1 - g\omega_0)}, \tag{3.187}$$

where $g = x_1/3$ is the asymmetry parameter. This important equation shows that the intensity in the deep layers of clouds decreases faster for smaller values of g

(less extended in the forward direction phase functions). Our derivations are valid as $\omega_0 \to 1$ only. So we can also write:

$$k = \sqrt{3(1-\omega_0)(1-g)}. \tag{3.188}$$

The approximate expression for the diffusion constant given here is of a great importance for cloud optics studies. In particular, we can derive from Eqs. (3.187), (3.178):

$$i(\eta) = 1 + \sqrt{3}s\eta, \tag{3.189}$$

where

$$s = \sqrt{\frac{1-\omega_0}{1-g\omega_0}} \tag{3.190}$$

is the similarity parameter. Surprising result is that the angular pattern $i(\eta)$ does not depend on the choice of the particular light scattering medium if s kept constant. The function $i(\eta)$ is completely determined by the similarity parameter s as $\omega_0 \to 1$. Therefore, cloudy media having different ω_0 and g but the same s have very similar light angular distributions in deep layers at $\omega_0 \approx 1$.

Let us introduce the ratio $D = i(-1)/i(1)$. This ratio is equal to one for nonabsorbing media. However, it follows from Eq. (3.189) for weakly absorbing media: $D = 1 - \varsigma\sqrt{1-\omega_0}$, $\varsigma = 2\sqrt{3/(1-g)}$. Therefore, measurements of g and D can be used to find the probability of light absorption $\beta = 1 - \omega_0$. Namely, it follows: $\beta = (1-D)^2/\varsigma^2$.

The parameters k and s are of a crucial importance for the theory considered here. We expect that other asymptotic constants and functions must depend on these parameters as well. In particular, we derive using property 7 in Table 3.3:

$$M = \frac{8s}{\sqrt{3}} \tag{3.191}$$

as $k \to 0$.

3.6.3.2 The constant N and the escape function

The expansion of $u(\eta)$ with respect to the diffusion coefficient k can be presented as

$$u(\eta) = \sum_{n=0}^{\infty} k^n u_n(\eta). \tag{3.192}$$

We are interested only in the case of weak absorption. Then it follows:

$$u(\eta) = u_0(\eta) + ku_1(\eta). \tag{3.193}$$

The task is to calculate the function $u_1(\eta)$. This will be performed in two steps. First of all we note that the weak absorption of light does not alter single scattering angular pattern considerably. The angular distribution of emerging light $u(\eta)$ is determined largely by the multiple scattering processes. So it is safe to assume that $u(\eta) \approx u_0(\eta)$ as $k \to 0$ or $u_1(\eta) = bu_0(\eta)$, where the constant b should be determined. Clearly, due to physical reasons we should have: $u(\eta) < u_0(\eta)$ and $b < 0$. Therefore, absorption plays the role of a veil in this case. It reduces the contrast but it does not change details of the scattering pattern. We start from the expression:

$$2\int_0^1 u(\eta)i(\eta)\eta d\eta = 1. \tag{3.194}$$

Let us use the following expansions in this formula:

$$u(\eta) = u_0(\eta)(1 + bk) \tag{3.195}$$

and

$$i(\eta) = 1 + ak\eta, \tag{3.196}$$

where $a = (1 - g\omega_0)^{-1}$ as underlined above.

Then it follows (see Eqs. (3.188), (3.189)):

$$2\int_0^1 u_0(\eta)\eta d\eta + 2bk\int_0^1 u_0(\eta)\eta d\eta + 2ak\int_0^1 u_0(\eta)\eta^2 d\eta = 1 \tag{3.197}$$

or

$$b = -2a\int_0^1 u_0(\eta)\eta^2 d\eta, \tag{3.198}$$

where we accounted for the fact that (see property 6 at $\omega_0 = 1$ ($i = 1$) in Table 3.3)

$$2\int_0^1 u_0(\eta)\eta d\eta = 1 \tag{3.199}$$

and we neglect the terms of second order with respect to k.

Finally, it follows:

$$b = -\frac{2\delta}{1 - g\omega_0}, \tag{3.200}$$

where we accounted for the fact that $a = (1 - g\omega_0)^{-1}$ and

$$\delta = \int_0^1 u_0(\eta)\eta^2 d\eta \tag{3.201}$$

is the second moment of the escape function. Therefore, one finally derives:

$$u(\eta) = \left(1 - \frac{2\delta k}{1 - g\omega_0}\right) u_0(\eta). \tag{3.202}$$

This equation allows to find the constant N as $k \to 0$. Namely, it follows from property 8 in Table 3.3:

$$N = 2\int_{-1}^{1} d\eta u_0(\eta) \left\{1 - \frac{2\delta k}{1 - g\omega_0}\right\} \left\{1 - \frac{k\eta}{1 - g\omega_0}\right\} \tag{3.203}$$

or

$$N = 1 - \frac{3\delta k}{2(1 - g\omega_0)}, \tag{3.204}$$

where we neglected terms of the second order with respect to k. We can also write:

$$N = 1 - \frac{3\sqrt{3}s\delta}{2}. \tag{3.205}$$

Note that due to the reciprocity principle functions $u_0(\mu)$ enter asymptotic formulae in the combination: $F(\eta, \xi) = Mu(\eta)u(\xi)$. This means that one can use the following approximation valid as $k \to 0$ (see Eq. (3.191)):

$$F(\eta, \xi) = \frac{8s}{\sqrt{3}} u_0(\eta)u_0(\xi). \tag{3.206}$$

3.6.3.3 The reflection function of a semi-infinite layer $R_\infty(\xi, \eta)$

The last point in our derivations of asymptotics as $\omega_0 \to 1$ is the derivation of the weak absorption approximation for the reflection function of a semi-infinite medium $R_\infty(\xi, \eta)$. This will be done in two steps.

Step 1.
The expression for a plane albedo of a semi-infinite medium is written by a definition as

$$r_d(\xi) = 2\int_0^1 R_\infty(\xi, \eta)\eta d\eta. \tag{3.207}$$

We will use the following expansion of $R_\infty(\xi, \eta)$ with respect to k:

$$R_\infty(\xi, \eta) = R_{0\infty}(\xi, \eta) - kR_{1\infty}(\xi, \eta), \tag{3.208}$$

where $R_{1\infty}(\xi, \eta)$ is the function we need to derive. The minus signifies the fact that $R_\infty(\xi, \eta) \leq R_{0\infty}(\xi, \eta)$ due to reduction of reflection by absorption processes. One can see that

$$r_d(\xi) = 1 - kJ(\xi), \tag{3.209}$$

where

$$J(\xi) = 2\int_0^1 R_1(\xi, \eta)\eta d\eta \tag{3.210}$$

and we used the property:

$$2\int_0^1 R_{0\infty}(\xi, \eta)\eta d\eta = 1. \tag{3.211}$$

Eq. (3.211) follows from Eq. (3.207) and the fact that $r_d = 1$ at $\omega_0 = 1$.

Step 2.
We derive now the asymptotic equation for $r_d(\xi)$ as $k \to 0$ using other set of equations. This will allow us to give a relationship between $J(\xi)$ and $u_0(\xi)$. We start from the following equation derived above (see property 4 in Table 3.3):

$$i(-\xi) = 2\int_0^1 i(\eta)R_\infty(\xi, \eta)\eta d\eta. \tag{3.212}$$

Substituting expansions with respect to k and ignore high-order terms, we obtain:

$$1 - \frac{k\xi}{1 - g\omega_0} = 2\int_0^1 \left(1 + \frac{k\eta}{1 - g\omega_0}\right)(R_{0\infty}(\xi, \eta) - kR_{1\infty}(\xi, \eta))\eta d\eta. \tag{3.213}$$

This means that

$$1 - \frac{k\xi}{1 - g\omega_0} = 1 - kJ + \frac{2k}{1 - g\omega_0}\int_0^1 R_{0\infty}(\xi, \eta)\eta^2 d\eta \tag{3.214}$$

or

$$-\frac{\xi}{1 - g\omega_0} = -J + \frac{2}{1 - g\omega_0}\int_0^1 R_{0\infty}(\xi, \eta)\eta^2 d\eta, \tag{3.215}$$

where [see Eq. (3.209)]

$$J = \frac{1 - r_d(\xi)}{k}. \tag{3.216}$$

This means that

$$(1 - g\omega_0)(1 - r_d(\xi))k^{-1} = 2\int_0^1 R_{0\infty}(\xi, \eta)\eta^2 d\eta + \xi \tag{3.217}$$

or

$$r_d(\xi) = 1 - \frac{k}{1 - g\omega_0}\left\{\xi + 2\int_0^1 R_{0\infty}(\xi, \eta)\eta^2 d\eta\right\}. \tag{3.218}$$

On the other hand, we have (see property 5 in Table 3.3):

$$i(\xi) = Mu(\xi) + 2\int_0^1 i(-\eta)R_\infty(\xi,\eta)\eta d\eta \tag{3.219}$$

or as $k \to 0$:

$$1+\frac{k\xi}{1-g\omega_0}=\frac{8ku_0(\xi)}{3(1-g\omega_0)}+2\int_0^1\left(1-\frac{k\eta}{1-g\omega_0}\right)(R_{0\infty}(\xi,\eta)-kR_{1\infty}(\xi,\eta))\eta d\eta. \tag{3.220}$$

This means that

$$\frac{k\xi}{1-g} = \frac{8ku_0(\xi)}{3(1-g)} - \frac{2k}{1-g}\int_0^1 R_{0\infty}(\xi,\eta)\eta^2 d\eta - kJ(\xi) \tag{3.221}$$

or

$$\xi = \frac{8}{3}u_0(\xi) - 2\int_0^1 R_{0\infty}(\xi,\eta)\eta^2 d\eta - (1-g\omega_0)J(\xi). \tag{3.222}$$

We remind that (see Eq. (3.216))

$$J(\xi) = 2\int_0^1 R_{1\infty}(\xi,\eta)\eta d\eta = (1-r_d(\xi))k^{-1}. \tag{3.223}$$

Therefore, it follows:

$$(1-r_d(\xi))k^{-1} = (1-g\omega_0)^{-1}\left(\xi + 2\int_0^1 R_{0\infty}(\xi,\eta)\eta^2 d\eta\right) \tag{3.224}$$

and

$$J(\xi) = (1-g)^{-1}\left(\xi + 2\int_0^1 R_{0\infty}(\xi,\eta)\eta^2 d\eta\right) \tag{3.225}$$

or (see Eq. (3.222) and Eq. (3.225))

$$\xi = \frac{8u_0(\xi)}{3} - \xi - 4\int_0^1 R_{0\infty}(\xi,\eta)\eta^2 d\eta \tag{3.226}$$

and

$$\frac{8u_0(\xi)}{3} = 2\xi + 4\int_0^1 R_{0\infty}(\xi,\eta)\eta^2 d\eta. \tag{3.227}$$

This allows us to derive the following important relationship:

$$u_0(\xi) = \frac{3}{4}\left[\xi + 2\int_0^1 R_{0\infty}(\xi,\eta)\eta^2 d\eta\right]. \tag{3.228}$$

Comparing this formula with Eq. (3.224), we obtain:

$$r_d(\xi) = 1 - \frac{4ku_0(\xi)}{3(1-g\omega_0)}. \tag{3.229}$$

But also we derived:

$$r_d(\xi) = 1 - kJ(\xi). \tag{3.230}$$

This means that

$$J(\xi) = 2\int_0^1 R_{1\infty}(\xi, \eta)\eta d\eta = \frac{4u_0(\xi)}{3(1 - g\omega_0)}. \tag{3.231}$$

Due to the reciprocity principle, the function $R_{1\infty}(\xi, \eta)$ must be symmetric with respect to the pair (ξ, η). Therefore, it follows:

$$R_{1\infty}(\xi, \eta) = cu_0(\xi)u_0(\eta). \tag{3.232}$$

Substituting this formula in Eq. (3.231) given above, we derive for the constant c:

$$c = \frac{4}{3(1 - g\omega_0)}, \tag{3.233}$$

where we used the property 11 in Table 3.3

$$2\int_0^1 u_0(\eta)\eta d\eta = 1. \tag{3.234}$$

Finally, we have:

$$R_\infty(\xi, \eta) = R_{0\infty}(\xi, \eta) - \frac{4k}{3(1 - g\omega_0)}u_0(\xi)u_0(\eta) \tag{3.235}$$

or

$$R_\infty(\xi, \eta) = R_{0\infty}(\xi, \eta) - 4su_0(\xi)u_0(\eta). \tag{3.236}$$

This also means that the spherical albedo (see Table 3.1)

$$r = 1 - \frac{4}{\sqrt{3}}s \tag{3.237}$$

and

$$r_d(\xi) = 1 - \frac{4}{\sqrt{3}}su_0(\xi). \tag{3.238}$$

Main asymptotic equations valid as $k \to 0$ are given in Table 3.4. It follows that R and T in the case of weak absorption can be easily calculated if the functions $u_0(\xi)$ and $R_{0\infty}(\xi, \eta)$ are known. Moreover, Eq. (3.228) can be used to find $u_0(\xi)$ from $R_{0\infty}(\xi, \eta)$.

The choice of the normalization condition for the function $u(\xi)$ (and also for $i(\xi)$ and derived parameters like M) is arbitrary. We followed notations of Sobolev (1975). They differ from corresponding equations used by van de Hulst (1980). For

Table 3.4. Asymptotic equations valid as $k \to 0$ $\left(\delta = \int_0^1 u_0(\xi)\xi^2 d\xi, s = \sqrt{\frac{1-\omega_0}{1-g\omega_0}}\right)$.

$R_\infty(\xi, \eta, \varphi)$	$R_{0\infty}(\xi, \eta, \varphi) - \dfrac{4k}{3(1-g\omega_0)} u_0(\xi)u_0(\eta)$
$u(\xi)$	$\left(1 - \dfrac{2\delta k}{(1-g\omega_0)}\right) u_0(\xi)$
M	$\dfrac{8k}{3(1-g\omega_0)}$
N	$1 - \dfrac{\delta k}{1-g}$
$Mu(\xi)u(\eta)$	$\dfrac{8k}{3(1-g\omega_0)} u_0(\xi)u_0(\eta)$
k	$\sqrt{3(1-\omega_0)(1-g\omega_0)}$
r	$1 - 4s/\sqrt{3}$
$r_d(\xi)$	$1 - 4su_0(\xi)/\sqrt{3}$

instance, van de Hulst's diffusion pattern $P(\xi)$ must be divided by ω_0 to yield $i(\xi)$. His escape function $K(\xi)$ must be multiplied by ω_0 to yield $u(\xi)$, and his Mequals to that used by Sobolev multiplied by ω_0^2. These differences do not lead to any extra factors in main equations. However, they must be remembered. Clearly, all differences between normalizations disappear for the case of nonabsorbing clouds. This case will be considered in the next Section.

3.6.4 Nonabsorbing Optically Thick Clouds

3.6.4.1 Main equations

Let us assume that there is no absorption in the medium (e.g., water clouds in the visible). Then it follows using Table 3.4 and Eqs. (3.152) and (3.153):

$$R(\xi, \eta, \varphi) = R_{0\infty}(\xi, \eta, \varphi) - tu_0(\xi)u_0(\xi) \tag{3.239}$$

and

$$T(\xi, \eta) = tu_0(\xi)u_0(\xi), \tag{3.240}$$

where we accounted for the fact that the transmittance of a thick cloud layer does not depend on the azimuth φ and

$$t = \frac{1}{\alpha + 0.75(1-g)\tau}, \tag{3.241}$$

where $\alpha = 3\delta$. The plane albedo $r_d(\xi)$, the spherical albedo r, the diffuse transmittance $t_d(\xi)$ and the global transmittance t are given as (see Table 3.1)

$$r_d(\xi) = 2\int_0^1 R(\xi, \eta)\eta d\eta, \tag{3.242}$$

$$r = 2\int_0^1 r_d(\xi)\xi d\xi, \tag{3.243}$$

$$t_d(\xi) = 2\int_0^1 T(\xi, \eta)\eta d\eta, \tag{3.244}$$

$$t = 2\int_0^1 t_d(\xi)\xi d\xi. \tag{3.245}$$

This allows to derive the following analytical relationships:

$$r_d(\xi) = 1 - tu_0(\xi), r = 1 - t, t_d(\xi) = tu_0(\xi) \tag{3.246}$$

and also confirm that t given by Eq. (3.241) coincides with the global transmittance. It follows that the calculation of reflection and transmission functions of optically thick nonabsorbing cloud layers is reduced to the calculation of the reflection function of a semi-infinite nonabsorbing cloud $R_{0\infty}(\xi, \eta, \varphi)$. The functions $u_0(\xi)$ can be calculated from Eq.(3.228) and the parameter α is defined as

$$\alpha = 3\int_0^1 u_0(\eta)\eta^2 d\eta. \tag{3.247}$$

We will show later that $\alpha \approx 1.07$ independent of the phase function (Kokhanovsky et al., 2004a). The function $R_{0\infty}(\xi, \eta, \varphi)$ can be derived from the numerical solution of the corresponding integral equation (Ambartsumian, 1943).

In the next section we introduce useful approximations for $R_{0\infty}(\xi, \eta, \varphi)$ and also for $u_0(\xi)$. The important property of these functions is the fact that they do not depend on the pair (ω_0, τ) and that they are completely determined by the phase function. Moreover, the dependence on the phase function is rather weak because functions $u_0(\xi)$, $R_{0\infty}(\xi, \eta, \varphi)$ are related to the problems involving light diffusion in semi-infinite nonabsorbing media. So multiple light scattering is quite important in this case. It leads to the averaging of the scattering features characteristic for a single-scattering event. This also means that a good starting point for the derivation of approximate solutions for $u_0(\xi)$, $R_{0\infty}(\xi, \eta, \varphi)$ valid at arbitrary g is the case of $g = 0$ (isotropic scattering).

3.6.4.2 Auxiliary functions

We start the consideration of auxiliary functions from the well studied case of isotropic scattering. Then the nonlinear integral equation for the reflection function of a nonabsorbing semi-infinite medium can be presented in the following form (Ambartsumian, 1943):

$$R_{0\infty}(\xi,\eta)=\frac{1+2\xi\int_0^1 R_{0\infty}(\eta,\eta')d\eta'+2\eta\int_0^1 R_{0\infty}(\xi,\eta')d\eta'+G(\xi,\eta)}{4(\xi+\eta)}, \tag{3.248}$$

where

$$G(\xi,\eta)=4\xi\eta\int_0^1\int_0^1 R_{0\infty}(\xi,\eta')R_{0\infty}(\eta,\eta'')d\eta'd\eta''. \tag{3.249}$$

The inspection of this equation shows that it can be reduced to the following more simple form:

$$R_{0\infty}(\xi,\eta)=\frac{H(\xi)H(\eta)}{4(\xi+\eta)} \tag{3.250}$$

with

$$H(\xi)=1+2\xi\int_0^1 R_{0\infty}(\xi,\eta')d\eta'. \tag{3.251}$$

The last two equations allow to formulate the integral equation for the function $H(\xi)$:

$$H(\xi)=1+0.5\xi H(\xi)\int_0^1\frac{H(\eta)}{\xi+\eta}d\eta. \tag{3.252}$$

It follows immediately: $H(0)=1.0$. Numerical calculations show that the function $H(\xi)$ can be approximated by the linear function [$H(\xi)=1+2\xi$ (see Fig. 3.5)]. The substitution of this linear approximation into the expression for $R_{0\infty}(\xi,\eta)$ gives:

$$R_{0\infty}(\xi,\eta)=\frac{1+2(\xi+\eta)+4\xi\eta}{4(\xi+\eta)}. \tag{3.253}$$

This is a rather accurate approximation of the reality in the isotropic scattering case. Further, we note that the value of $R_{0\infty}(\xi,\eta)$ can be separated in two parts:

$$R_{0\infty}(\xi,\eta)=R^s_{0\infty}(\xi,\eta)+R^m_{0\infty}(\xi,\eta), \tag{3.254}$$

where the first term is due to single scattering [$R^s_{0\infty}(\xi,\eta)=0.25(\xi+\eta)^{-1}$, see Eq. (3.62) at $p=1,\ \omega_0=1,\ \tau_0\to\infty$] and the second one ($R^m_{0\infty}(\xi,\eta)=[0.5+\xi\eta(\xi+\eta)^{-1}]$) is due to multiple light scattering.

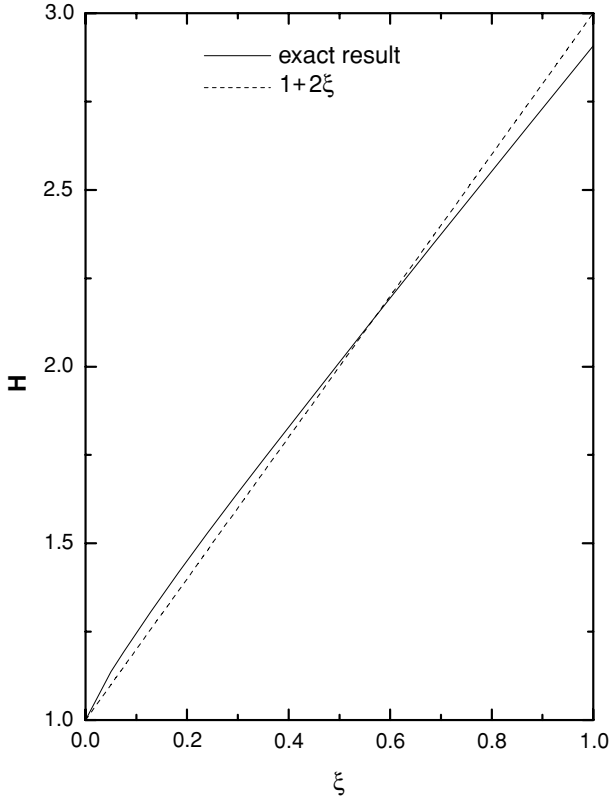

Fig. 3.5. Dependence of the H-function on the cosine of incidence angle using exact calculations and approximation $H(\xi) = 1 + 2\xi$.

We make the same separation for the anisotropic ($g \neq 0$) scattering case. Then we have:

$$R^s_{0\infty}(\xi, \eta) = 0.25 p(\theta)(\xi + \eta)^{-1} \tag{3.255}$$

and we assume that it holds for anisotropic multiple light scattering:

$$R^m_{0\infty}(\xi, \eta) = \frac{A + B(\xi + \eta) + C\xi\eta}{4(\xi + \eta)}, \tag{3.256}$$

where A, B and C are constants to be determined. There are different ways to get these constants. In particular integral relationships involving the function $R_{0\infty}(\xi, \eta)$ can be used.

They can be also found using the following fitting technique. The function $R_{0\infty}(\xi, \eta, \varphi)$ is calculated using the exact radiative transfer equation and then functions $\Xi(\xi, \eta, \varphi) = 4(\xi + \eta)\tilde{R}_{0\infty}(\xi, \eta, \varphi)$, where $\tilde{R}_{0\infty}(\xi, \eta, \varphi) =$

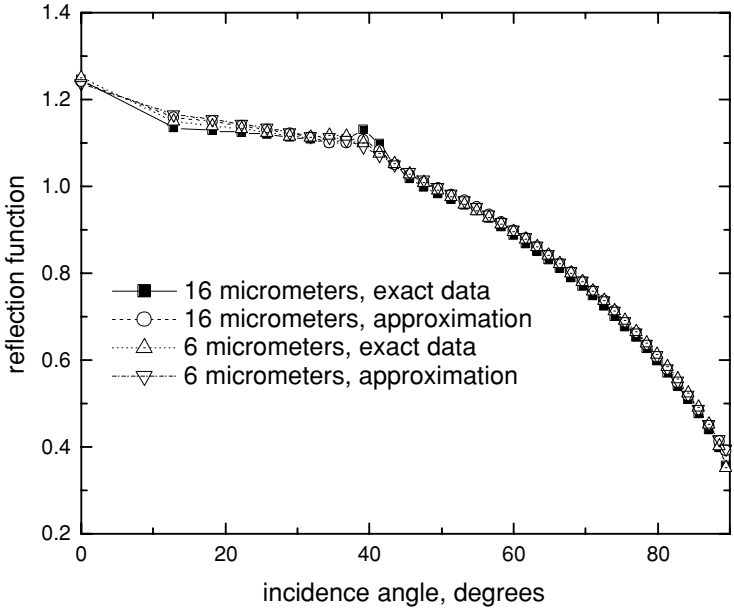

Fig. 3.6. Dependence of reflection function at the nadir observation of a semi-infinite cloud on the solar zenith angle at $a_{ef} = 4,\ 16$ μm and $\lambda = 0.55$ μm. The gamma PSD with $\mu = 6$ was used in calculations. Results both exact and approximate calculations are shown.

$R_{0\infty}(\xi, \eta, \varphi) - R^s_{0\infty}(\xi, \eta, \varphi)$, are fitted by linear functions of the argument assuming, e.g., $\eta = 1$.This technique gives: $A = 3.944$, $B = -2.5$, $C = 10.664$ for water clouds, and $A = 1.247$, $B = 1.186$, $C = 5.157$ for ice clouds as discussed by Kokhanovsky (2004b, 2005). The results of numerical calculations of $R_{0\infty}(\xi, \eta, \varphi)$ are given in Fig. 3.6. It follows that the reflection function of clouds having different values of a_{ef} almost coincide at $\omega_0 = 1$ [although phase functions do depend on the size of particles (see Fig. 3.7)]. Note that the shape of particles has some influence on functions $R_{0\infty}(\xi, \eta, \varphi)$ as shown in Fig. 3.8.

The next point is to derive the corresponding equation for the function $u_0(\xi)$. This can be done in the following way.

It was shown above that the following relationship holds:

$$u_0(\xi) = \frac{3}{4}\left[\xi + 2\int_0^1 R_{0\infty}(\xi, \eta)\eta^2 d\eta\right]. \tag{3.257}$$

Let us substitute $R_{0\infty}(\xi, \eta)$ for the isotropic case in this equation. Then it follows:

$$u_0(\xi) = \frac{3}{4}\left[\xi + \frac{1}{2}\int_0^1 \frac{H(\xi)H(\eta)}{\xi + \eta}\eta^2 d\eta\right]. \tag{3.258}$$

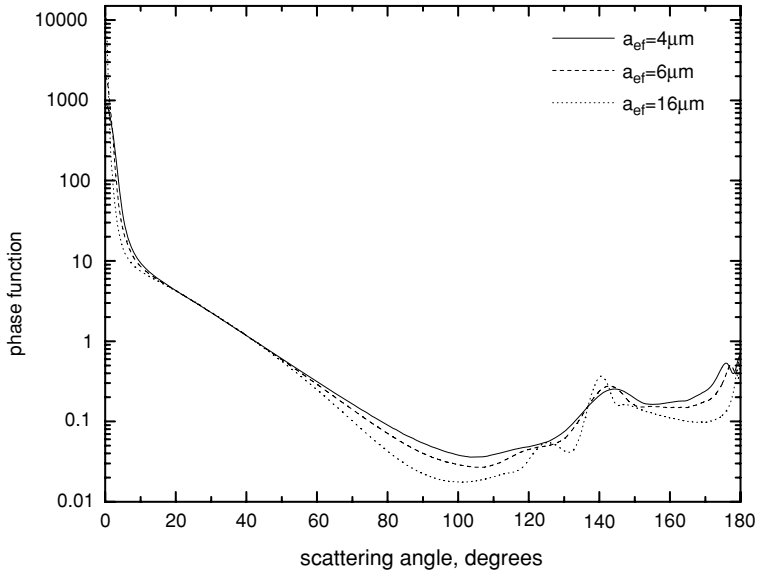

Fig. 3.7. Dependence of the cloud phase function on the effective size of water droplets at $\lambda = 0.55$ μm. The gamma PSD with $\mu = 6$ was used in calculations.

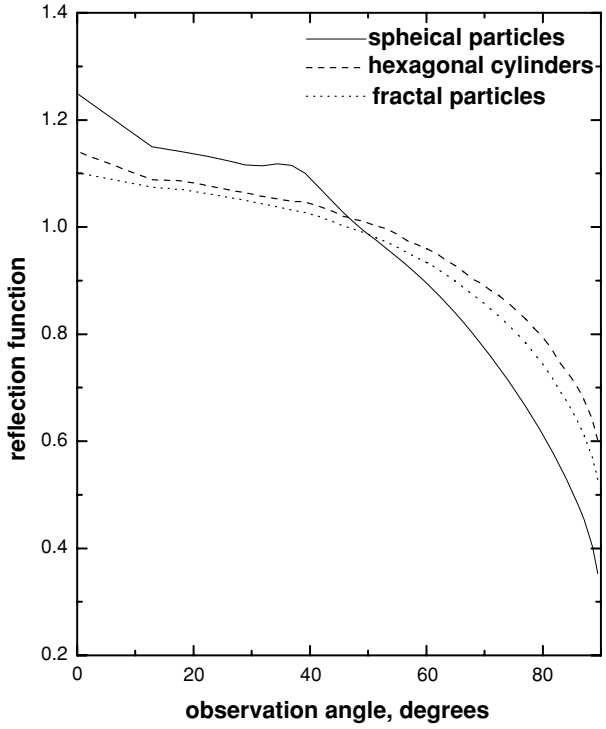

Fig. 3.8. Dependence of reflection function at the nadir observation of a semi-infinite cloud on the solar zenith angle for spherical particles (gamma PSD, $a_{ef} = 6$ μm, $\mu = 6$), hexagonal randomly oriented ice cylinders with aspect ratio 1.0 and ice fractal particles calculated using exact radiative transfer code (Mishchenko et al., 1999) at $\lambda = 0.55$ μm.

We can represent $H(\eta)\eta(\xi+\eta)^{-1}$ as $H(\eta)(1-\xi(\xi+\eta)^{-1})$. So we have:

$$u_0(\xi)=\frac{3}{4}\left[\xi+\frac{1}{2}H(\xi)\int_0^1 H(\eta)\eta d\eta-\frac{H(\xi)\xi}{2}\int_0^1\frac{H(\eta)}{\xi+\eta}\eta d\eta\right]. \tag{3.259}$$

This can be written as

$$u_0(\xi)=\frac{3}{4}\left[\xi+\frac{1}{2}\mathrm{C}H(\xi)-\Psi\xi\right], \tag{3.260}$$

where

$$\mathbb{C}=\int_0^1 H(\eta)\eta d\eta \tag{3.261}$$

and (see Eq. (3.250))

$$\Psi=2\int_0^1 R_{0\infty}(\xi,\eta)\eta d\eta. \tag{3.262}$$

But we have, due to property 11 (see also property 4) in Table 3.3 (the conservation energy law): $\Psi=1$ and

$$u_0(\xi)=\frac{3\mathrm{C}}{8}H(\xi). \tag{3.263}$$

This means that the function $u_0(\xi)$ is proportional to $H(\xi)$. The constant $\mathbb{C}$ can easily be derived for the isotropic scattering. For this we multiply the last equation by 2ξ and integrate with respect to ξ. Then it follows:

$$\mathbb{C}=\frac{2}{\sqrt{3}}, \tag{3.264}$$

where we used normalization conditions. Therefore, we establish an important relationship:

$$u_0(\xi)=\frac{\sqrt{3}}{4}H(\xi). \tag{3.265}$$

Surprisingly, two completely separate radiative transfer problems [for the determination of $H(\xi)$ and $u_0(\xi)$] have shown themselves to be interrelated in the case under study. This important theoretical result, valid for isotropic scattering allows to derive approximate equations for $u_0(\xi)$ just using the corresponding equations for $H(\xi)$. A number of parameterizations and approximations can be derived in such a way.

We will use the fact that $H(\xi)$ is well approximated by the function $1+2\xi$ (see Fig. 3.5). Then it follows:

$$u_0(\xi)=\mathbb{Q}(1+2\xi), \tag{3.266}$$

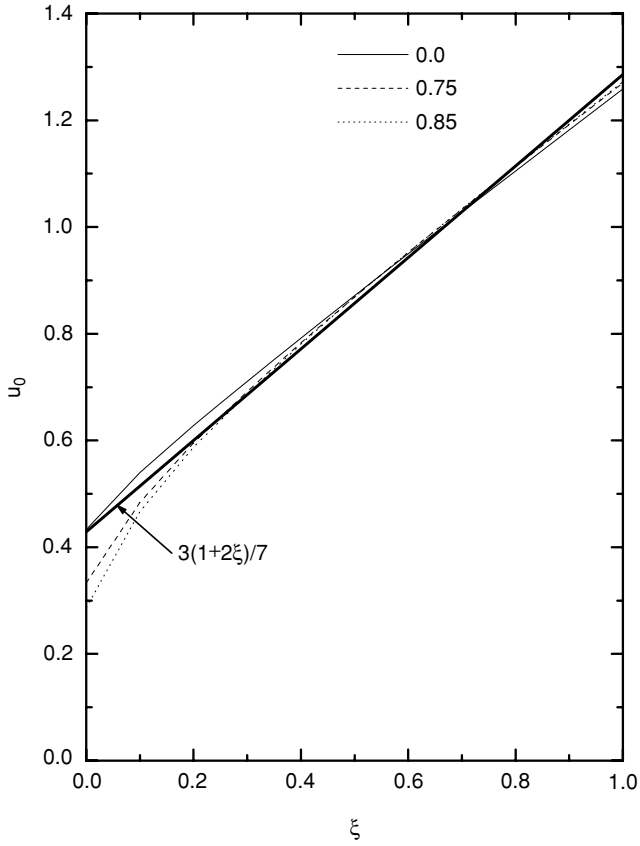

Fig. 3.9. Dependence of the escape function on the cosine of the zenith observation angle at g = 0, 0.75, and 0.85. Results of calculations obtained using the approximation $u_0(\xi) = 3(1 + 2\xi)/7$ are also shown.

where $\mathbb{Q} = \sqrt{3}/4 \approx 3/7$. We use the approximate equality (the error is under 1%) here to satisfy the normalization condition (see property 11 in Table 3.3). So finally, we have:

$$u_0(\xi) = \frac{3}{7}(1 + 2\xi). \tag{3.267}$$

Although this result is strictly valid only for isotropic scattering, we find that the error of this approximation is below 2% at $\xi \geq 0.2$ (see Fig. 3.9). This also allows to derive the value of $\delta = 15/42$ (see property 9 in Table 3.3). Therefore, one can use for α [see Eq. (3.247)]:$\alpha \equiv 3\delta \approx 1.07$. This completes our derivations for the nonabsorbing case.

3.6.5 Exponential Approximation

3.6.5.1 Statistical physics approach

Asymptotic solutions for weak absorption derived above allow for the consideration of the influence of light absorption on cloud radiative characteristics for small values of the probability of photon absorption $\beta = 1 - \omega_0$, if correspondent characteristics are known for the nonabsorbing case. The results are limited to a very narrow range of β (typically, $\beta \leq 0.001$). There are two possibilities to avoid this problem. One is related to the derivation of higher order corrections to the results given in Table 3.4 (generally, following the same path as described above).

Yet another approach is based on the exponential approximation often used in the diffusion theory. To demonstrate this technique, we represent the spherical albedo as a series with respect to ω_0 :

$$r(\omega_0) = \sum_{n=1}^{\infty} a_n \omega_0^n, \tag{3.268}$$

where

$$r(\omega_0) = 2 \int_0^1 r_d(\xi) \xi d\xi. \tag{3.269}$$

with

$$r(1) = \sum_{n=1}^{\infty} a_n. \tag{3.270}$$

However, it also follows by the definition: $r(1) = 1$, which is due to the energy conservation law. Thus, one obtains that

$$\sum_{n=1}^{\infty} a_n = 1 \tag{3.271}$$

and numbers a_n can be interpreted in terms of the probability theory. Such an approach is often used in statistical physics. In particular, the value of a_1 gives us the probability that a photon will be singly scattered before escaping a cloud. The probabilities of scattering events $a_1, a_2, a_3, \ldots$ do not depend on each other. The theorem of adding independent probabilities brings us to Eq. (3.268) as well. Let us substitute the following exact expansion in Eq. (3.268):

$$\omega_0^n \equiv (1 - \beta)^n = \sum_{j=0}^{n} (-1)^j \binom{n}{j} \beta^j, \tag{3.272}$$

where

$$\binom{n}{j} \equiv \frac{n!}{j!(n-j)!}. \tag{3.273}$$

Then it follows from Eq. (3.268):

$$r(\beta) = \sum_{n=1}^{\infty} a_n \sum_{j=0}^{n} (-1)^j \binom{n}{j} \beta^j \tag{3.274}$$

or in the explicit form:

$$r(\beta) = \sum_{n=1}^{\infty} a_n \left[1 - \beta n + \frac{\beta^2 n(n-1)}{2} - \frac{\beta^3 n(n-1)(n-2)}{6} + \dots\right], \tag{3.275}$$

where we accounted for equalities:

$$\binom{n}{0} = 1, \binom{n}{1} = n, \binom{n}{2} = \frac{n(n-1)}{2}, \binom{n}{3} = \frac{n(n-1)(n-2)}{6}. \tag{3.276}$$

Equation (3.275) can be rewritten in the following form:

$$r = 1 - \beta\bar{n} + \frac{\beta^2 \overline{n(n-1)}}{2} - \frac{\beta^3 \overline{n(n-1)(n-2)}}{6} + \dots, \tag{3.277}$$

where we used the normalization condition (3.271) and defined the following averages:

$$\bar{n} = \sum_{n=1}^{\infty} n a_n, \overline{n(n-1)} = \sum_{n=1}^{\infty} n(n-1) a_n, \overline{n(n-1)(n-2)} = \sum_{n=1}^{\infty} n(n-1)(n-2) a_n. \tag{3.278}$$

and so on. Here $\bar{n}$ is the average number of scattering events in the medium.

Equation (3.277) is an exact formula. We did not make any approximations so far. Now we should make some assumptions to have a possibility to sum series in Eq. (3.277). First of all, we assume that the value of $\bar{n}$ is large and, consequently, $\overline{n(n-1)} \approx \overline{n^2}$, $\overline{n(n-1)(n-2)} = \overline{n^3}$ and so on. Clearly, such an approximation is valid as $\beta \to 0$ only. This gives us instead of Eq. (3.277):

$$r = 1 - \beta\overline{n} + \frac{\beta^2}{2}\overline{n^2} - \frac{\beta^3}{6}\overline{n^3} + \dots \tag{3.279}$$

or

$$r = \overline{\exp(-\beta n)}, \tag{3.280}$$

where we used the expansion

$$\exp(-\beta n) = \sum_{k=0}^{\infty} \frac{(-1)^k (\beta n)^k}{k!}. \tag{3.281}$$

Thus, the value of r is given by

$$r = \sum_{n=1}^{\infty} \exp(-\beta n) a_n. \tag{3.282}$$

Applying the sum formula

$$\sum_{n=1}^{\infty} f(n) = \int_0^{\infty} f(x) dx, \tag{3.283}$$

we have:

$$r = \int_0^{\infty} \exp(-\beta x) a(x) dx. \tag{3.284}$$

It follows from the mean value theorem:

$$r = \exp(-\beta \overline{x}). \tag{3.285}$$

We also used the integral form of the normalization condition (3.271):

$$\int_0^{\infty} a(x) dx = 1. \tag{3.286}$$

We did not specify any specific laws of a scattering event in the derivation of Eq. (3.277). Thus, Eq. (3.285) can be applied in a much broader context than just scattering of light by particles in clouds. The comparison of Eqs. (3.277) and (3.285) shows us that $\bar{x} \to \bar{n}$ as $\beta \to 0$. However, generally speaking, $\bar{x} \neq \bar{n}$. This is due to the differences $\sigma_2 = \overline{n^2} - \bar{n}^2$, $\sigma_3 = \overline{n^3} - \bar{n}^3$ and so on, which are not necessary to be exact zeros.

The problem we face now is the determination of the parameter $\bar{x}$. For this we will use the well-known asymptotic result of the radiative transfer theory derived above (see Table 3.4):

$$r = 1 - \sqrt{\frac{16\beta}{3(1-g)}}, \tag{3.287}$$

which is valid as $\beta \to 0$.

Eq. (3.285) takes the following form as $\beta \to 0$:

$$r = 1 - \beta \overline{x}. \tag{3.288}$$

So, comparing Eqs. (3.287) and (3.288) we have

$$\overline{x} = \frac{4}{k}, \tag{3.289}$$

where $k = \sqrt{3(1 - g\omega_0)\beta}$ is the diffusion exponent of the radiative transfer theory. Therefore, it follows:

$$r = \exp\left(-4\sqrt{\frac{1-\omega_0}{3(1-g\omega_0)}}\right). \tag{3.290}$$

We notice that the combination of local optical characteristics, given by

$$y = 4\sqrt{\frac{1-\omega_0}{3(1-g)}} \tag{3.291}$$

completely determines the spherical albedo. The value of $y = 4s/\sqrt{3}$ can be also measured experimentally ($y = \ln(1/r)$).

By analogy, relationships similar to Eq. (3.290) must be valid also for other asymptotic parameters. This allows to derive the following relationships using Table 3.4 (Zege et al., 1991):

$$R_\infty(\xi, \eta, \varphi) = R_{0\infty}(\xi, \eta, \varphi)\exp(-yu_0(\xi)u_0(\eta)R_{0\infty}^{-1}(\xi, \eta, \varphi)), \tag{3.292.a}$$

$$r_{d\infty}(\xi) = \exp(-yu_0(\xi)), \tag{3.292.b}$$

$$M = 1 - \exp(-8k/(3(1 - g\omega_0)), \quad N = \exp(-3\delta k/2(1 - g\omega_0)), \tag{3.292.c}$$

$$Mu(\xi)u(\eta) = (1 - \exp(-8k/3(1 - g\omega_0)))u_0(\xi)u_0(\eta). \tag{3.292.d}$$

We obtain using these relationships:

$$R(\xi, \eta, \varphi) = R_{0\infty}\exp(-yu(\xi, \eta, \varphi)) - t\ \exp(-x - y)u_0(\xi)u_0(\eta), \tag{3.293}$$

$$T(\xi, \eta) = tu_0(\xi)u_0(\eta), \tag{3.294}$$

where we introduced a new parameter $x = k\tau$, $u(\xi, \eta, \varphi) = u_0(\xi)u_0(\eta)\,/\,R_{0\infty}(\xi, \eta, \varphi)$. The global transmittance t is given by:

$$t = \frac{\sinh y}{\sinh(\alpha y + x)}. \tag{3.295}$$

We can also derive the analytical results for the plane and spherical albedos and the diffuse transmittance. Corresponding equations are summarized in Table 3.5.

Equation (3.293) transforms into Eq. (3.239) [and also Eq. (3.294) transforms into Eq. (3.240)] as $\beta = 0$. However, Eq. (3.292a) unlike Eq. (3.239) allows to consider absorbing media as well. It is important that no new angular functions arise in Eq. (3.292a) as compared to Eq. (3.239). This is in contrast with Eq. (3.152), where

Table 3.5. Radiative transfer characteristics in the framework of the exponential approximation ($r_{d\infty}(\xi) = \exp(-yu_0(\xi))$, $u_0(\xi) = \frac{3}{7}(1 + 2\xi)$, $r_\infty = e^{-y}$, $x = k\tau$, $y = k\tau$, $k = \sqrt{3(1-\omega_0)(1-g\omega_0)}$, $\alpha = 1.07$).

Radiative characteristic	Symbol	Equation
Plane albedo	$r_d(\xi)$	$r_{d\infty}(\xi) - (r_\infty - r)u_0(\xi)$
Spherical albedo	r	$r_\infty - t\exp(-x-y)$
Diffuse transmittance	$t_d(\xi)$	$tu_0(\xi)$
Global transmittance	t	$\dfrac{\sinh(y)}{\sinh(x+\alpha y)}$

parameters and functions have an implicit and complex dependence on the probability of photon absorption, β. Equation (3.293) can be used for the rapid estimations of light reflection from cloudy media and also for the speeding up cloud retrieval algorithms (Kokhanovsky et al., 2003).

The range of applicability of the exponential approximation (3.293) with respect to cloud optical thickness can be extended using correction terms derived from the numerical solution of the radiative transfer equation. In particular, we find that the accuracy of Eq. (3.293) for cloudy media can be increased using the following substitutions: $u \to u\ (1 - 0.05y)$ (in the argument of the exponent in Eq. 3.293), $t \to t - \Delta$, where

$$\Delta = \frac{a + b\mu\xi + c\mu^2\mu_0^2}{\tau^3}\exp(x) \tag{3.296}$$

and $a = 4.86$, $b = -13.08$, $c = 12.76$. Therefore, the final equation for the cloud reflection function can be written as

$$R(\eta,\xi,\varphi,\tau) = R_{0\infty}\exp(-y(1-0.05y)u(\eta,\xi,\varphi)) - (t-\Delta)\exp(-x-y) \times u_0(\eta)u_0(\xi). \tag{3.297}$$

Equation (3.297) is called the Modified Exponential Approximation (MEA). We show the accuracy of the MEA given by Eq. (3.297) in Figs. 3.10 and 3.11 for the nadir observation conditions, the solar zenith angle 60° and wavelengths 865 and 2130 nm. These wavelengths are often used in cloud retrieval techniques. Note that the single-scattering albedo is equal to 1.0 and 0.9872 at these wavelengths, respectively. The asymmetry parameter is 0.8435 for the smaller wavelength. It is 0.8054 for the wavelength 2130 nm. Exact data shown in Fig. 3.10 are obtained using the vector radiative transfer code based on the discrete ordinate approach and thoroughly tested against tabular results presented by Siewert (2000). It follows that the accuracy of the approximation is better than 6% for the cloud optical thickness $\tau \geq 4$ in the case considered.

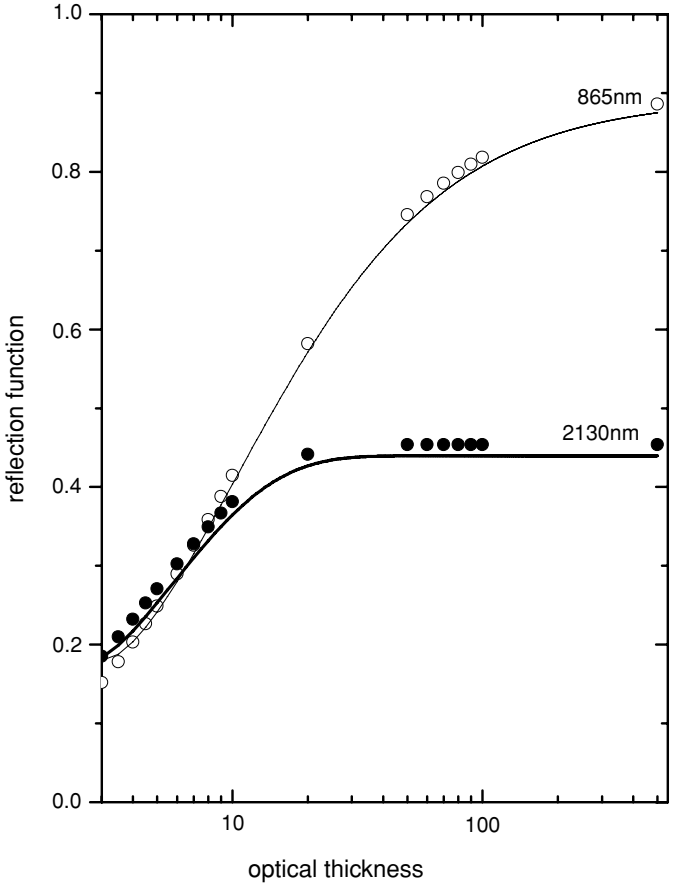

Fig. 3.10. Dependence of reflection function on the optical thickness at wavelengths 865 and 2130 nm calculated using the Cloud C1 PSD model. Solid lines give the approximate results according to exponential approximation and points are obtained solving the exact radiative transfer equation using SCIATRAN (Rozanov et al., 2005).

Calculations performed for other angles and cloud optical thicknesses show (see Figs. 3.12–3.18) that the accuracy only weakly depends on the geometry, providing that grazing observation and illumination conditions are excluded (Kokhanovsky and Rozanov, 2003). It means that the top-of-atmosphere reflectance over cloudy scenes can be accurately modelled in the framework of the MEA (even as compared to the vector radiative transfer model). It follows from Fig. 3.11 that the accuracy of the MEA could be increased if the exact result for the reflection function of a semi-infinite layer is used in calculations. Note that we used in Eq. (3.297) the following simple formula valid for the nadir observation conditions only (Kokhanovsky,

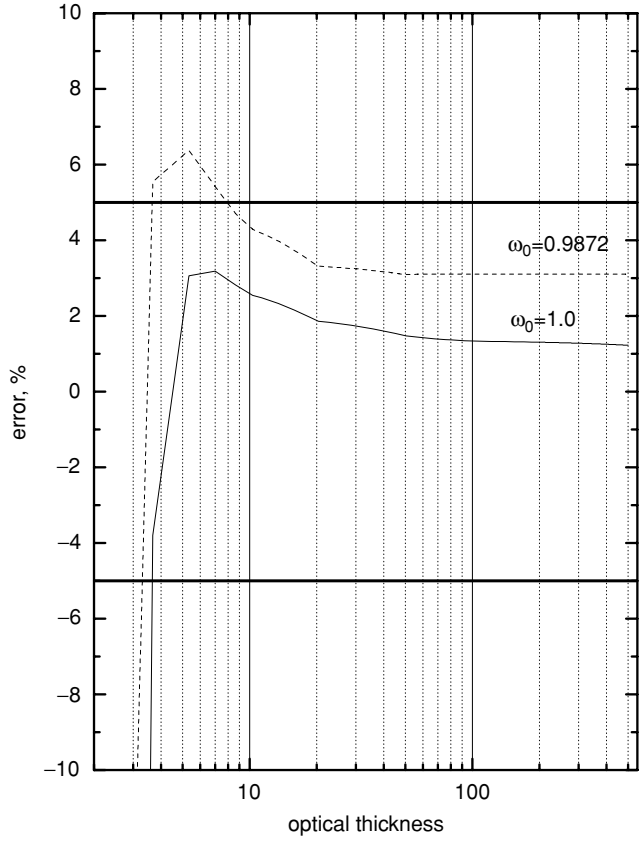

Fig. 3.11. Errors of exponential approximation calculated using data shown in Fig. 3.10. Upper curve corresponds to the wavelength 2130 nm, where single-scattering albedo is equal to 0.9872. Lower curve corresponds to a nonabsorbing cloud at $\lambda = 865$ nm.

2002):

$$R_{0\infty}(\eta, \xi, \varphi) = \frac{0.37 + 1.94\xi}{1 + \xi}. \tag{3.298}$$

The accuracy of Eq. (3.298) can be further increased adding the function $F = 0.25p(1 - \arccos(\mu_0))$ to the nominator.

The analysis of Figs. 3.12–3.18 shows that the exponential approximation is applicable for $\tau \geq 5$ and most solar angles for the nadir observation. Also these figures show main dependencies related to light reflection from cloud media, like the increase in reflection with τ (see Fig. 3.12) and a high sensitivity of reflectances in the infrared to the size of particles (see Fig. 3.17). This sensitivity is almost negligible in the visible (see Fig. 3.12).

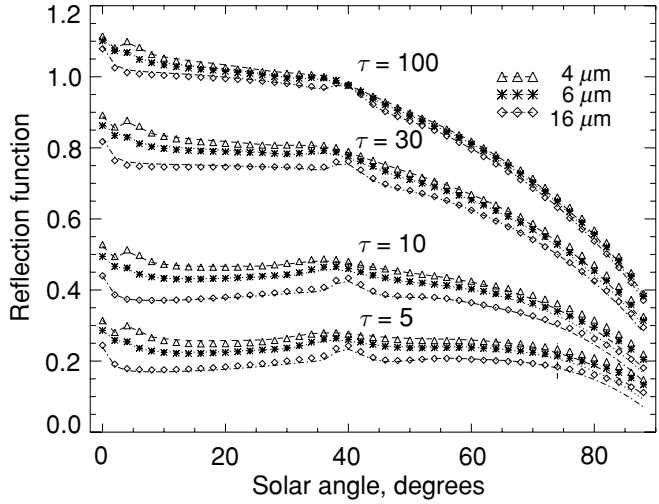

Fig. 3.12. Dependence of cloud reflection on the solar zenith angle at $\tau = 5, 10, 30, 100$ and $a_{ef} = 4, 6, 16$ μm (the gamma PSD with $\mu = 6$) for nadir observations. Symbols show exact calculations and lines are obtained using the approximate result at $\lambda = 0.55$ μm.

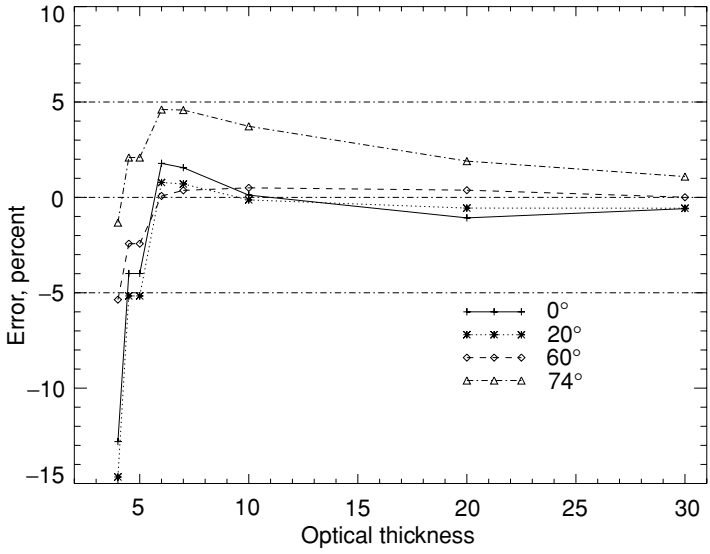

Fig. 3.13. Relative errors of the approximation as functions of the optical thickness for several solar zenith angles calculated using data shown in Fig. 3.12 at $a_{ef} = 6$ μm.

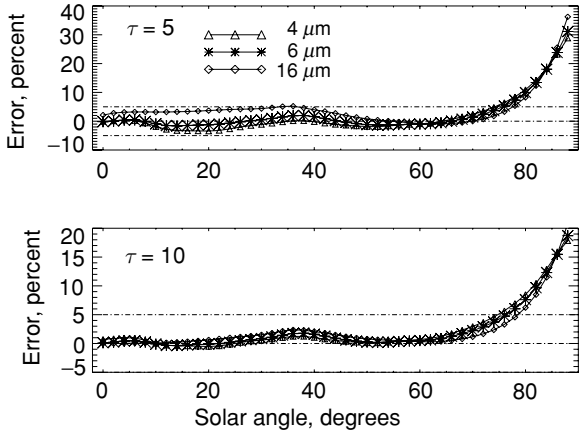

Fig. 3.14. Relative errors of the approximation as functions of the solar zenith angle at the optical thickness 5 and 10 and $a_{ef} = 4,\ 6,\ 16$ μm calculated using data shown in Fig. 3.12.

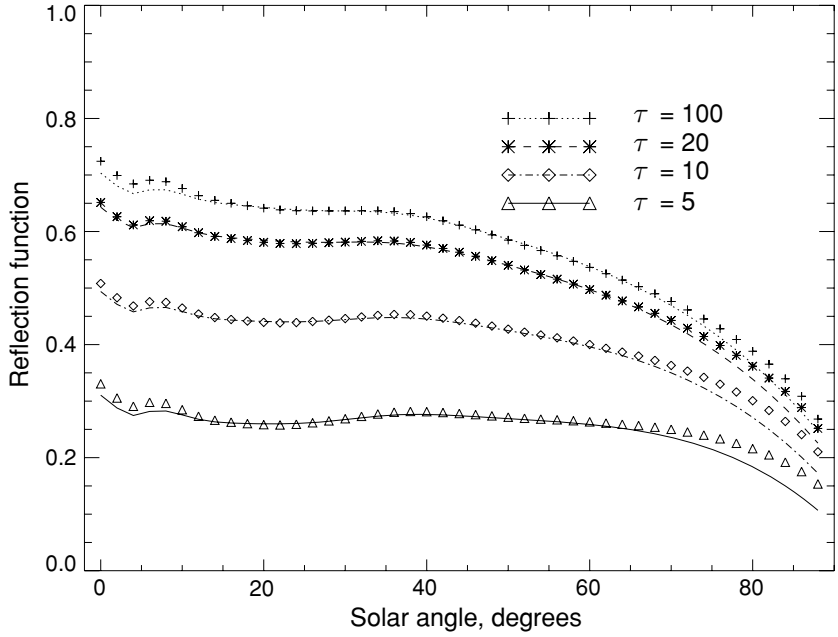

Fig. 3.15. Dependence of cloud reflection on the solar zenith angle at $\tau = 5, 10, 20, 100$ and $a_{ef} = 6$ (the gamma PSD with $\mu = 6$) for nadir observations at $\lambda = 1.55$ μm. Symbols show exact calculations and lines are obtained using the approximate result.

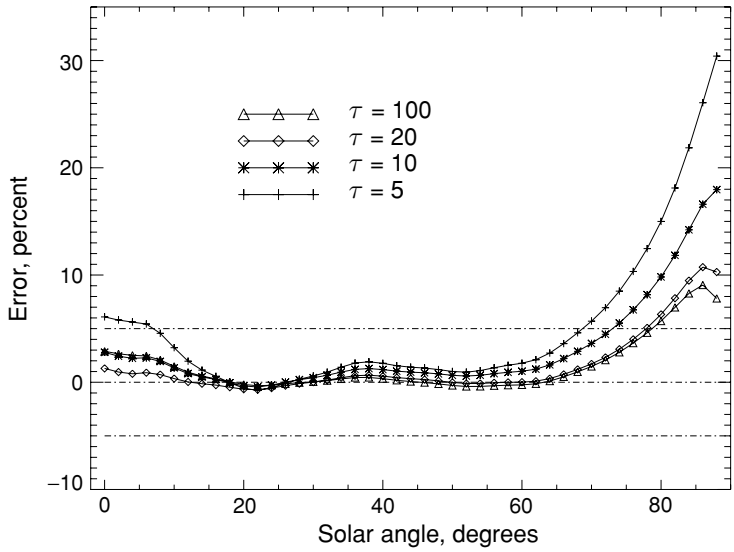

Fig. 3.16. Relative errors of the approximation as functions of the solar zenith angle at the optical thickness 5, 10, 20, and 100 and $a_{ef} = 6$ μm calculated using data shown in Fig. 3.15.

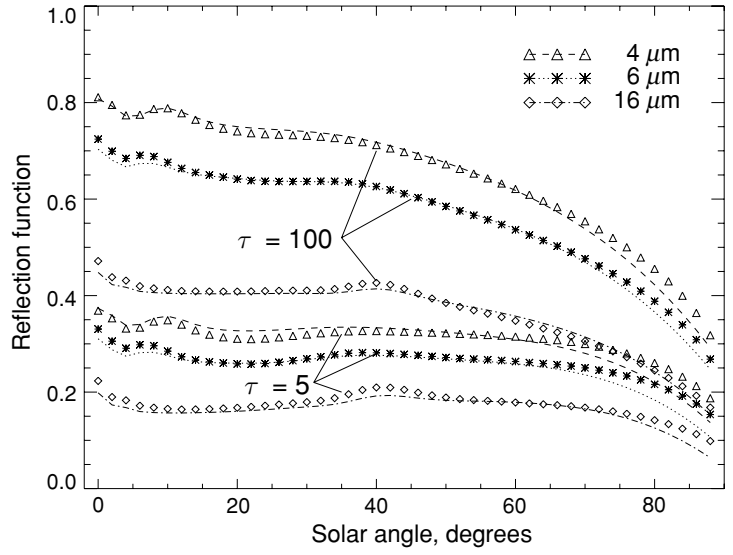

Fig. 3.17. Dependence of cloud reflection on the solar zenith angle at $\tau = 5,\ 100$ and $a_{ef} = 4,\ 6,\ 16$ μm (the gamma PSD with $\mu = 6$) for nadir observations at $\lambda = 1.55$ μm. Symbols show exact calculations and lines are obtained using the approximate result.

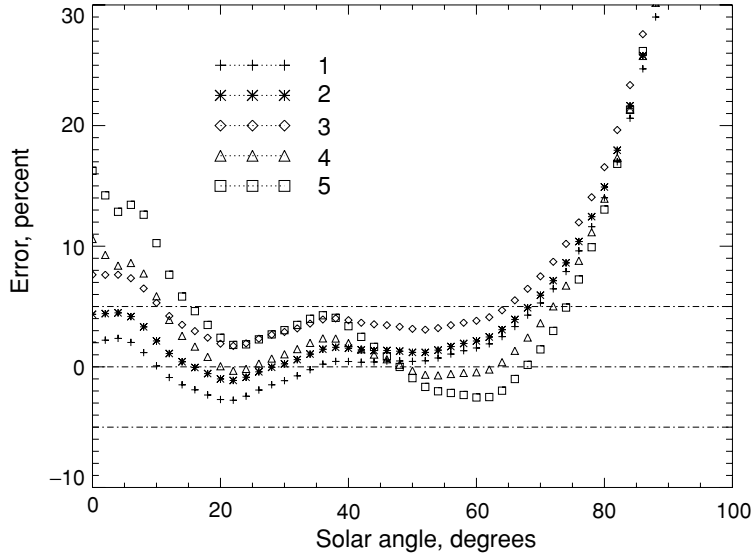

Fig. 3.18. Errors of the approximation at various values of the single-scattering albedo as functions of the solar zenith angle at the nadir observation and $\tau = 5$. The curves 1–5 were obtained using phase functions and single-scattering albedos derived from the Mie theory for the C1 PSD at the wavelength 1.55 μm assuming that the refractive index is equal to $1.3109 - i\chi$ with $\chi = 0.00001(1),\ 0.00005(2),\ 0.0001(3),\ 0.0005(4)$, and $0.001(5)$. The values of $\beta = 1 - \omega_0$ were equal to 0.0005(1), 0.0034(2), 0.0047(3), 0.0226(4), and 0.0435(5).

3.6.5.2 The radiative transfer in the gaseous absorption band

The exponential approximation presented above can be easily extended to account for the gaseous absorption. Then one should use the following substitutions in equations given above: $\tau \to \tau + \tau_g,\ \beta \to (\sigma_{abs} + \sigma_{abs,g})/(\sigma_{ext} + \sigma_{abs,g})$, where the subscript '$g$' relates the correspondent value to the gaseous absorption process. The phase function does not need to be modified because we ignore molecular scattering. This could easily be accounted for if necessary. However, we account for the additional light absorption in the atmosphere above a cloud. Therefore, it follows for the cloud reflection function $\bar{R}$ in the gaseous absorption band: $\bar{R} = T_1 R T_2$, where we omitted arguments for the sake of simplicity. The value of R is given by Eq. (3.297) and $T_j = \exp(-m_j \tau_{abs})$, $j = 1, 2$, where $m_1 = 1/\xi$, $m_2 = 1/\eta$, and

$$\tau_{abs} = \sum_{i=1}^{N} \int_{z_1}^{z_2} C_{abs,i}(z) \varsigma_i(z) dz, \tag{3.299}$$

where $C_{abs,i}$ is the ith gas absorption cross section, N is the total number of gases present and $\varsigma_i(z)$ is the concentration of the ith gas at a given height. The integration extends from the upper cloud boundary position z_1 to the height of the optical instrument z_2. The accuracy of the MEA for the gaseous absorption band can be increased if the single-scattering contribution in the signal from the

atmospheric layer above the cloud R_s (Kokhanovsky and Rozanov, 2004) is also taken into account. Then it follows:

$$\bar{R} = T_1 R T_2 + R_s \tag{3.300}$$

We checked the accuracy of Eq. (3.300) by performing exact calculations using the radiative transfer code SCIATRAN (Rozanov et al., 2005) for the oxygen absorption A-band located at wavelengths 758–768 nm. The atmospheric model used in calculations coincides with that described by Kokhanovsky and Rozanov (2004). The values of $\bar{R}$ are averaged with respect to the Gaussian instrument response function with the half-width of 0.225 nm. The absorption by the oxygen was accounted for by using the HITRAN 2000 (Rothman et al., 2003) database in conjunction with the correlated k-distribution approximation (Kokhanovsky and Rozanov, 2004). To increase the accuracy of the model, we accounted for light scattering and absorption below the cloud layer using the approximate technique developed by Kokhanovsky and Rozanov (2004). Results are given in Fig. 3.19

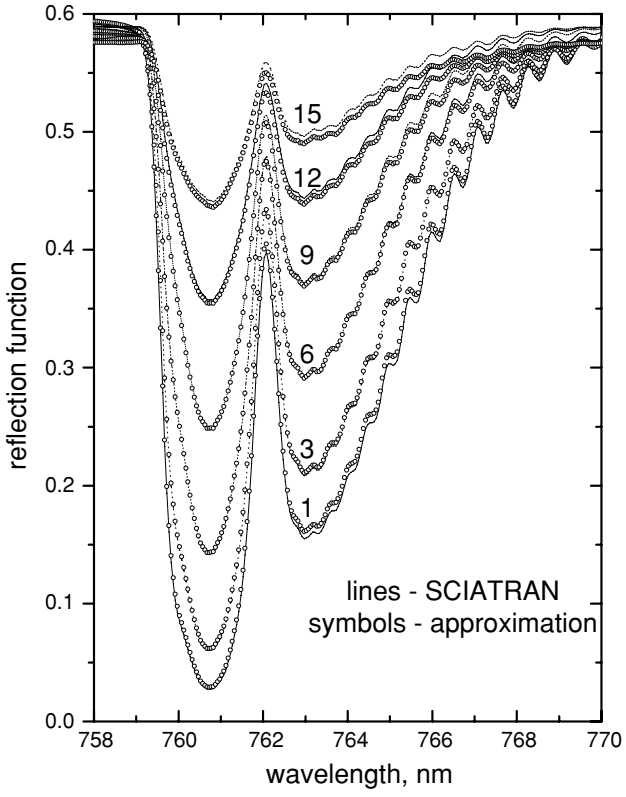

Fig. 3.19. Oxygen A-band cloud reflectance spectrum calculated using the approximate theory and SCIATRAN solver at $\tau = 20$, the cloud geometrical thickness equal to 1 km and the cloud top altitudes 1, 3, 6, 9, 12, and 15 km for the nadir observation and the solar zenith angle 60°.

for different cloud top heights. It follows from the analysis of the data presented that the accuracy of approximate calculations is better than 5% (see Fig. 3.20) in most cases. The errors increase for low clouds having larger values of τ due to the simplicity of our model, which accounts for the cloud – upper atmospheric layer interaction in a first coarse approximation only (Kokhanovsky and Rozanov, 2004). This interaction becomes more important for lower thick clouds (see Fig. 3.20).

The parameterization developed here is useful for cloud top altitudes retrievals from airborne and satellite-based optical sensors. We see that the depth of the oxygen A-band depends on cloud altitude. Although other gaseous absorption bands (see Fig. 3.21) can be used for this purpose, the vertical distribution of the gaseous concentration must be known in advance. This is a difficult task, e.g., for water vapour, which has a lot of absorption bands in the optical range. However, unlike oxygen, this gas does not belong to the category of well-mixed gases with stable vertical profiles and concentrations.

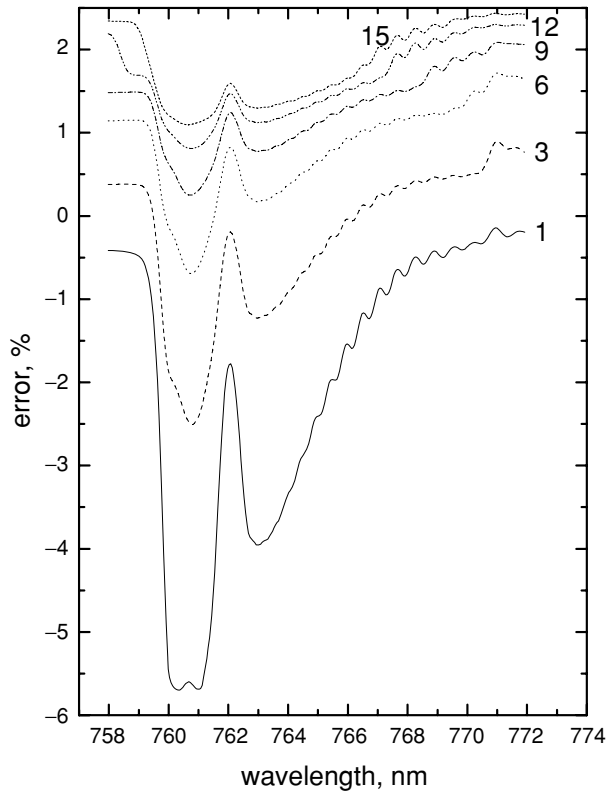

Fig. 3.20. Relative errors of the approximation obtained using Fig. 3.18.

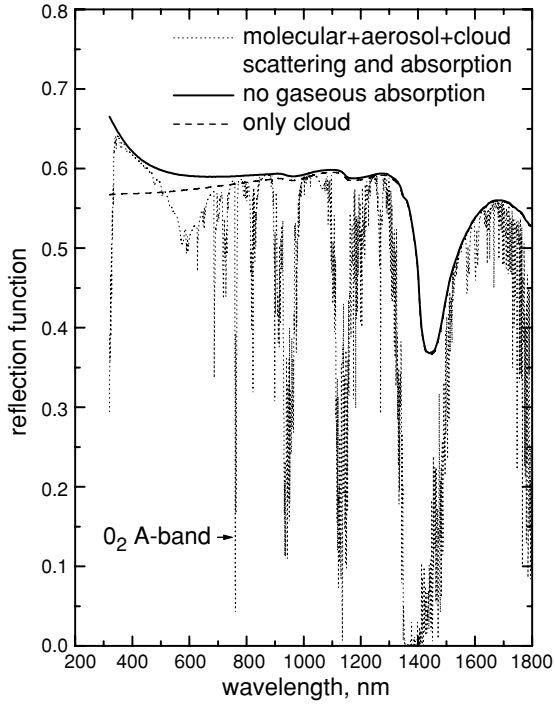

Fig. 3.21. The cloud reflection function calculated with SCIATRAN (Rozanov et al., 2005) accounting for molecular and aerosol scattering and absorption using forward model described by Kokhanovsky and Rozanov (2004) at the nadir observation, the solar incidence angle 60°, and $\tau = 20$. Results of calculations for the artificial case with no gaseous absorption are also shown. Dashed line corresponds to the artificial case, when only cloud presents in atmosphere. Rayleigh scattering enhances the reflection function at short wavelengths. The decrease in the reflection function (dashed line) in UV is due to the gaseous absorption.

Note that approximations for optically thick layers discussed here are of great importance for cloud optics, because such clouds are very common (see Fig. 3.22).

3.6.6 Polarization of Light by Optically Thick Clouds

Equations for optically thick clouds presented in the previous section can be generalized to account for polarization. Corresponding equations for azimuthally averaged reflection $\hat{R}$ and transmission $\hat{T}$ matrices were obtained by Domke (1978a,b). They have the following forms for isotropic symmetric light scattering media:

$$\hat{R}(\xi, \eta) = \hat{R}_\infty(\xi, \eta) - N\hat{T}(\xi, \eta)\exp(-k\tau), \tag{3.301}$$

$$\hat{T}(\xi, \eta) = \frac{M\exp(-k\tau)}{1 - N^2\exp(-2k\tau)}\vec{K}(\eta)\vec{K}^T(\xi), \tag{3.302}$$

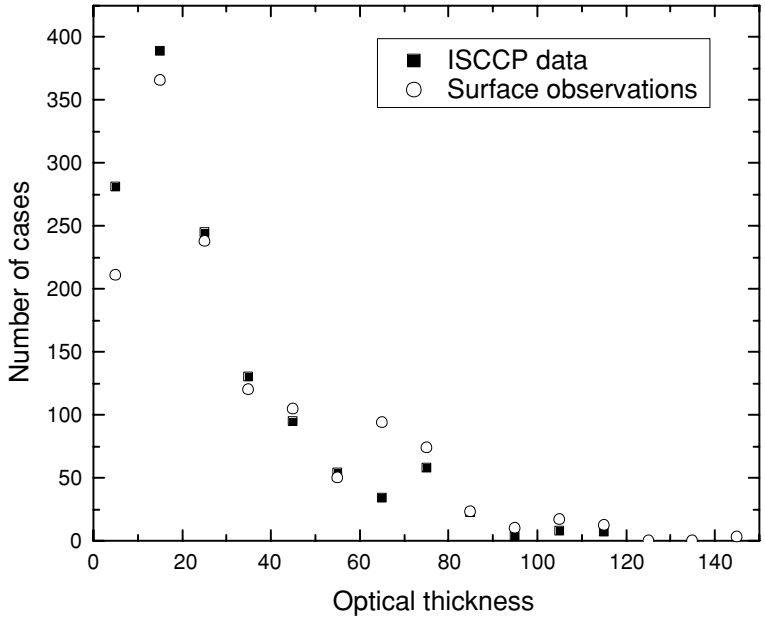

Fig. 3.22. Frequency of a given cloud optical thickness as observed using ground and satellite observations. (Trishchenko and Liu, 2001)

where only two-dimensional matrices and vectors are involved. Other components of generally four-dimensional matrices and vectors vanish due the azimuthal averaging. Note that this is also the case for a normal illumination of the scattering layer. Then the azimuth does not enter theory at all. Here $\hat{R}_\infty(\xi, \eta)$ is the azimuthally averaged reflection matrix of a semi-infinite medium with the same optical characteristics as a finite slab under study. One can also introduce the vector $\vec{\mathrm{K}}(\mu)$, which describes the intensity and degree of light polarization in deep layers of a semi-infinite scattering medium (in a so-called asymptotic regime, when the intensity and polarization angular distributions are symmetrical with respect to the normal to a scattering layer and exponentially decrease with the depth $\sim \exp(-k\tau)$). Functions $\hat{R}_\infty(\xi, \eta)$ and $\vec{\mathrm{K}}(\eta)$ determine all parameters in the equations given above. The explicit equations for their calculation are discussed by Domke (1978a,b).

We see, therefore, that intensity and polarization characteristics of reflected and transmitted light for optically thick turbid media are determined by the reflection matrix of a semi-infinite layer and the angular distribution of the light intensity and polarization in deep layers of the same medium. This reduction of a problem for a finite optical thick slab to the case of a semi-infinite medium is of a general importance for the radiative transfer theory. Note that the matrix $\hat{R}_\infty$ and vector $\vec{\mathrm{K}}$ are obtained from solutions of the well-known integral equations, which can be found elsewhere (van de Hulst, 1980; de Rooij, 1985).

Equations (3.301) and (3.302) are valid only for the azimuthally averaged matrices. In practice, however, measurements are performed for a fixed azimuth. The transmission matrix is azimuthally independent in the case of optically thick layers. The azimuthal dependence in the reflected light disappears in some specific cases (e.g., for the case of normal illumination of an isotropic light scattering plane-parallel slabs).

Equations (3.301) and (3.302) are simplified for nonabsorbing media. Then it follows:

$$\hat{R}(\xi, \eta) = \hat{R}_{0\infty}(\xi, \eta) - \hat{T}(\xi, \eta), \tag{3.303}$$

$$\hat{T}(\xi, \eta) = \frac{4}{3(\tau + 2q_0)(1 - g)} \vec{K}_0(\xi)\vec{K}_0^T(\eta), \tag{3.304}$$

where

$$q_0 = \frac{2}{1 - g} \int_0^1 d\eta \eta^2 \vec{K}_0^T(\eta)\vec{j}. \tag{3.305}$$

Here

$$\vec{j} = \begin{pmatrix} 1 \\ 0 \end{pmatrix} \tag{3.306}$$

is the unity vector,

$$g = \frac{1}{4} \int_0^\pi p(\theta) \sin 2\theta d\theta \tag{3.307}$$

is the asymmetry parameter,

$$\vec{K}_0(\eta) = \frac{3}{4} \left[\eta + 2 \int_0^1 d\xi \xi^2 \hat{R}_{0\infty}(\xi, \eta) \right] \vec{j} \tag{3.308}$$

and $\hat{R}_{0\infty}(\mu, \mu_0)$ is the azimuthally averaged reflection matrix of a semi-infinite nonabsorbing medium. This matrix is completely determined by the phase matrix $\hat{P}$, introduced above. It does not depend on the single-scattering albedo and optical thickness by definition. Clearly, the first component of the vector $\vec{K}_0$ coincides with the escape function u_0 discussed above.

Eqs. (3.301), (3.302) are simple in form. However, they can be used only if auxiliary functions and parameters are known. Their calculations, however, can be quite a complex procedure.

However, it appears that for weakly absorbing media, when single-scattering albedo $\omega_0 = \sigma_{sca}/\sigma_{ext}$ is close to one, simplifications are possible. Then it follows (Kokhanovsky, 2003a,b):

$$\hat{R}(\xi, \eta) = \hat{R}_{0\infty}(\xi, \eta) \exp(-y\hat{D}(\xi, \eta)) - \hat{T}(\xi, \eta) \exp(-x - y), \tag{3.309}$$

$$\hat{T}(\xi, \eta) = t\vec{K}_0(\xi)\vec{K}_0^T(\eta). \tag{3.310}$$

where

$$x = k\tau,\ y = 4\sqrt{\frac{1-\omega_0}{3(1-g\omega_0)}},\ k = \sqrt{3(1-\omega_0)(1-g\omega_0)},$$
$$\hat{D}(\xi,\eta) = \hat{R}_{0\infty}^{-1}(\xi,\eta)\vec{K}_0(\xi)\vec{K}_0(\eta),$$

$t = \dfrac{\sinh y}{\sinh(x+\alpha y)}$ is the global transmittance of a scattering layer, $\alpha = \frac{1}{2}\int_0^1 u_0(\eta)\eta^2 d\eta \approx 1.07$ and $\hat{R}_{0\infty}(\mu,\mu_0)$ is the reflection matrix of a semi-infinite nonabsorbing layer with the same phase matrix as an absorbing layer of a finite thickness under study. The two-dimensional vector $\vec{K}_0(\mu)$ describes the polarization and intensity of light in the Milne problem for nonabsorbing semi-infinite media (Wauben, 1992). The components $K_{01}(\mu)$ and $K_{02}(\mu)$ of this vector were calculated by Chandrasekhar (1950) for Rayeigh particles ($g = 0$) and by Wauben (1992) for spherical particles with the refractive index $n = 1.44$ and the gamma particle size distribution (1.5) with $\mu = 11.3, a_0 = 0.83$ μm. The wavelength λ was equal to 0.55 μm. Note, that the model of spheres with $\mu = 11.3, r_0 = 0.83$ μm and $n = 1.44$ is generally used to characterize particles in clouds on Venus (Hansen and Hovenier, 1974). It follows for the effective size a_{ef}, the effective variance Δ_{ef}, and the asymmetry parameter g, respectively, in this case: $a_{ef} = 1.05$ μm, $\Delta_{ef} = 0.07$ μm, $g = 0.718$. It was found that the ratio $p_l = -K_{02}/K_{01}$, which gives the degree of polarization for transmitted light is very low. It changes from zero to 1.2% while the escape angle changes from 0 till 90°. Note that for Rayleigh scattering we have a change from 0 till 11.7% for the same conditions. This means that light transmitted by thick clouds is almost unpolarized. It is possible to understand this on general grounds. Indeed, the polarization of unpolarized solar light occurs due to single-scattering events. Multiple light scattering leads to an increase of entropy and the reduction of initial polarization arising in single-scattering events.

Note that the ellipticity is equal to zero in this case and that $P_l \le 0$, which means that light is polarized in the plane perpendicular to the meridional plane.

Formulae (3.309) and (3.310) can be simplified for nonabsorbing media (y= 0):

$$\hat{R}(\xi,\eta) = \hat{R}_{0\infty}(\xi,\eta) - \hat{T}(\xi,\eta), \tag{3.311}$$
$$\hat{T}(\xi,\eta) = t\vec{K}_0(\xi)\vec{K}_0^T(\eta), \tag{3.312}$$

where

$$t = \frac{1}{\alpha + \frac{3}{4}\tau(1-g)} \tag{3.313}$$

is the global transmittance.

Let us apply Eq. (3.311) to a particular problem, namely, to the derivation of a relation between the spherical albedo $r = 1 - t$ and the degree of polarization of reflected light $p_l(\eta)$ at the illumination along the normal to the scattering layer

($\xi = 1$) by a wide, unidirectional unpolarized light beam. The value of $p_l(\mu)$ is given simply by $-R_{21}(1, \mu)/R_{11}(1, \mu)$ in this case. Thus, it follows from Eq. (3.311):

$$p_l(\eta) = \frac{p_{l\infty}(\eta)}{1 - (1 - r)\mathrm{N}(\eta)}, \tag{3.314}$$

where

$$\mathrm{N}(\eta) = \frac{u_0(1)u_0(\eta)}{R_{0\infty}(1, \mu)} \tag{3.315}$$

$$p_{l\infty}(\eta) = -\frac{R_{\infty 21}(1, \eta)}{R_{\infty}(1, \eta)} \tag{3.316}$$

and we accounted for the equality: $K_{02}(1) = 0$.

Our calculations show that the value of $\mathrm{N}(\eta)$ is close to 1 for most of observation angles, which implies the inverse proportionality between the brightness of a turbid medium and the degree of polarization of reflected light ($r p_l \approx p_{l\infty}$). The accuracy of Eq. (3.314) is shown in Fig. 3.23.

This inverse proportionality between the spherical albedo r and the degree of polarization p_l was discovered experimentally by Umow (1905). Equation (3.314) can be considered as a manifestation of this important law, which has important applications in reflectance spectroscopy (Hapke,1993).

Equation (3.314) is easily generalized to account for the absorption of light in a medium using the exponential approximation described above. Namely, it follows:

$$p_l(\eta) = \frac{p^*_{l\infty}(\eta)}{1 - \mathrm{N}^*(\eta)t \exp(-x - y)}, \tag{3.317}$$

where

$$t = \frac{\sinh y}{\sinh(x + \alpha y)} \tag{3.318}$$

and

$$\mathrm{N}^*(\eta) = \frac{u_0(1)u_0(\eta)}{R^*_{\infty}(1, \eta)}. \tag{3.319}$$

Values of $p^*_{l\infty}(\eta)$ and $R^*_{\infty}(1, \eta)$ represent the degree of polarization and reflection function of a semi-infinite weakly absorbing medium at the nadir illumination. Note, that Eq. (3.317) can be written in the following form:

$$p_1(\eta) = c(\eta, \tau)p^*_{l\infty}(\eta), \tag{3.320}$$

where

$$c(\eta, \tau) = \frac{1}{1 - \mathrm{N}^*(\eta)t \exp(-x - y)} \tag{3.321}$$

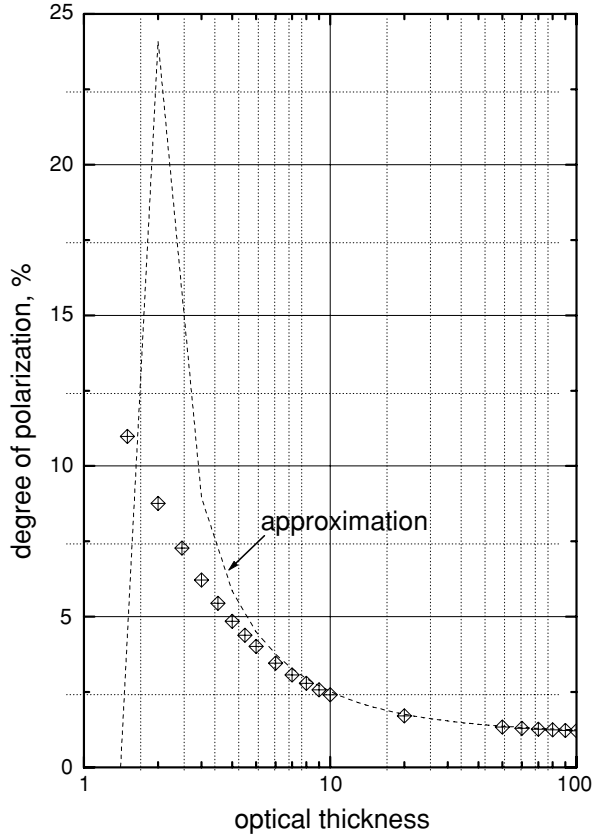

Fig. 3.23. Degree of linear polarization of light reflected from a cloudy atmosphere as the function of the cloud optical thickness at $a_{ef} = 6\mu$m (the gamma PSD with $\mu = 6$) for nadir observations at $\lambda = 0.55\mu$m. The solar zenith angle is equal to 60°. Both exact (symbols) and approximate (lines) results are shown.

can be interpreted as the polarization enhancement factor, which is solely due to a finite cloud depth. It follows for semi-infinite layers that the transmittance t is equal to zero and $c = 1$ as it should be. Also it follows from Eq. (3.320) that zeroes of polarization curves for semi-infinite and optically thick finite layers almost coincide, which is supported by numerical calculations with the radiative transfer code (see Fig. 3.24). This is due to the fact that the function $\mathrm{N}^*(\eta)$ only weakly depends on the angle.

Multiple light scattering fails to produce the polarization of incident unpolarized light. It only diminishes the polarization of singly scattered light. Thus, the angles where polarization is equal to zero for semi-infinite layers are almost equal to those for the case of single light scattering.

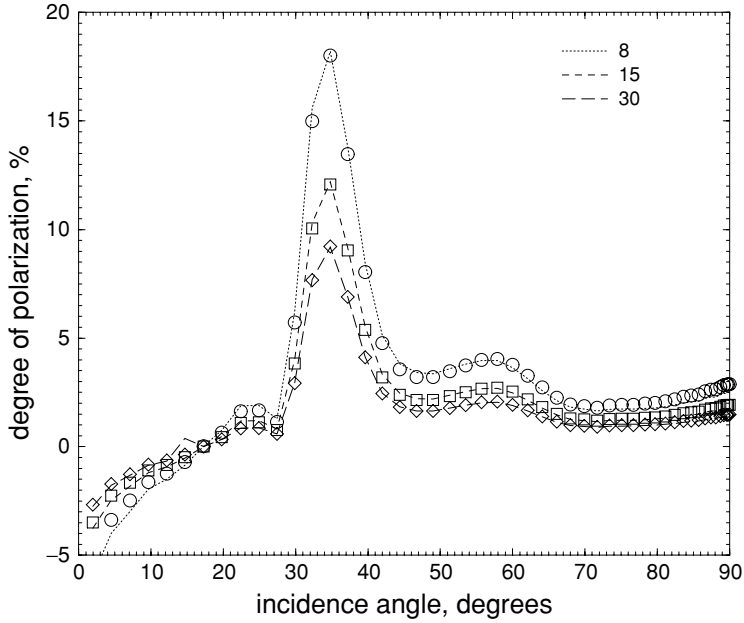

Fig. 3.24. Degree of linear polarization of light reflected from a cloudy atmosphere as the function of the solar zenith angle at the cloud optical thickness 8, 15, and 30, $a_{ef} = 6$ μm (the gamma PSD with $\mu = 6$) for nadir observations at $\lambda = 0.55$ μm. The solar zenith angle is equal to 60°. Both exact (symbols) and approximate (lines) results are shown.

The exact calculations for the case of a cloudy atmosphere takes much more computer time as compared to molecular scattering. This is not related to the larger optical thickness of clouds, which can reach 100 and more, but solely due to the peaked phase functions of water clouds. This means that one must account for many Legendre polynomials in the correspondent expansions. This also leads to a large number N of qaussian quadrature points required to solve this problem ($N \approx L/2$). This obstacle can be avoided using the so-called delta-M approximation (Nakajima and Tanaka, 1988; Min and Duan, 2004).

We show the cloud reflection function calculated using exact vector code in Fig. 3.25a. As one might expect, the reflection function increases with τ. It reaches an asymptotic value for a semi-infinite cloud at $\tau \approx 11$ for wavelength 2130 nm. For a nonabsorbing wavelength the asymptotic value is reached at much higher values of τ ($\tau \sim 500$ at wavelength 865 nm, see Fig. 3.25a). The single-scattering approximation (SSA) works quite well for $\tau \approx 0.03$ and below. So it can be used for the estimation of scattering characteristics of subvisual Cirrus, but not for most water and ice clouds present in the troposphere. The performance of the SSA for the polarization difference $D = -\pi Q_r / F_0 \mu_0$ is much better. It is valid at least

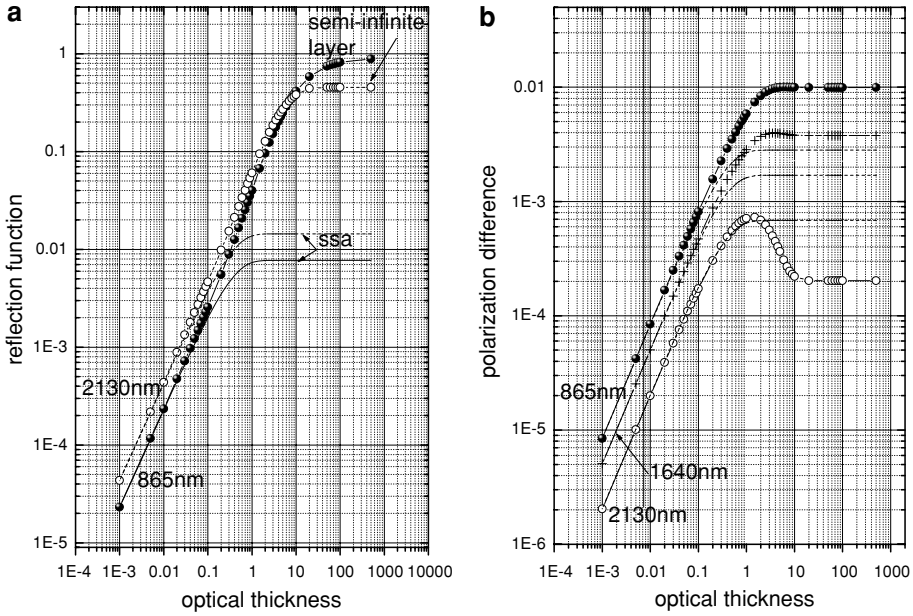

Fig. 3.25. Dependence of the cloud reflection function on the cloud optical thickness at wavelengths 865 and 2130 nm. The results for the semi-infinite layer and the single-scattering approximation are also shown. The solar zenith angle is 60°. The observation zenith angle is 0°. The phase function was calculated using Mie theory for the Deirmendjian's Cloud C1 model (Deirmendjian, 1969). (b) Dependence of the polarization difference D on the cloud optical thickness at wavelengths 865, 1640, and 2130 nm. The results for the semi-infinite layer and the single-scattering approximation are also shown. The solar zenith angle is 60°. The observation zenith angle is 0°. The phase function was calculated using Mie theory for the Deirmendjian's Cloud C1 model.

up to $\tau = 0.1$ (and even up to $\tau = 1.0$ for the wavelength $\lambda = 2130$ nm, see Fig. 3.25b).

There is a peculiarity in the behavior of the function $D(\tau)$ at $\lambda = 2130$ nm shown in Fig. 3.25b. In particular, there is a maximum around $\tau = 1$. Such maxima are not particularly pronounced for other solar angles shown in Fig. 3.26. The existence of the maximum cannot be explained on physical grounds because the difference D does not have a direct physical meaning. Physically based quantities I_l, I_r, R, and also the degree of polarization

$$p = \frac{D}{R} \tag{3.322}$$

all behave in a monotonous way [see, e.g., Fig. 3.27)]. Yet another peculiarity of the function $D(\tau)$ is that it reaches its asymptotical value for a semi-infinite cloud D_∞ at relatively small values of $\tau = \tau_\infty$ ($\tau_\infty = 1 - 4$, depending on the

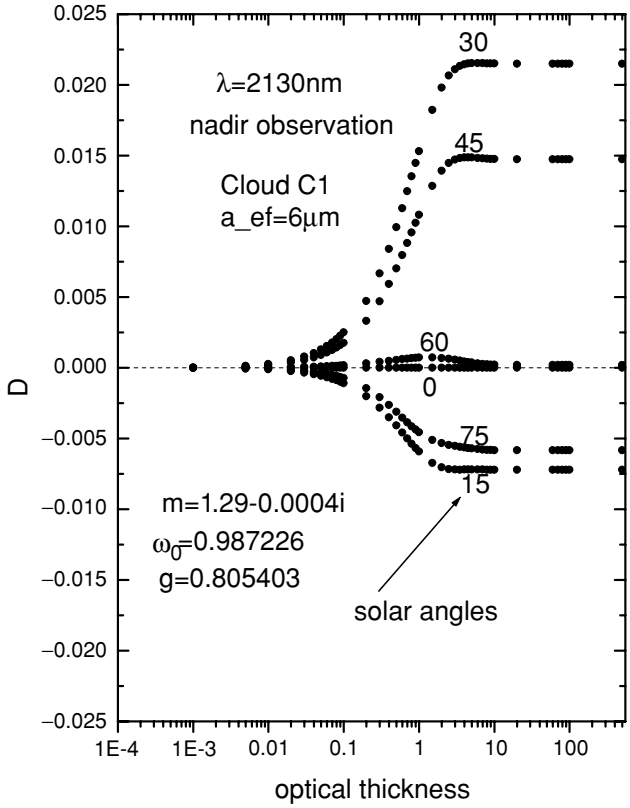

Fig. 3.26. Dependence of D on τ for various solar zenith angles at the wavelength 2130 nm. The refractive index used in calculations of the phase function using Mie theory for the Deirmendjian's Cloud C1 model is also shown. Values of ω_0 and g give correspondent values of the single-scattering albedo and the asymmetry parameter.

wavelength, see Fig. 3.26), which is not the case for R and P (see Figs. 3.25a and 3.27). The optical thickness of clouds is usually larger than τ_∞. It means that the value of D is *a priori* known for a given wavelength and the effective radius of droplets. Such a peculiarity can be used to estimate the sub-pixel cloud fraction K from remote sensing measurements. Indeed, the values of R and D can be presented as

$$R = K R_c + (1 - K)R_a, \quad D = K D_c + (1 - K)D_a, \tag{3.323}$$

for a partially cloudy scene, where the symbol c shows that the correspondent characteristic is related to the cloudy portion of the pixel and a denotes the characteristic of a cloudless atmosphere. It is known that values of R_a and D_a are determined mostly by the molecular scattering in the UV region of the electromagnetic spectrum

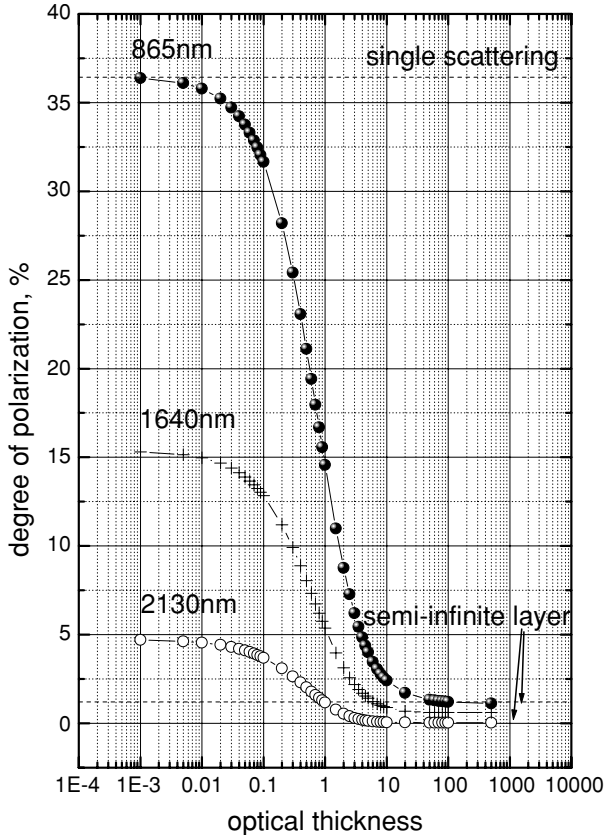

Fig. 3.27. The same as in Fig. 3.25b but for the degree of polarization in percent.

($R_a \to R_m$, $D_a \to D_m$, where m denotes the pure molecular scattering case (no clouds and aerosols)). This contribution is known a priori due to the relative stability of the Rayleigh optical thickness for a given wavelength. Then it follows in the UV:

$$K = \frac{D - D_m}{D_\infty - D_m},\ R_c = K^{-1}R - (K^{-1} - 1)R_m, \tag{3.324}$$

which allows also to find the cloud optical thickness in a partially cloudy scene. Another interesting possibility arises at geometries, where $D_c = 0$ (and, therefore, $P = 0$). Then it follows from Eq. (3.324): $K = 1 - DD_m^{-1}$. So if the measured value of D is equal to D_m, then we have: $K = 0$. K is equal to one for a completely cloudy atmosphere ($D = 0$ for clouds at the chosen favorable geometry). It follows from Fig. 3.24 that $D_c \approx 0$ at the solar angle 22° and the nadir observation. This corresponds to a scattering angle of 158°. So if one constructs the device capable to

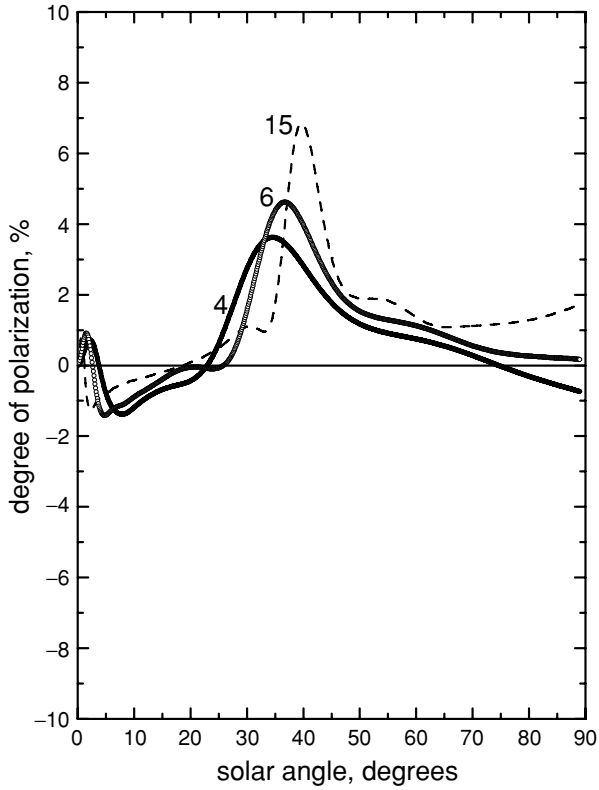

Fig. 3.28. Dependence of the degree of polarization P on the solar zenith angle at the optical thickness 500, nadir observation, and several effective radii of droplets. The phase function was calculated using Mie theory for the Deirmendjian's Cloud C1 model but with different effective radii $a_{ef} = 4$, 6, and 15 μm at the wavelength 865 nm. The maximum corresponds to the size dependent rainbow scattering.

measure D at this scattering angle, one will be able to determine the cloud fraction K quite accurately. The origin of a minimum at $\theta = 158^\circ$ is due to peculiarities of single scattering by water droplets. Note that multiple scattering hardly moves the positions, where the degree of polarization of singly scattered light vanishes (Kokhanovsky, 2003a).

The degree of polarization of light reflected from clouds for several values of a_{ef} is shown in Fig. 3.28. We see that the degree of polarization is more pronounced at the rainbow geometry.

Studies of polarization characteristics of solar light transmitted and reflected by cloudy media have a long history. However, the real burst of research in this area was given by a launch of the POLDER (Polarization and Directionality of Earth

Reflectances) instrument on board of Japanese ADEOS-I and ADEOS-II satellites. The POLDER (Goloub et al., 2000) was able to transmit to the Earth a huge amount of information about polarization characteristics of light reflected from cloudy media, aerosols and underlying surfaces at several wavelengths. Specifically, the first three components of the Stokes vector $\vec{S}_r(I, Q, U, V)$ have been measured for wavelengths λ equal to 443, 670 and 865 nm. There is no doubt that even more advanced polarimeters with wide spectral coverage will appear on board of different satellites in future, which makes further theoretical studies of polarization characteristics of cloudy media extremely important. This is due to potential possibilities for global retrievals of cloud microstructure, the shape of particles and the optical thickness of clouds based on polarization measurements.

Of course, similar information can be obtained from reflected intensity measurements. However, it could well appear that the degree of polarization can be used as a source of additional information about cloud particle size distributions close to the top of a cloud. Indeed, the high proportion of photons scattered from a thin upper layer of a cloud in creating light polarization is quite understandable. Multiply scattered light fluxes from deep layers are hardly polarized at all. Radiative characteristics, on the other hand, represent the cloud as a whole. Thus, the effective radius derived from radiative measurements is an average of large ensembles of possibly very different particle size distributions, presented in different parts of cloudy media.

The polarization characteristics of cloudy media can be studied applying numerical codes, based on the vector radiative transfer equation solution. However, one can also use the fact that cloud fields are optically thick in most cases. This allows to apply asymptotic analytical relations, derived for optically thick disperse media with arbitrary phase functions and absorption. These solutions help us to explain physical mechanisms and main features behind the polarization change due to the increase of the size of droplets or the thickness of a cloud. Analytical solutions also provide an important tool for the simplification of the inverse problem. They can be used, e.g., in studies of the information content of polarimetric measurements (Deschamps et al., 1994).

3.7 Clouds Over Reflective Surfaces

Equations for R and T derived above can be easily generalized to account for the underlying surface reflection.

Light intensity observed in a direction specified by the pair (ϑ, φ) can be considered as composed of two parts: due to the cloud itself (I_1) and due to surface contribution (I_2). The contribution I_2 can be also separated into two terms (I_{21}, I_{22}),

namely

$$I_{21} = I_s t(\eta) \tag{3.325a}$$

for the contributions of the surface in the diffused light ($\eta = \cos\vartheta$) and

$$I_{22} = I_s e^{-\tau/\eta} \tag{3.325b}$$

for the contribution of the surface in the direct light.

Summing up, we have:

$$I(\eta, \varphi) = I_1(\eta, \varphi) + I_s t(\eta) + I_s e^{-\tau/\eta}, \tag{3.326}$$

where we assumed that the surface is Lambertian. This means that the upward intensity I_s for the light emerging from the ground surface does not depend on angle. Let us relate I_s to the albedo A of underlying Lambertian surface. For this we note that the upward flux density is

$$F_u = \int_{2\pi} I_s \cos\vartheta d\Omega = \int_0^{2\pi} d\varphi \int_0^{\pi/2} d\vartheta I_s \cos\vartheta \sin\vartheta = \pi I_s. \tag{3.327}$$

We have for the ideally reflecting Lambertian surface ($A = 1$): $F_u = F_d$ or $F_d = \pi I_s$, where F_d is the downward flux density. F_d is composed of three components: the direct transmission component $F_{dir} = \xi F_0 e^{-\tau/\xi}$, the diffuse transmission component $F_{dif} = \xi F_0 t(\xi)$ and the component coming from the surface but reflected by a scattering layer back to the underlying surface: $F_{ref} = r F_u$, where r is the spherical albedo of a scattering layer under illumination from below. Obviously, for the underlying surface with arbitrary ground albedo A, we have:

$$F_u = A F_d \tag{3.328}$$

and, therefore,

$$\pi I_s = A\left[\xi F_0 \left(t(\xi) + e^{-r/\xi}\right) + \pi r I_s\right]. \tag{3.329}$$

The intensity I_s can be easily found from this equation. Namely, it follows:

$$I_s = \frac{A t^*(\xi) \xi F_0}{\pi(1 - Ar)} \tag{3.330}$$

where

$$t^*(\xi) = t(\xi) + e^{-\tau/\xi} \tag{3.331}$$

is the total transmittance. Therefore, we have (Liou, 2002):

$$I(\eta, \varphi) = I_1(\eta, \varphi) + \frac{A t^*(\eta) t^*(\xi) \xi F_0}{\pi(1 - Ar)} \tag{3.332}$$

or

$$R(\eta, \xi\varphi) = R_b(\eta, \xi\varphi) + \frac{At^*(\eta)t^*(\xi)}{1 - Ar}, \tag{3.333}$$

where $R_b(\eta, \xi, \varphi) \equiv R(\eta, \xi, \varphi)$ at $A = 0$. All functions presented in this equation have been studied in the previous section. A similar simple account for the Lambertian underlying surface can be performed also for the transmitted component. Namely, we have then:

$$I_{tr}(\eta, \varphi) = I_{1tr}(\eta, \varphi) + I_s r_d(\eta), \tag{3.334}$$

where the first component is due to light transmission by a cloud itself and the second component accounts for the reflection of the diffuse light (I_s) coming from the surface, $r_d(\eta)$ is the plane albedo for illumination from below. Finally, we have:

$$I_{tr}(\eta, \varphi) = I_{1tr}(\eta, \varphi) + \frac{At^*(\xi)r_d(\eta)\xi F_0}{\pi(1 - Ar)} \tag{3.335}$$

or for the transmission function:

$$T(\xi, \eta, \varphi) = T_b(\xi, \eta, \varphi) + \frac{Ar_d(\xi)t^*(\eta)}{1 - Ar}, \tag{3.336}$$

where $T_b(\xi, \eta, \varphi) \equiv T(\xi, \eta, \varphi)$ at $A = 0$.

3.8 Vertically Inhomogeneous Clouds

Vertically inhomogeneous disperse media are of frequent occurrence both in nature (e.g., multi-level cloud systems, snow deposited at different times at a given place, terrestrial atmosphere and ocean, biological tissues, etc.) and technological applications (multi-layered painted surfaces, paper, etc.). This explains a great interest in studies of radiative transfer in vertically inhomogeneous media. Recent advances in this area have been summarized by Yanovitskij (1997). A great number of exact (see, e. g., Minin, 1988; Rozanov et al., 2005) and approximate (Germogenova and Konovalov, 1974; Minin, 1988; Melnikova and Vasilyev, 2005) techniques has been developed. At present there is no problem to account for an arbitrary vertical inhomogeneity of a horizontally homogeneous plane-parallel light scattering medium. However, it appears that one needs to perform quite complex numerical calculations with the use of up-to-date computer technology. On the other hand, the practical work requires simple approximate solutions, which can be used to perform rapid estimations of the influence of vertical inhomogeneity on light reflection and transmission by cloudy media. Such results are presented in this section. To derive approximate solutions, we make an assumption that the

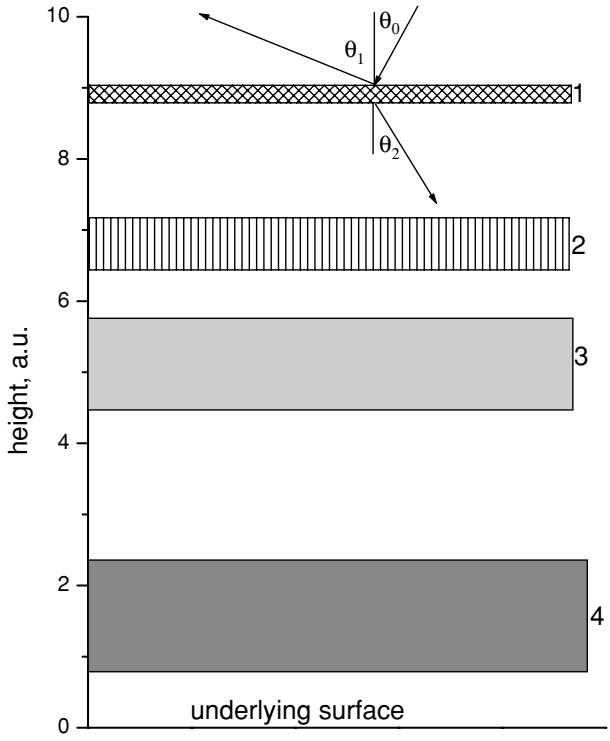

Fig. 3.29. Geometry of the problem.

probability of light absorption by droplets in a cloud is small and the exponential approximation can be applied.

Let us assume that a cloudy medium is composed of several cloud layers having different light scattering characteristics (e.g., the phase function $p(\theta)$, the absorption σ_{abs} and extinction σ_{ext} coefficients). The geometry of the problem is shown in Fig. 3.29. Light enters a disperse medium at the angle θ_0. The reflected light is observed at the angle θ_1 and the diffusely transmitted light is observed in the direction specified by the angle θ_2. We need to model the intensity of diffusely reflected and transmitted beams taking into account effects of vertical inhomogeneity of the medium under consideration.

Note that we put no limitations on the number of layers in a cloudy medium. The region which separates clouds is assumed to be free of light scattering and absorption. This means that the situation we consider is equivalent to the touching light scattering layers (e.g., several snow layers). This assumption, however, is not crucial for the theory developed here [e.g., absorption and scattering of light by gases and aerosols between clouds can be accounted for, if needed (see, e.g., Kokhanovsky and Rozanov, 2004)]. We assume that all layers are optically thick

($l_i \gg \ell_i$, where l_i is the geometrical thickness of i-layer and ℓ_i is the photon free path length in the layer, which is equal to the inverse value of the extinction coefficient in a given layer) and weakly absorbing (the probability of photon absorption $\beta = \sigma_{abs}/\sigma_{ext} \to 0$). We need these assumptions to apply the exponential approximation as discussed above. There is no limitation on the type of the cloud phase function, however. Although our assumptions severely restrict the applicability of the model to many natural clouds, they do provide an accurate approach to the solution of a number of important problems.

The starting point is the expression for the reflection function of a single homogeneous, optically thick, weakly absorbing layer. This can be written in the following form for a scattering layer above a Lambertian surface with albedo A:

$$R_A(\xi, \eta, \tau) = R(\xi, \eta, \tau) + \frac{A t_d(\xi) t_d(\eta)}{1 - Ar}, \tag{3.337}$$

where

$$R(\xi, \eta, \tau) = R_\infty(\xi, \eta) - t \exp(-x - y) u_0(\xi) u_0(\eta) \tag{3.338}$$

is the reflection function of a scattering layer for the black ($A = 0$) underlying surface, $R_A(\xi, \eta, \tau)$ is the same function but for the scattering layer–underlying surface system, $x = k\tau$, $k = \sqrt{3\beta(1-g)}$ is the diffusion exponent, g is the asymmetry parameter, $\tau = \sigma_{ext} l$ is the optical thickness, l is the geometrical thickness of a scattering layer, $y = 4k/3(1-g)$, r is the spherical albedo of a scattering layer for an illumination from below at $A = 0$, $t_d(\xi)$ is the diffuse transmittance for the illumination in the direction $\theta_0 = \arccos(\xi)$, t is the global transmittance at $A = 0$. The function $t_d(\eta)$ is the diffuse transmittance for the illumination in the direction $\theta_2 = \arccos(\eta)$. The dependence of the reflection function in Eq. (3.338) on the azimuth is omitted for simplicity. Also we neglect the direct light transmittance, which takes rather small values for optically thick layers. Convenient approximate equations for functions $t_d(\xi)$, $R_\infty(\xi, \eta)$ and r are presented above.

Let us proceed further now. It is known that the reflection of light from an optically thick weakly absorbing strongly light scattering layer is rather close to that of a Lambertian reflector. This is due to well-developed multiple light scattering in the medium in this case. Therefore, to find the reflectance from a multi-layered system as given in Fig. 3.29, one can use Eq. (3.337) with A substituted by the spherical albedo r_2^* of the multi-layered system below the upper layer (see Fig. 3.29). Other functions in Eq. (3.337) then refer to the first layer from the illumination side. Such an approach was proposed and successfully used by Melnikova and Minin (1977) for studies of light fluxes in a cloudy atmosphere.

The spherical albedo r_2^* can be easily found integrating Eq. (3.337). Indeed, it follows from Eq. (3.337):

$$r_2^* = r_2 + \frac{t_2^2 r_3^*}{1 - r_2 r_3^*}. \tag{3.339}$$

Here r_3^* is the spherical albedo of the system starting from the 3rd layer down (see Fig. 1), t_2 is the global transmittance of the second layer, r_2 is the spherical albedo of the second scattering layer for an illumination from below. The spherical albedo r_3^* can be found using equation similar to Eq. (3.339):

$$r_3^* = r_3 + \frac{t_3^2 r_4^*}{1 - r_3 r_4^*} \tag{3.340}$$

with meaning of all parameters similar to those in Eq. (3.339). Clearly, we need to repeat this procedure till the underlying surface is reached. Then we have:

$$r_n^* = r_n + \frac{t_n^2 A}{1 - r_n A} \tag{3.341}$$

and the procedure is complete.

Let us check the accuracy of the straightforward procedure outlined above using the exact solution of the radiative transfer equation with SCIATRAN (Rozanov et al., 2005) for a two-layered disperse system over a black surface. Then A in Eq. (3.339) should be substituted by the spherical albedo of a lower layer r_2. All other parameters in Eq. (3.339) refer to an upper layer. Note that SCIATRAN is a well-documented and thoroughly tested radiative transfer code based on the discrete ordinates approach. Its accuracy is better than 1%.

The results of comparisons are shown in Figs. 3.30a–c. In particular, we give the dependence of the reflection function of a disperse medium on the incidence angle for the nadir observation. Due to the reciprocity principle, our calculations are also valid for the nadir illumination and varying observation angles.

The middle curves in Figs. 3.30a–c correspond to a two-layered cloud system with an optical thickness of the bottom layer $\tau_b = 30$ and an optical thickness of the upper layer $\tau_u = 10$. We assume that the upper layer does not absorb incident radiation. The single-scattering albedo of the bottom layer is equal to 0.9945 (Fig. 3.30a), 0.9982 (Fig. 3.30b), 0.9681 (Fig. 3.30c).

The upper curves in these figures correspond to a single layer having an optical thickness $\tau = \tau_b + \tau_u$ and the single-scattering albedo equal to 1. Lower curves in Figs. 3.30a–c correspond to a single layer having an optical thickness $\tau = \tau_b + \tau_u$ and the single-scattering albedo equal to 0.9945 (Fig. 3.30a), 0.9982 (Fig. 3.30b), 0.9681 (Fig. 3.30c). Exact results are shown by symbols. Lines correspond to calculations according to the approximation developed here.

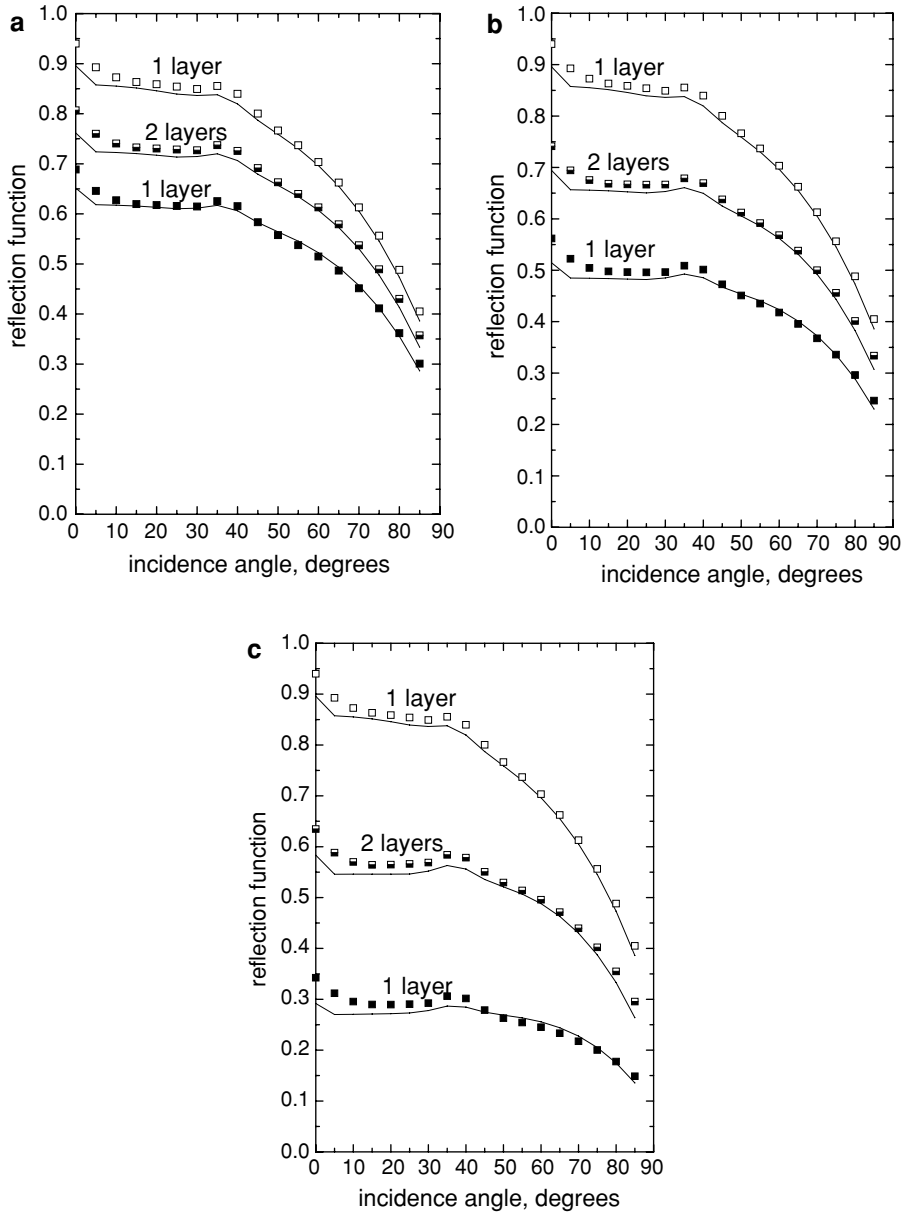

Fig. 3.30. (a) The dependence of the reflection function of a cloud medium on the incidence angle for the nadir observation. Symbols give exact results and lines are due to the approximation (see details in text). The curve in the middle was obtained for an upper nonabsorbing layer and the absorbing layer with $\omega_0 = 0.9945$ at the bottom. Upper curves correspond to a nonabsorbing single layer. Lower curves correspond to an absorbing single layer. The total optical thickness is kept constant for all calculations ($\tau = 40$). The phase function was calculated using Mie theory for the gamma droplet distribution with $a_{ef} = 10$ μm, $\mu = 1/9$, $\lambda = 0.65$ μm, and the refractive index $1.331 - i\chi$, $\chi = 0$ (upper curve) and $\chi = 0.00005$ (lower curve). (b) The same as in Fig. 3.30a except $\chi = 0.0001$ for a lower curve and $\omega_0 = 0.9892$. (c) The same as in Fig. 3.30a except $\chi = 0.0003$ for a lower curve and $\omega_0 = 0.9691$.

The phase function was found using the narrow gamma droplet size distribution with the effective radius 10 μm and the effective variance equal to 1/9 at wavelength $\lambda = 0.65\mu$m for water droplets with the refractive index m equal to 1.331-0i (Figs. 3.29a–c, upper curves), 1.331–0.00005i (Fig. 3.30a, lower curves), 1.331–0.0001i (Fig. 3.30b, lower curves), 1.331–0.0003i (Fig. 3.30c, lower curves).

Note that the variation of the imaginary part of the refractive index allows us to model various levels of cloud pollution (e.g., due to black carbon). The phase function differs not significantly for all layers. For instance, the asymmetry parameter is equal to 0.85 at $m = 1.331–0i$, 0.8513 at $m = 1.331–i0.00005i$, 0.8525 at $m = 1.331–0.0001i$ and 0.8571 at $m = 1.331–0.0003i$. This is according to the general fact that the phase function of weakly absorbing particles is not particularly affected by the level of light absorption. However, note that there is a slight tendency to the general increase of the asymmetry parameter with the imaginary part of the refractive index.

It follows from Figs. 3.30a–c that the accuracy of our simple approximation is quite high for the case considered. In fact it is comparable with the accuracy of corresponding equations for a single layer or even higher than that. This paradox is explained by the fact that the accuracy of the approximation is highly influenced by the value of ω_0. The average value of ω_0 is, however, lower for a two-layered system (with a nonabsorbing upper layer) as compared to a single absorbing layer having the same optical thickness.

We see that the two-layered system with total optical thickness 40 has values of R intermediate between those for an upper layer (at $\tau = 40$) and lower layer (also at $\tau = 40$). This can be expected on general grounds as well. Errors are generally below 5% but they increase for oblique incidence angles. The accuracy decreases with β. The value of $\beta \approx 0.03$ can be considered as an upper boundary for the application of this theory. Although it can be applied to slightly larger values of β if the accuracy is not a primary concern (e.g., for rapid estimations of vertical inhomogeneity effects).

It is interesting to see the performance of equations for larger and smaller values of τ_b, τ_u. This is shown in Figs. 3.31a and 3.31b for an absorbing lower layer and nonabsorbing upper layer. We see that the accuracy of our equations is robust against change of the turbid layer thickness. Note that the variation of the optical thickness of a lower layer (see Fig. 3.31a) does not change the reflection function very much. This is due to the fact that the spherical albedo of a lower absorbing cloud does not depend strongly on τ_b. On the other hand, the variation of the upper layer optical thickness τ_u (see Fig. 3.31b) changes the result considerably. Clouds become much brighter with a larger thickness of the upper layer. Obviously, for a very thick upper layer the sensitivity of the reflection function to the presence of a turbid layer at the bottom is lost. This is similar to the effect of the disappearance of objects in a heavy fog. Therefore, we conclude that high nonabsorbing clouds

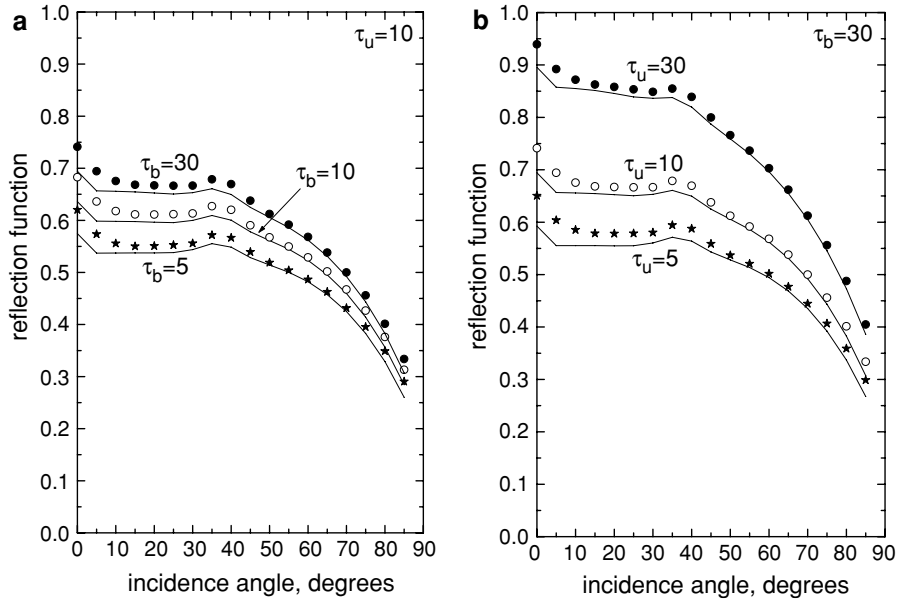

Fig. 3.31. (a) The dependence of the reflection function of a two-layered cloud medium on the incidence angle for the nadir observation at $\tau_u = 10$ and $\tau_b = 5, 10, 30$. The upper layer does not absorb radiation. The bottom layer is characterized by the single-scattering albedo 0.9892. Symbols give exact results and lines are due to the approximation (see details in the text). (b) The dependence of the reflection function of a two-layered cloud medium on the incidence angle for the nadir observation at $\tau_u = 5, 10, 30$ and $\tau_b = 30$. The upper layer does not absorb radiation. The bottom layer is characterized by the single-scattering albedo 0.9892. Symbols give exact results and lines are due to the approximation (see details in the text).

can shield lower (and possibly) polluted clouds. This can lead to important climatic effects not accounted for in Global Circulation Models at the moment.

To make this point more clear, we present the reflection function of a single absorbing cloud layer with the optical thickness 30 in Fig. 3.32. Then we add a nonabsorbing cloud at the higher level in the atmosphere. It follows that the reflection of the system considerably increases both for warm water and cold ice upper-level clouds. The phase function of an ice cloud was taken from a study by Mishchenko et al. (1999) (the fractal particle model) and the phase function of the water cloud was calculated as indicated above (at $m = 1.331 - 0.0001i$ for a lower cloud and $m = 1.331$ for an upper cloud in the two-layered system). The increase in the reflection is much more pronounced for crystalline clouds. It means that ice clouds not only warm the system by trapping terrestrial radiation. They also may shield lower polluted cloud systems (e. g., in urban areas) and increase general reflection of the surface–atmosphere system. This indicates the complexity of the issue of cloud influence on the climate.

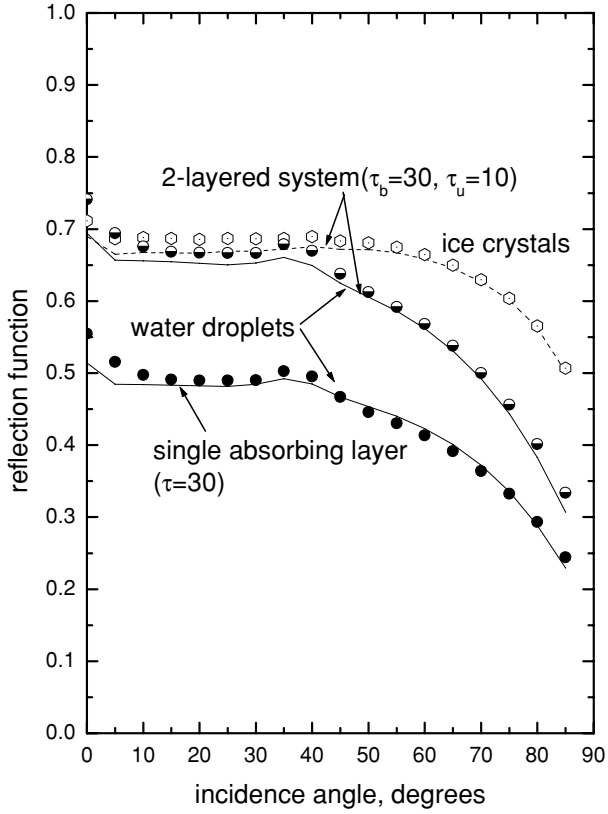

Fig. 3.32. The dependence of the reflection function on the incidence angle for the nadir observation for a two-layered cloud medium at $\tau_u = 10$, $\tau_b = 30$ (upper curves) and for an absorbing single cloud layer with $\tau = 30$ (lower curves). The upper layer does not absorb radiation and composed either of water droplets or ice crystals. The bottom layer and a single absorbing layer is characterized by the single-scattering albedo 0.9892. Symbols give exact results and lines are due to the approximation (see details in text).

The question arises if the model presented above can be applied to studies of light transmission. The answer on this question is positive. Indeed, we have for the transmission function of a single homogeneous disperse layer over a Lambertian surface with surface albedo A :

$$T_A(\xi, \eta, \tau) = T(\xi, \eta, \tau) + \frac{A t_d(\xi) r_d(\eta)}{1 - Ar}. \tag{3.342}$$

Here $r_d(\eta)$ is the plane albedo of the layer for the illumination from below. Again assuming that the layers below the upper one can be substituted by a Lambertian reflector, we have for the transmission function $\bar{T}_1(\xi, \eta)$ of the first layer in the

n-layer system:

$$\bar{T}_1(\xi, \eta) = T_1(\xi, \eta) + \frac{t_{d1}(\xi) r_{d1}(\eta) r_2^*}{1 - r_1 r_2^*}, \tag{3.343}$$

where we omitted the dependence on the optical thickness and r_2^* is found using the iterative procedure starting from the ground surface as underlined in the previous section. Functions $T_1(\xi, \eta)$, $t_{d1}(\xi)$, r_1 and $r_{d1}(\eta)$ have the same meaning as in Table 3.1 but for the first layer.

Let us consider now the transmittance under the second layer. The second layer is illuminated by the diffuse light transmitted by the first layer. It follows that the diffuse transmittance $\bar{t}_{d1}(\xi)$is given by:

$$\bar{t}_{d1}(\xi) = t_{d1}(\xi) + \frac{t_{d1}(\xi) r_1 r_2^*}{1 - r_1 r_2^*} \tag{3.344}$$

or

$$\bar{t}_{d1}(\xi) = \frac{t_1(\xi)}{1 - r_1 r_2^*}. \tag{3.345}$$

Also we have for the global transmittance:

$$\bar{t}_1 = \frac{t_1}{1 - r_1 r_2^*}. \tag{3.346}$$

Therefore, the transmission function $\bar{T}_2$ after the second layer in the n-layered system is given as

$$\bar{T}_2(\xi, \eta) = \bar{t}_{d1}(\xi) \bar{t}_{d2}(\xi)(\eta), \tag{3.347}$$

where

$$\bar{t}_{d2}(\eta) = \frac{\bar{t}_{d2}(\eta)}{1 - r_2 r_3^*}. \tag{3.348}$$

Following this procedure, we can obtain the transmission function under the third layer:

$$\bar{T}_3(\xi, \eta) = \bar{t}_{d1}(\xi) \bar{t}_2 \bar{t}_{d3}(\eta), \tag{3.349}$$

where $\bar{t}_2 = t_2/(1 - r_2 r_3^*)$ and we accounted for the fact that the second layer is illuminated from above by diffuse light and that it also serves as a diffuse light source for the third layer. Repeating this procedure for each layer, we can arrive finally to the transmission function of a whole system:

$$\bar{T}_n(\xi, \eta) = \bar{t}_{d1}(\xi) \bar{t}_2 \bar{t}_3 \ldots \bar{t}_{n-1} \bar{t}_{dn}(\eta), \tag{3.350}$$

where $\bar{t}_j = t_j/(1 - r_j r^*_{j+1})$ and $r_{n+1} \equiv A$. Interestingly, Eq. (3.350) can be written in the form similar to that for a homogeneous layer:

$$\bar{T}_n(\xi, \eta) = t_{ef} K_0(\xi) K_0(\eta), \tag{3.351}$$

where the effective global transmittance is given by:

$$t_{ef} = \frac{\prod_{j=1}^{n} t_j}{\prod_{j=1}^{n} \left(1 - r_j r^*_{j+1}\right)} \tag{3.352}$$

with all parameters defined in the theory for a single layer. Note that we have used here the equality: $t_{dj} = t_j u_0(\xi)$, where $u_0(\xi)$ is the escape function.

Let us check the applicability of our assumptions making comparisons with exact radiative transfer calculations using SCIATRAN (Rozanov et al., 2005) for a special case of a two-layered medium over a black surface. Then Eq. (3.350) is reduced to the following form:

$$\bar{T}_2(\xi, \eta) = \frac{t_1 t_2 u_0(\xi) u_0(\eta)}{1 - r_1 r_2}, \tag{3.353}$$

where we accounted for the fact that $t_{ef} = t_1 t_2 (1 - r_1 r_2)^{-1}$ in this case. Note that if neither of both layers absorb radiation, the sensitivity of transmitted light to the vertical inhomogeneity is low and in a good approximation one can use the reflection function for a single layer having the optical thickness equal to the sum of optical thicknesses of both layers and the average value of the asymmetry parameter (Sobolev, 1972).

The results of calculations using simple approximation (3.353) are shown in Figs. 3.33–3.37 as functions of the observation angle together with corresponding errors and outcome of exact calculations for the incident angle equal to 60° and the azimuth equal to 0°. In particular, we give the dependence of the transmission function on the observation angle for a single layer having the optical thickness equal to 40 at $\omega_0 = 0.9945$ and $\omega_0 = 1.0$ in Fig. 3.33. The results of computations for a two-layered medium having the total optical thickness 40 but $\omega_0 = 0.9945$ in the bottom layer ($\tau_b = 30$) and $\omega_0 = 1.0$ in upper layer ($\tau_u = 10$) are also given in the same figure (the middle line). Note that phase functions in all calculations given here are very close to each other. So the change of transmission is mostly due to the absorption effect. As expected the largest transmission is observed for a nonabsorbing single layer. It is reduced considerably if absorption is introduced in the bottom part of a layer. Of course, the minimum of transmission occurs for a single absorbing layer (see, e.g., a lower line in Fig. 3.33). It follows that exact and approximate results are quite close to each other for observation angles smaller than 70°. Then the error of approximation is smaller than 5%. The error increases for slabs having larger absorption, however. This is illustrated in Fig. 3.34, where we show a dependence similar to that in Fig. 3.33 but now for the increased

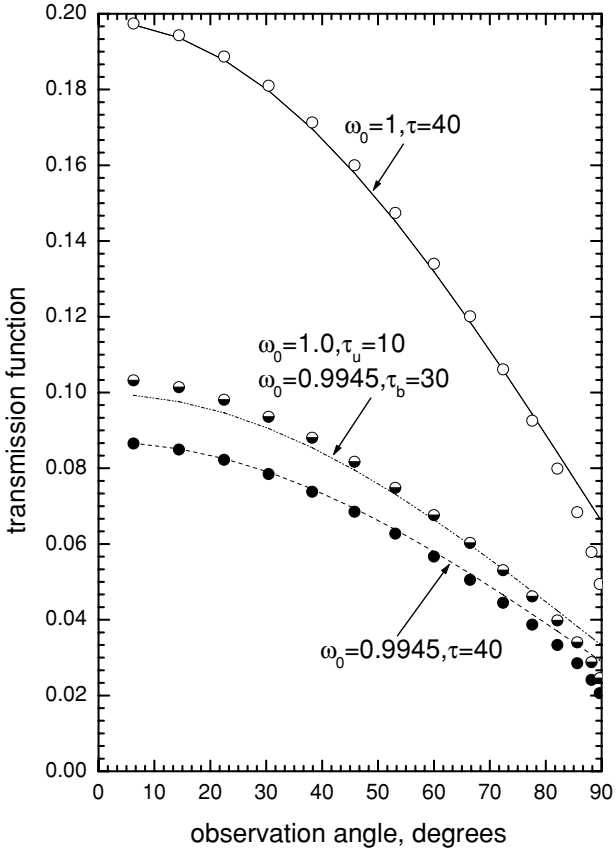

Fig. 3.33. The dependence of the transmission function on the zenith observation angle at the zenith incidence angle equal to 60° and the azimuth equal to 0° for a single homogeneous layer and a two – layered turbid medium with the total optical thickness equal to 40. The single-scattering albedo is equal to 0.9945. Lines correspond to Eq. (3.353) and symbols are obtained from exact calculations. Further explanations are given in the text.

absorption ($\omega_0 = 0.9892$). It is interesting that the error of Eq. (3.353) for a two-layered medium is smaller than that for a single layer with the optical thickness 40 and $\omega_0 = 0.9892$. This points to the fact that the accuracy of the technique is mostly influenced by the total light absorption and transmission and not by a number of layers. Note that the accuracy of reflected light calculation is generally higher than that for the diffusely transmitted light (for a given level of absorption).

Calculations for a two-layered turbid slab with the optical thickness of a lower absorbing layer equal to 30 for various thicknesses of a nonabsorbing upper layer are shown in Fig. 3.35. The middle lines in this figure coincide with the middle line in Fig. 3.33. We see that the accuracy is better than 5% in this case. The decrease of

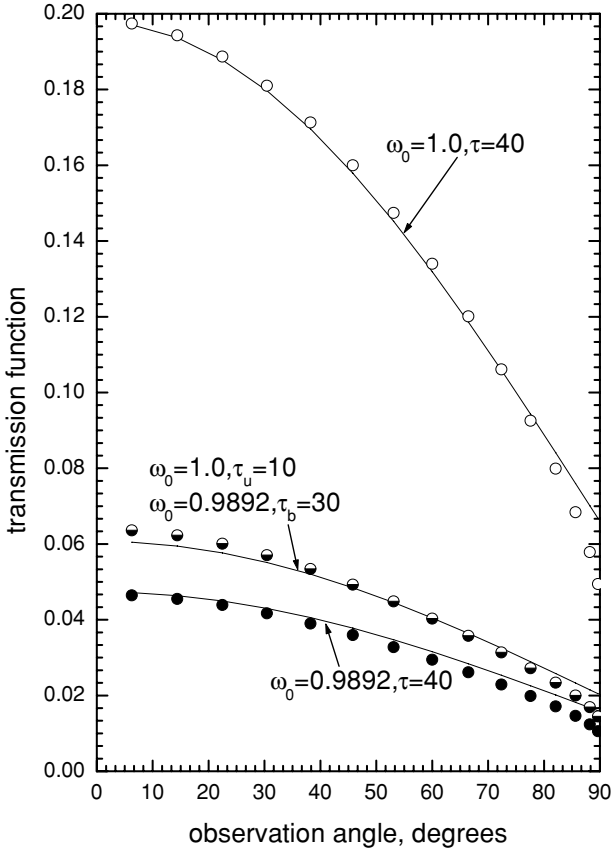

Fig. 3.34. The same as in Fig. 3.33 but at $\omega_0 = 0.9892$.

the optical thickness of an upper layer leads to the increase of the light transmission as one might expect.

Fig. 3.36 is similar to Fig. 3.35, but now the optical thickness of an absorbing layer at the bottom is varied from 5 till 30. The optical thickness of an upper layer is fixed and equal to 10. Clearly, the error approximation increases for thinner layers, which is in accordance with general assumptions of our approximation, which is valid only for weakly absorbing optically thick layers (Kokhanovsky and Rozanov, 2003). However Eq. (3.353) has a comparatively high accuracy even at such comparatively small values of τ as 5 (see Fig. 3.36).

In conclusion, we show the transmission function of a single absorbing layer having optical thickness 40 at $\omega_0 = 0.9945$ in Fig. 3.37 (middle line) in comparison with transmission functions of a two-layered system having $\omega_0 = 0.9945$ in the upper layer ($\tau_u = 30$) and $\omega_0 = 0.9892$ in the layer at the bottom ($\tau_b = 10$) (lower line

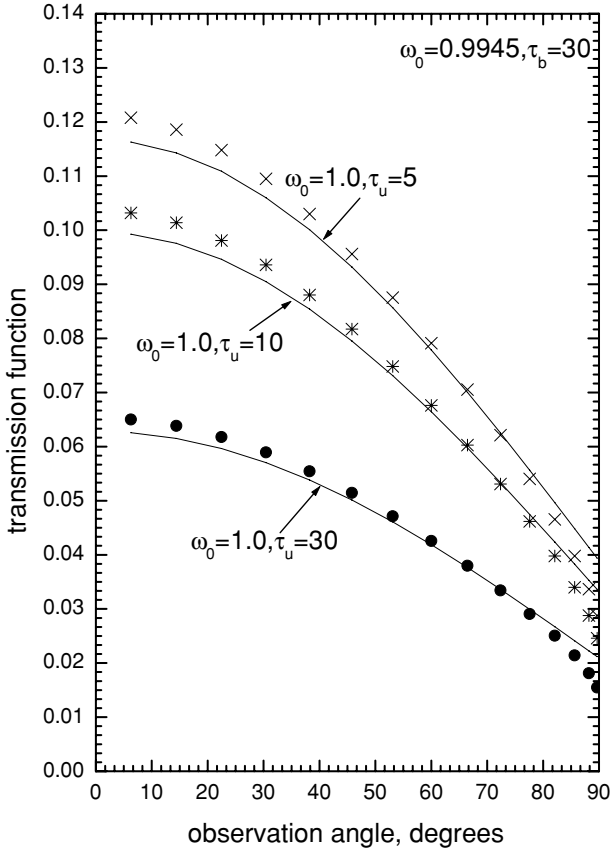

Fig. 3.35. The same as in Fig. 3.33 but for other values of optical thickness of an upper layer.

in Fig. 3.37). Clearly, in the later case the transmission should be lower. Figure 3.37 quantifies this decrease. The upper line in Fig. 3.37 corresponds to a two-layered system with total optical thickness equal to 40 and local optical characteristics of a lower layer equal to that of a single layer shown by the middle line in Fig. 3.37 but having a nonabsorbing scattering layer at the top of the system ($\tau_u = 10$). Then, due to the general decrease of absorption in the system, transmission should increase. This is confirmed by Fig. 3.37. It follows from Fig. 3.37 that the error of Eq. (3.353) is smaller than 5%, which is acceptable for a broad range of applications (e.g., rapid estimations of stratification effects on diffusely transmitted and reflected light fields).

Detailed studies of radiative transfer in vertically inhomogeneous clouds including those with smooth vertical profiles of scattering and absorption characteristics have been performed by Yanovitskij (1997).

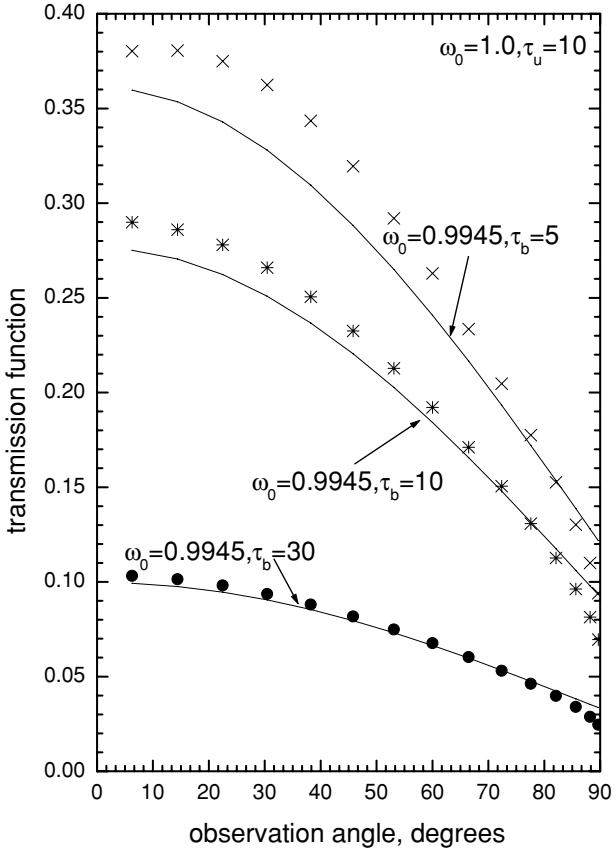

Fig. 3.36. The same as in Fig. 3.33 but for other values of optical thickness of a bottom layer.

3.9 Horizontally Inhomogeneous Clouds

3.9.1 Independent Pixel Approximation

The influence of the horizontal inhomogeneity of clouds on their radiative characteristics is a major subject of modern cloud optics studies (Cahalan et al., 1994, 2001; Barker et al., 1996; Loeb and Davies, 1996; Marshak et al., 1998; Platnick, 2001; Scheirer and Macke, 2001; Davis and Marshak, 2002). In particular, it was found that the horizontal inhomogeneity of clouds effects their abilities to absorb, reflect and transmit solar light (Feigelson, 1981; Scheirer and Macke, 2001). Thus, cloud remote sensing techniques, based on the spectral reflectance method (Kondratyev and Binenko, 1984; Arking and Childs, 1985; Nakajima and King, 1990; Nakajima et al., 1991; King et al., 1992; Han et al., 1994; Rossow et al.,

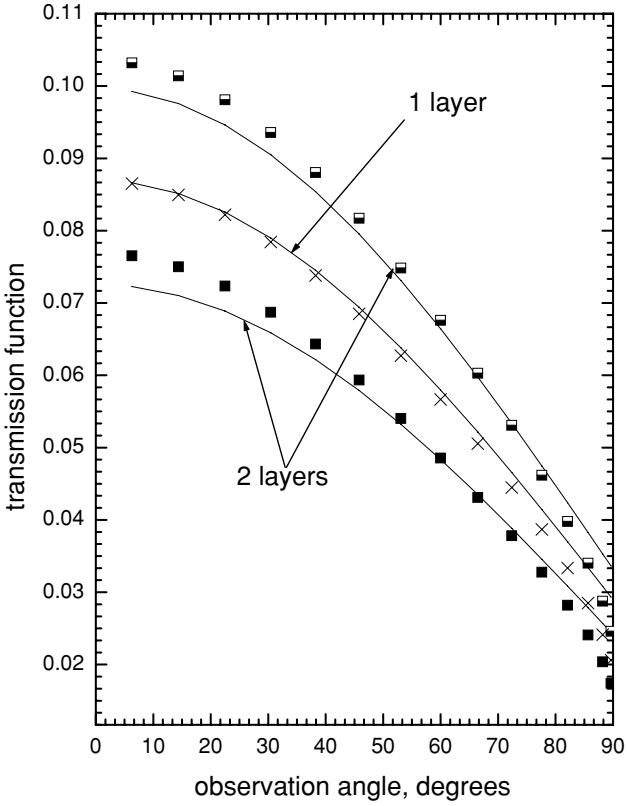

Fig. 3.37. The dependence of the transmission function on the zenith observation angle at the zenith incidence angle equal to 60° and the azimuth equal to 0° for a single homogeneous layer (middle line, $\omega_0 = 0.9945$, $\tau = 40$) and a two-layered turbid medium [$\omega_0 = 0.9945$, $\tau = 30$ for a lower layer and $\omega_0 = 1.0$, $\tau = 10$ for an upper layer (upper line) and $\omega_0 = 0.9892$, $\tau = 10$ for a lower layer and $\omega_0 = 0.9945$, $\tau = 30$ for an upper layer (lower line)]. Lines correspond to results obtained with Eq. (3.353) and symbols are obtained from exact calculations. Further explanations are given in text.

1989; Rossow and Schiffer, 1999), must account for the sub-pixel cloud horizontal inhomogeneity. This is not generally the case so far.

It is known that pixels with inhomogeneous clouds are darker than pixels with homogeneous cloud layers, having the same average optical thickness (Cahalan et al., 1994). This leads to the underestimation of cloud optical thickness by modern satellite retrieval techniques. There are semi-empirical approaches to overcome this problem. They are based on the artificial increase of the measured reflection function to account for the horizontal inhomogeneity of a cloud field under study. The correct magnitude of these adjustments, however, cannot be assumed *a priori*.

So they lack a physical basis. This issue is discussed in detail by Pincus and Klein (2000). Also cloud inhomogeneity could lead to unphysical dependencies of the retrieved cloud optical thickness on illumination and viewing geometry (Loeb and Davies, 1996).

Another way to solve the problem is to use 3-D Monte Carlo calculations (see, e.g., Scheirer and Macke, 2001). However, they are time-consuming for realistic clouds and can be used mostly for theoretical studies and not as a core of operational cloud satellite retrieval algorithms. Monte Carlo calculations have shown, however, that in some cases a high accuracy can be achieved if a 3-D cloud field is substituted by N noninteracting vertical columns or cells. A cloud field in each cell is modelled as a horizontally homogeneous plane-parallel layer of an infinite horizontal extent. The optical thickness (and, possibly, microstructure) of each cell varies, depending on its position in a cloud field. Such an approach is called the Independent Column Approximation (ICA) or the Independent Pixel Approximation (IPA). The range of applicability of the ICA was studied by Davis et al. (1997) and Scheirer and Macke (2001).

Effectively, the ICA reduces the 3-D radiative transfer problem to N standard radiative transfer problems for homogeneous media. The number N can be large. Thus, the problem remains computationally very expensive.

It can be simplified, however, if one applies approximate solutions of the radiative transfer problem for each cloud cell. This is done usually in the framework of the two-stream approximation (Barker, 1996; Barker et al., 1996; Barker and Fu, 2000). In particular, one can assume that the cloud optical thickness for a given cloud field obeys the probability distribution law (e.g., as those given in Fig. 3.38). However, the accuracy of two-stream approximations is rather low as compared to exact radiative transfer calculations (King and Harshvardhan, 1986; Thomas and Stamnes, 1999). In particular, for some cases errors introduced by the approximation can be larger than differences of radiative fluxes for horizontally homogeneous and inhomogeneous cloud fields themselves. Also this approximation does not allow consideration of the bi-directional reflection function of clouds, which is routinely measured by various radiometers and spectrometers on satellite platforms. With this in mind, Kokhanovsky (2003b) proposed to use the exponential approximation of the radiative transfer theory to solve each of N standard radiative problems, discussed above. Then it follows for the whole cloud field under observation:

$$\langle R(\xi, \eta, \phi)\rangle = \int_0^\infty R(\xi, \eta, \phi, \tau) f(\tau) d\tau, \tag{3.354}$$

where $f(\tau)$ is the cloud optical thickness distribution and $R(\xi, \eta, \phi, \tau)$ is the reflection function of a cloud with given τ. This equation and also similar formulae for other cloud radiative characteristics allow us to study the influence of cloud

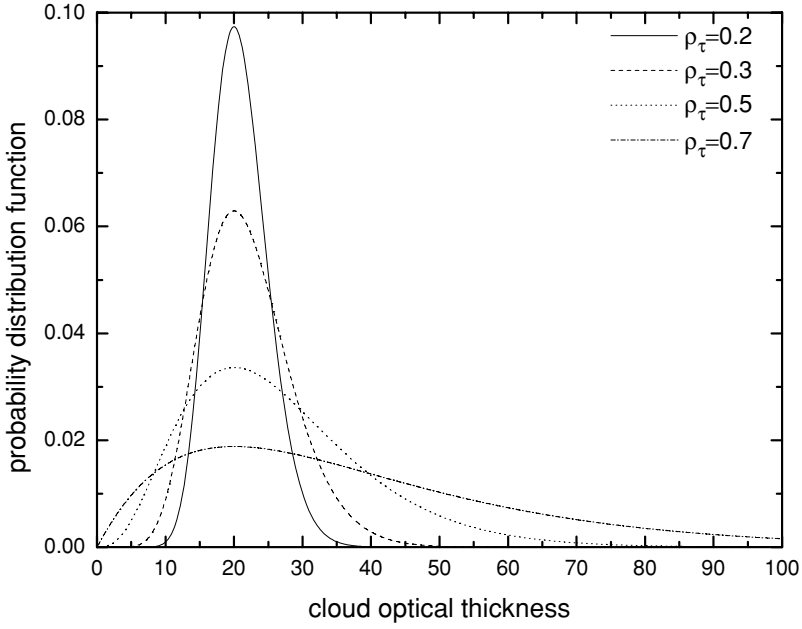

Fig. 3.38. Spatial optical thickness distribution modeled using the gamma distribution for different values of ρ_τ defined as $\Delta/\langle\tau\rangle$, where Δ is the standard deviation of the optical thickness and $\langle\tau\rangle$ is the average optical thickness.

inhomogeneity parameters on the measured reflection function for a given cloudy scene in a simple way. In particular, it follows for a nonabsorbing case:

$$\langle R(\xi,\eta,\phi)\rangle = R_\infty(\xi,\eta,\phi) - \langle t\rangle u_0(\xi)u_0(\eta), \tag{3.355}$$

where $R_\infty(\xi,\eta,\phi)$ does not depend on τ by definition (see Fig. 3.39) and

$$\langle t\rangle = \int_0^\infty t(\tau)f(\tau)d\tau. \tag{3.356}$$

Let us assume that $\tau \to \infty$. Then we have:

$$t(\tau) \approx \frac{4}{3\tau(1-g)} \tag{3.357}$$

and

$$\langle t\rangle = \frac{4\left(1+\frac{1}{\mu}\right)}{3\langle\tau\rangle(1-g)}, \tag{3.358}$$

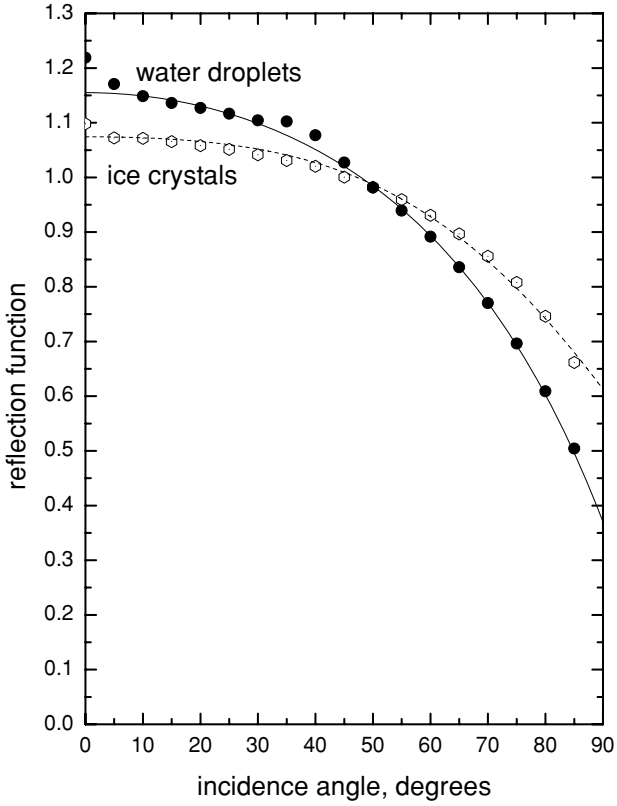

Fig. 3.39. Dependence of reflection functions of a semi-infinite nonabsorbing water and ice cloud on the incidence angle at the nadir observation. Symbols give exact results and lines are due to the approximation (Kokhanovsky, 2004b, 2005).

where we used the following distribution:

$$f(\tau) = \Lambda \tau^{\mu} \exp\left(-\mu \frac{\tau}{\tau_0}\right) \tag{3.359}$$

with

$$\Lambda = \frac{\mu^{\mu+1}}{\tau_0^{\mu+1}\Gamma(\mu+1)} \tag{3.360}$$

and $\langle \tau \rangle = \tau_0(1 + (1/\mu))$ is the average optical thickness defined as

$$\langle \tau \rangle = \int_0^{\infty} \tau f(\tau) d\tau. \tag{3.361}$$

So we have:

$$\langle t(\tau)\rangle / t(\langle\tau\rangle) \approx \left(1 + \frac{1}{\mu}\right) \tag{3.362}$$

as $\langle\tau\rangle \to \infty$. It means that $\langle t(\tau)\rangle / t(\langle\tau\rangle) \geq 1$, where we accounted for the fact that $\mu > 1$. Also because of this we have: $\langle R(\xi, \eta, \phi, \tau)\rangle < R(\xi, \eta, \phi, \langle\tau\rangle)$. It means that reflectances of inhomogeneous cloud fields, calculated assuming that the optical thickness is equal to the average optical thickness, give larger values as compared to measured reflectances. So we conclude that inhomogeneity leads to darkening of correspondent pixels as compared to the case of homogeneous clouds with the same optical thickness $\langle\tau\rangle$. On the other hand, the transmission of light by inhomogeneous clouds increases as compared to the case of a horizontally homogeneous cloud with the cloud optical thickness equal to $\langle\tau\rangle$.

3.9.2 Multidimensional Radiative Transfer in Clouds

3.9.2.1 General remarks

Radiative transfer in a cloudy atmosphere is usually studied in the framework of the plane-parallel approximation or the IPA as shown above. Then the diffuse light field changes only along the vertical direction for wide solar beam illumination conditions. There is no any change in the radiation field in the horizontal direction. Although this approximation, which is often called 1-D case, is very important for the case of extended cloudiness (e.g., extended fields of Stratocumulus clouds), it cannot be applied for the majority of cloudy scenes. Indeed cloudiness has a horizontal structure (e.g., holes between clouds).

These effects can be accounted for in the framework of the 3-D radiative transfer equation, where the spatial variation of local optical properties is fully accounted for. Various approaches to deal with 3-D clouds are known (Liou, 2002). The most popular techniques are the Monte Carlo method (Marchuk et al., 1980; Shreier and Macke, 2001), the diffusion approximation (Liou, 2002), the spherical harmonics discrete ordinate method (Evans, 1998), and the iteration technique (Nikolaeva et al., 2005).

In the iteration technique, the phase function in the scattering integral is represented by the spherical harmonics and the integral is replaced by a quadrature sum. Spatial grids are introduced and obtained partial differential equations are approximated by the system of linear algebraic equations. To solve it, the successive-orders-of-scattering (SOS) approach is applied.

Each partial differential equation is integrated along its characteristic throughout the whole calculation region in the framework of the well-known Evans's algorithm (Evans, 1998). These methods have some advantages and some deficiencies.

In particular, some of them may be non-conservative, e.g., do not conserve the number of photons in the transport problem. This defect can lead to significant errors in the solution obtained.

Other spherical harmonics discrete ordinate methods use the local approximation for partial differential equations. Such methods were widely used in various neutron and photon transport problems in the last 50 years. They are conservative and economic since they use very simple equations and do not apply complicated logic (all spatial meshes are calculated successively). In particular, such methods have been incorporated in the RADUGA 3-D solver described by Nikolaeva et al. (2005).

3.9.2.2 The three-dimensional radiative transfer equation

The 3-D radiative transfer equation can be written in the following form:

$$\xi \frac{\partial I(x,y,z,\theta,\phi)}{\partial x} + \eta \frac{\partial I(x,y,z,\theta,\phi)}{\partial y} + \beta \frac{\partial I(x,y,z,\theta,\phi)}{\partial z} + \sigma_{ext}(x,y,z) \times I(x,y,z,\theta,\phi) = \frac{1}{4\pi}\sigma_{sca}(x,y,z)\int_0^{\pi} \sin\theta' d\theta' \int_0^{2\pi} I(x,y,z,\theta',\phi') p(x,y,z, \chi(\theta,\phi,\theta',\phi'))d\phi' + \frac{1}{4\pi}\sigma_{sca}(x,y,z)F_0 p(x,y,z,\chi(\theta,\phi,\Theta,\Phi))\exp(-t), \tag{3.363}$$

where σ_{sca} and σ_{ext} are scattering and extinction coefficients, $p(x, y, z, \chi)$ is the phase function. The function $I(x, y, z, \theta, \phi)$ is the diffuse light intensity at the point (x, y, z) propagated in the direction (θ, ϕ), see Fig. 3.40. Also we have: $\xi = \sin\theta\cos\phi$, $\eta = \sin\theta\sin\phi$, $\beta = \cos\theta$. Scalar product χ is defined by the following relation

$$\chi(\theta,\phi,\theta',\phi') = \cos\theta\cos\theta' + \sin\theta\sin\theta'\cos(\phi-\phi'). \tag{3.364}$$

The value ot t in Eq. (3.363) is the optical path between two points defined by radius vector $\vec{r}_0$ and $\vec{r}$: $t = \int_0^d \sigma_{ext}(\vec{r}_0 + \zeta\vec{r})d\zeta$, where $d = |\vec{r} - \vec{r}_0|$.

The vector $\vec{r}_0$ defines the crossing point of the light beam with the boundary of the scattering medium under study.

We assume that there is no diffuse light entering the medium. Therefore, boundary conditions have the following form:

$$I(\vec{r},\vec{\Omega}) = 0 \text{ at } \vec{\Omega}\vec{n}(\vec{r}) < 0 \text{ for all } \vec{r}(x,y,z) \in G_{\text{finite}},$$
$$I(\vec{r},\vec{\Omega}) = I(\vec{r}^*,\vec{\Omega}) \text{ at } \vec{\Omega}\vec{n}(\vec{r}) < 0 \text{ for all } \vec{r}(x,y,z) \in G_{\text{infinite}},$$

Here G_{finite} is the finite part of the medium boundary (on z), G_{infinite} is the infinite one (on x and y), $\vec{r}^*$ is an inner point for the periodic boundary conditions.

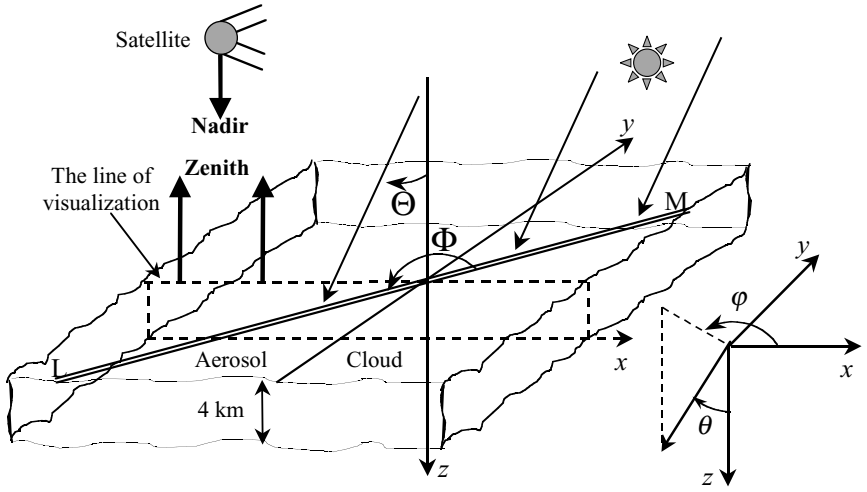

Fig. 3.40. Geometry of the problem.

This full 3-D transport equation is reduced to 2-D equation in some particular cases. For instance, let us assume that the line LM (see Fig. 3.40) coincides with the visualization line. This means that the solution becomes invariant in respect to the coordinate y. Then we can drop the dependence on y in Eq. (3.363) and arrive at the following simplified 2-D transport equation:

$$\xi \frac{\partial I(x, y, z, \theta, \phi)}{\partial x} + \beta \frac{\partial I(x, y, z, \theta, \phi)}{\partial z} + \sigma_{ext}(x, z) I(x, z, \theta, \phi) = \hat{F} I, \tag{3.365}$$

where

$$\hat{F} I \equiv \frac{1}{4\pi} \sigma_{sca}(x, z) \int_0^{\pi} \sin\theta' d\theta' \int_0^{2\pi} I(x, z, \theta', \phi') p(x, z, \chi(\theta, \phi, \theta', \phi')) d\phi' + \frac{1}{4\pi} \sigma_{sca}(x, z) F_0 p(x, z, \chi(\theta, \phi, \Theta, \Phi)) \exp(-t). \tag{3.366}$$

Equation (3.365) can be solved using the method of successive orders of scattering. Namely, at first we neglect the integral term in Eq. (3.366) and calculate the diffuse intensity $I(x, z, \theta, \phi)$ from the solution of the partial differential equation. Then the obtained diffuse intensity is substituted in the scattering integral in Eq. (3.366) and the next approximation for $I(x, z, \theta, \phi)$ is found from the solution of the partial differential equation (3.365). The algorithm is stopped when the convergence is reached.

Therefore, the problem at hand is reduced to the solution of the following transport equation:

$$\xi \frac{\partial I(x,y,\theta,\phi)}{\partial x} + \beta \frac{\partial I(x,y,\theta,\phi)}{\partial z} + \sigma_{ext}(x) I(x,z,\theta,\phi) = \Im(x,z,\theta,\phi), \tag{3.367}$$

where $I(x,z,\theta,\phi)$ is the diffuse light intensity at the point $\vec{r}(x,z)$ propagated in the direction (θ,ϕ), $\Im(x,z,\theta,\phi) = \hat{F}\tilde{I}(x,z,\theta,\phi)$ and $\tilde{I}(x,z,\theta,\phi)$ is a known function obtained from the previous iteration as described above.

We introduce an angular quadrature and replace functions $I(x,z,\theta,\phi)$, $\tilde{I}(x,z,\theta,\phi)$ and $\Im(x,z,\theta,\phi)$ by their values in quadrature nodes. Integral $\Im(x,z,\theta,\phi)$ is calculated using the following standard steps:

- the expansion of function $\tilde{I}(x,z,\theta,\phi)$ in terms of spherical harmonics,
- the representation of integral $\Im(x,z,\theta,\phi)$ by spherical harmonics,
- the calculation of $\Im(x,z,\theta,\phi)$ values in quadrature nodes.

A standard grid method to approximate the partial differential equation of the first order is used. In particular, grids with respect to spatial variables x and z are introduced:

$$x_{1/2} < \ldots < x_{k+1/2} < \ldots < x_{k+1/2}, z_{1/2} < \ldots < z_{\ell+1/2} < \ldots < z_{L+1/2}.$$

A single two-dimensional cell (k,l) has the following dimensions: $[x_{k-1/2}, x_{k+1/2}] \times [z_{\ell-1/2}, z_{\ell+1/2}]$. Correspondingly, its size is $[\triangle x_k] \times [\triangle z_l]$, where $\triangle x_k = x_{k+1/2} - x_{k-1/2}$ and $\triangle z_k = z_{K+1/2} - z_{k-1/2}$. Also the integral operator

$$\hat{\Lambda}_{k,\ell} = \frac{1}{\triangle x_k \triangle y_\ell} \int_{x_{k-1/2}}^{x_{k+1/2}} dx \int_{x_{\ell-1/2}}^{z_{\ell+1/2}} dz$$

is applied to both parts of Eq. (3.365). Then it follows:

$$\xi(I_{k+1/2,\ell} - I_{k-1/2,\ell})/\triangle x_k + \beta(I_{k,\ell+1/2} - I_{k,\ell-1/2})/\triangle z_\ell + \sigma_{ext}^{k,\ell} I_{k,\ell} = \Im_{k,\ell}, \tag{3.368}$$

where

$$I_{k,\ell} = \frac{1}{\triangle x_k \triangle z_\ell} \int_{x_{k-1/2}}^{x_{k+1/2}} dx \int_{x_{\ell-1/2}}^{z_{\ell+1/2}} dz I(x,z), \Im_{k,\ell} = \frac{1}{\triangle x_k \triangle z_\ell} \int_{x_{k-1/2}}^{x_{k+1/2}} dx \times \int_{x_{\ell-1/2}}^{z_{\ell+1/2}} dz \Im(x,z), \tag{3.369}$$

are the average values of the intensity and the source function, respectively, over a given cell and

$$I_{k\pm1/2,\ell} = \frac{1}{\triangle z_\ell}\int_{x_{\ell-1/2}}^{z_{\ell+1/2}} dz I(x_{k\pm1/2}, z),\ I_{k,\ell\pm1/2} = \frac{1}{\triangle x_k}\int_{x_{k-1/2}}^{x_{k+1/2}} dx I(x, z_{\ell\pm1/2}), \tag{3.370}$$

are correspondent average values of the intensity on boundaries of the cell (k, l). Fulfilment of Eq. (3.368) guarantees that a presented scheme is a conservative one.

Intensities $I_{k-1/2,l}$ and $I_{k,l-1/2}$ are known either from boundary conditions or from the result of the calculation for the previous cell. So we need to determine only values of $I_{k-1/2,l}$, $I_{k,l-1/2}$ and $I_{k,l}$. It is not possible to evaluate three parameters from a single equation (3.368). So we need to introduce two approximate relations among these three unknown parameters. They are given as follows:

$$I_{k,\ell} = (1-\nu_{x,k,\ell})I_{k+s(\xi)/2,\ell} + \nu_{x,k,\ell} I_{k-s(\xi)/2,\ell}, \tag{3.371}$$

$$I_{k,\ell} = (1-\nu_{z,k,\ell})I_{k,\ell+s(\beta)/2,\ell} + \nu_{z,k,\ell} I_{k,\ell-s(\beta)/2}, \tag{3.372}$$

where $s(\xi) = sign(\xi)$, $s(\beta) = sign(\beta)$, $\nu_{x,k,\ell} \in [0, 1)$ and $\nu_{z,k,\ell} \in [0, 1)$ are weight parameters. One can use values of weight parameters as follows:

$$\nu_{x,k,\ell} = 1/(2+h_{x,k,\ell}),\ \nu_{z,k,\ell}\frac{(h_{x,k,\ell}/h_{z,k,\ell})(1+h_{x,k,\ell})}{2+2h_{x,k,\ell}+h_{x,k,\ell}^2} \text{ at } h_{x,k,\ell} \le h_{z,k,\ell}, \tag{3.373}$$

$$\nu_{x,k,\ell} = \frac{(h_{z,k,\ell}/h_{x,k,\ell})(1+h_{z,k,\ell})}{2+2h_{z,k,\ell}+h_{z,k,\ell}^2}\nu_{z,k,\ell} = 1/(2+h_{z,k,\ell} \text{ at } h_{x,k,\ell} \ge h_{z,k,\ell}. \tag{3.374}$$

Optical steps $h_{x,k,\ell}$ and $h_{z,k,\ell}$ are defined as:

$$h_{x,k,\ell} = \sigma_{ext}^{k,\ell}\triangle x_k/|\xi|,\ h_{x,k,\ell} = \sigma_{ext}^{k,\ell}\triangle z_k/|\beta|. \tag{3.375}$$

This scheme defines outside fluxes $I_{k+s(\xi)/2,\ell}$, $I_{k,\ell+s(\beta)/2}$ via entering fluxes $I_{k-s(\xi)/2,\ell}$, $I_{k,\ell-s(\beta)/2}$ in a physically correct manner in any cell of any grid. It permits to obtain discontinuous solutions and solutions with large gradients accurately. This completes a brief description of this technique. Further details are given by Nikolaeva et al. (2005).

3.9.2.3 Numerical results

Let us consider results of numerical calculations for the case presented in Fig. 3.40, where a rectangular coordinate system *xyz* is introduced. Solar light is approximated by the monodirectional source having intensity $F_0\delta(\mu - \mathrm{M})\delta(\phi - \Phi)$. Here $M = \cos\Theta$, $\mu = \cos\theta$ and the pair (Θ, Φ) gives the direction of solar light propagation in the spherical coordinate system defined by the axis z and angles (θ, ϕ). The azimuth Φ is counted with respect to the positive direction of the axis x. In this chapter only results for $\Phi = 0$ and $\Phi = \pi$ will be reported. It means that solar light enters the atmosphere from the direction of the positive values of x (then

$\Phi = \pi$) or from the direction of the negative values of x (then $\Phi = 0$). The intensity of multiply scattered light is calculated along the axis x in the zenith direction as shown in Fig. 3.40 (see the line of visualization in Fig. 3.40).

We divide the terrestrial atmosphere in two equal semi-spaces separated by a local vertical plane. One part is filled by a cloudy medium and another one by the atmospheric aerosol. The processes of molecular scattering and absorption are neglected. Scattering media are assumed to be homogeneous and infinite in planes $z = const$. We assume that there are no light scattering particles at $z > 4$ km. All downwardly propagated photons, which reach the plane $z = 0$, are assumed to be absorbed. Therefore, the contribution of the ground albedo is neglected.

Droplets in a cloud are characterized by the Cloud C.1 particle size distribution with the effective radius equal to 6 μm. The single-scattering diagram for an elementary volume of a cloudy medium is calculated at wavelength 412 nm using the Mie theory. The phase function in the aerosol medium is represented by the Henyey–Greenstein formula. The asymmetry parameter of the cloud phase function g is equal to 0.85. The value of g for the aerosol phase function is equal to 0.7. The optical thickness of cloudy and aerosol portions of the scene are 30 and 1.2, respectively. Also we have studied the variation of the reflected light as observed from a satellite for a nadir observation geometry as the function of the solar angle Θ.

Under conditions specified above, the considered problem is reduced to the 2-D problem. Both aerosol and cloud are homogeneous around z-direction on the height interval (0 km, 4 km). They are contained in rectangular boxes. We will study the upwelling light field in the zenith direction along the line of visualization shown in Fig. 3.40. Clearly, the intensity of the reflected light field must depend on the coordinate x.

The largest gradients of the reflection function $R(x)$ are expected in the area closest to the cloud boundary. Because both an aerosol and a cloud are extended to infinity along axis x, this function far from boundaries must be equal to the value, which can be obtained from the 1-D radiative transfer equation.

The results of calculations using the RADUGA code (Nikolaeva et al., 2005) are given in Figs. 3.41 and 3.42. We also show comparisons with 3-D Monte Carlo code MYSTIC in Figs. 3.41 and 3.42. The MYSTIC (Mayer, 1999) is the Monte Carlo code for the physically correct tracing of photons in cloudy atmospheres. The MYSTIC is a forward Monte Carlo code which traces photons on their individual paths through the atmosphere, similar to what is described by Cahalan et al. (1994). Radiances are calculated using a local estimate technique. In this configuration, MYSTIC has been successfully validated in the intercomparison of 3-D radiation codes (see http://climate.gsfc.nasa.gov/I3RC). MYSTIC is operated within the libRadtran package (see http://www.libradtran.org), which prepares the optical properties of the atmosphere to be used in the model. A model domain of 80 km in x was used. A large domain size is important since MYSTIC uses periodic

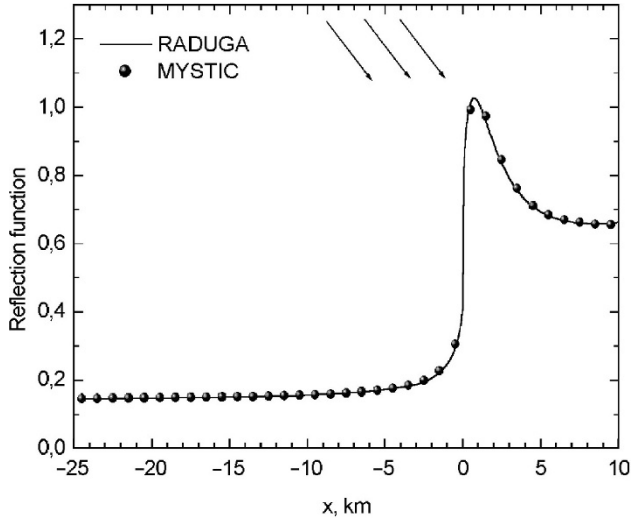

Fig. 3.41. The reflection function in the vicinity of the cloud edge in the nadir direction. Calculations are performed for the illumination from a clear sky side with the solar zenith angle 60°. The aerosol optical thickness is equal to 1.2 and the cloud optical thickness is equal to 30. Results of the RADUGA and MYSTIC codes in the direction perpendicular to the cloud band are shown (Nikolaeva et al., 2005).

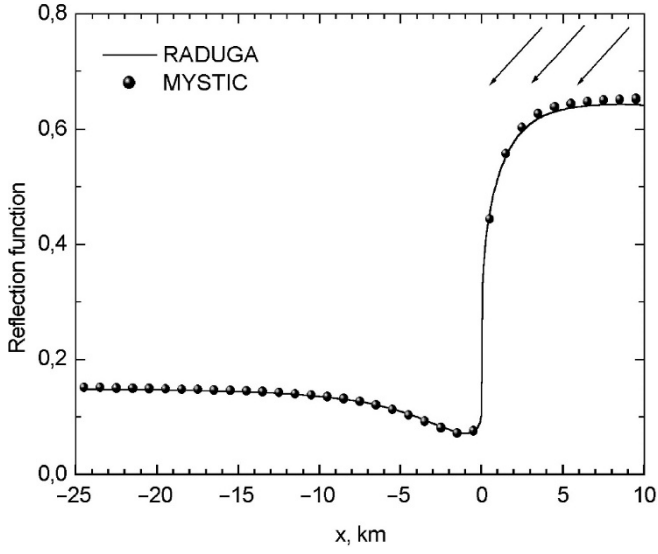

Fig. 3.42. The same as in Fig. 3.41 but for the illumination from the cloud side (Nikolaeva et al., 2005).

boundary conditions. The model resolution was set to 0.1 km; the MYSTIC results are, therefore, averages over 0.1 km bins.

It follows from results of comparisons as shown in Figs. 3.41 and 3.42 that differences are below 1%. Therefore, both the MYSTIC and RADUGA provide very accurate results as far as calculations of the light reflected by an aerosol-cloudy medium are concerned.

Some physical dependencies are clearly seen in Figs. 3.41 and 3.42. For instance, it follows from Fig. 3.42 that there is a shadow near the cloud border for the illumination from the cloud side ($\Phi = \pi$). It follows from geometrical considerations that the shadow extends from the cloud boundary up to the distance $\mathbb{Z} = Htg\vartheta_0$, where H is the cloud top altitude and ϑ_0 is the solar zenith angle. Therefore, the shadow covers a larger region for larger solar zenith angles.

Also we have a brightening effect in Fig. 3.41 due to the cloud side illumination effects ($\Phi = 0$). These two effects (*shadowing* and *brightening*) are primarily due to the direct light interaction with a scattering medium. They lead to roughening effects in 2-D–3-D transfer problems. We also observe (see Fig. 3.42) the decrease of the reflection near the border of the cloud (inside the cloud) as compared to the 1-D case. This is due to photon leaking in the area with a smaller extinction coefficient in the clear part of the scene. The increase in the aerosol reflection function in Fig. 3.41 close to the cloud is due to channelling of photons from a cloud to the aerosol side. These two effects (*photons channelling* and *leaking*) lead to a smoothening of the radiative field. The four effects considered here are valid not only for a simple case studied here but also for broken cloud systems (Varnai and Marshak, 2003).

Three-dimensional effects can be parameterized taking into consideration these four fundamental effects. The parameterization of 3-D effects is of a great importance for satellite remote sensing because calculations presented here are computationally expensive and can not be included in the operational aerosol/cloud retrieval algorithms. Also, these effects cannot be neglected. In particular, if satellite pixels contain areas corresponding to brightening/shadowing effects, then large biases in retrieved cloud/aerosol parameters are expected (see Figs. 3.41 and 3.42). This also points to the necessity of the development of the simultaneous aerosol-cloud (and surface) retrieval algorithm. This complex system should be considered in the retrieval process as a whole (Cahalan et al., 2001), which will allow us to obtain the most accurate estimations of the atmospheric and surface parameters from both airborne and satellite remote sensing measurements.